

Geobiology of the Zambales Ophiolite, Philippines and Coast Range Ophiolite, California

BY

CAITLIN CASAR
B.S., East Carolina University, 2012

THESIS

Submitted as partial fulfillment of the requirements for the
degree of Master of Science in Earth and Environmental Sciences
in the Graduate College of the University of Illinois at Chicago,
2015

Chicago, Illinois

Defense Committee:

D'Arcy Meyer-Dombard, Chair
Steve Guggenheim
Fabien Kenig

ACKNOWLEDGMENTS

I would like to thank my advisor, Dr. D'Arcy Meyer-Dombard, for giving me the opportunity to work with her. Her mentoring was invaluable, and I hope to work with her again in the future. I would also like to thank my committee members, Dr. Fabien Kenig and Dr. Steve Guggenheim for their support for the duration of this project. The collaboration of Dr. Dawn Cardace at the University of Rhode Island, Dr. Caloy Arcilla at the University of the Philippines, and Dr. Matt Schrenk at Michigan State University made this project possible. I'm also grateful to my lab mates Bharathi Vallalar and Kristin Woycheese for their support and friendship during my time spent at UIC. Alexander Simon was a huge part of the lab work for this research, and I'm grateful for his hard work and company during the long hours in the lab. I'm also very thankful for the technical and analytical support I received from Dr. Stefan Green, Olivia Thompson, Tad Daniel, and Ankur Naqib. I would also like to thank Christopher Marshall for his support for the final stretch of this project. I could not have completed this work without all of the amazing support I received, and I will always be very grateful to everyone who helped me through the journey to receiving my Master's degree.

TABLE OF CONTENTS

LIST OF TABLES	v
LIST OF FIGURES	vi
LIST OF ABBREVIATIONS	vii
SUMMARY	viii
I. INTRODUCTION: WHY STUDY THE DEEP SUBSURFACE?	1
A. Serpentinization Reactions in Ophiolites Support Life in the Subsurface	1
B. Global Biogeochemical Cycling Impacts	4
C. Extraterrestrial Analog Environments	4
D. Iron Metabolisms in Serpentinizing Systems	5
E. Ophiolite Study Sites	6
1. Coast Range Ophiolite, Lower Lake, California	6
2. Zambales Ophiolite, Philippines	9
F. Purpose of Proposed Study/Research Questions	9
1. Ubiquity of Microbial Communities Among Serpentinizing Systems	11
2. Microbial Alteration of Local Mineralogy	11
3. Iron Redox in Continental Serpentinizing Communities	12
II. METHODS	13
A. Sample Collection	13
B. Documenting Microbe-Mineral Interactions	13
1. Microcosm Setup	15
2. Experiment Observations	15
3. Fluorescence Microscopy	15
4. Scanning Electron Microscopy and X-ray Energy Dispersive Spectroscopy	16
5. X-ray Diffraction	16
C. Verifying Fe-Metabolisms	17
1. Fe-Enrichment Cultures	17
2. Experiment Observations	18
3. Fluorescence Microscopy	19
4. Scanning Electron Microscopy and X-ray Energy Dispersive Spectroscopy	19
5. X-ray Diffraction	20
6. X-ray Photo-electron Spectroscopy	20
D. DNA Sequencing/Analyses	20
E. Expected Results of Analyses	22
1. Documenting Microbe-Mineral Interactions	22
2. Verifying Fe Metabolisms	22
III. RESULTS	24
A. Documenting Microbe-Mineral Interactions	24
1. Experiment Observations	25
2. Fluorescence Microscopy	27
3. Scanning Electron Microscopy and X-ray Energy Dispersive Spectroscopy	29
4. X-ray Diffraction	32
5. DNA Sequencing	35

B. Verifying Fe-Metabolisms	38
1. Experiment Observations.	39
2. Fluorescence Microscopy.	44
3. Scanning Electron Microscopy and X-ray Energy Dispersive Spectroscopy.	47
4. X-ray Photoelectron Spectroscopy.	51
5. X-ray Diffraction	52
6. DNA Sequencing	54
C. DNA Sequence Analyses.	57
D. Summary of Results.	58
1. Documenting Microbe-Mineral Interactions	58
2. Verifying Fe-Metabolisms	59
IV. DISCUSSION.	61
A. Ubiquity of Microbial Communities Among Serpentinizing Systems.	61
B. Microbial Alteration of Mineralogy	64
1. Mineralogy of Microcosm Sediments.	64
2. Secondary Precipitation on Microcosm Rock Chip Surfaces	64
C. Iron Redox in Continental Serpentinizing Systems.	67
1. Visual Indications of Redox Reactions	67
2. Oxidation States of Iron Precipitates in Cultures.	68
3. Putative Nanowires and Iron Redox in Iron Enrichment Cultures	70
4. Nitrate as an Electron Acceptor for Anaerobic Iron Oxidation	73
D. Comparison of Taxa in this Study	75
1. Alpha Diversity.	75
2. Beta Diversity.	78
E. Biosignature and Energy Signature Implications	81
VI. CONCLUSION	83
1. Ubiquity of Microbial Communities Among Terrestrial Serpentinizing Systems	83
2. Microbial Alteration of Mineralogy	84
3. Iron Redox in Terrestrial Serpentinizing Communities	85
CITED LITERATURE	86
APPENDIX A. DOCUMENTING MICROBE-MINERAL INTERACTIONS	91
APPENDIX B. VERIFYING FE-METABOLISMS	126
VITA.	133

LIST OF TABLES

1. Site Fluid Chemistry	8
2. Microcosm Mineralogy (XRD)	31
3. Culture and Inoculum Sediment Bulk Elemental Chemistry (Wt%) (XEDS)	44
4. Culture Mineralogy (XRD)	44
5. DNA Sequence Summary	52

LIST OF FIGURES

1. Global map of serpentinizing locations	2
2. Predicted iron metabolisms in subsurface serpentinizing systems worldwide	7
3. Predicted iron metabolisms in serpentinizing systems in the Philippines	7
4. Coast Range ophiolite study site	8
5. Zambales ophiolite study site	10
6. Microcosm setup	14
7. Iron enrichment culture setup	18
8. Documenting microbe-mineral interactions flowchart of analyses	24
9. Phase I microcosm images	26
10. Fluorescence microscopy images of Phase I microcosm fluids	28
11. SEM images of rock chips from Phase I microcosm experiments	31
12. Phase I microcosm XRD patterns overlain with standard pattern for lizardite	33
13. Relative abundances of genera in Phase I microcosm experiments	36
14. Verifying Fe-metabolisms flowchart of analyses	38
15. Images of California (QV1,3) cultures	40
16. Images of Philippines (ML2) cultures	41
17. Images of orange and black precipitates in Philippines (ML2) cultures	42
18. Images of nitrate cultures	43
19. Fluorescence microscopy images of California (QV1,3) cultures	45
20. Fluorescence microscopy images of Philippines (ML2) cultures	46
21. Fluorescence microscopy images of nitrate cultures	48

22. SEM images of California (QV1,3) and Philippines (ML2) culture precipitates	49
23. XPS spectra of precipitates from iron enrichment cultures	51
24. Culture XRD patterns overlain with standard pattern for halite	53
25. Relative abundances of genera in culture experiments	56
26. Documenting microbe-mineral interactions - summarized results	60
27. Verifying Fe-metabolisms - summarized results	60
28. Relative abundances of phyla in global serpentinizing systems	62
29. SEM images of precipitate morphologies on rock chips from microcosm experiments	65
30. XPS iron oxidation peak shifts from iron culture precipitates	60
31. Alpha diversity (family level)	76
32. Alpha diversity (species level)	77
33. Beta diversity (weighted unifrac)	78
34. Beta diversity (unweighted unifrac)	80
APPENDIX A. FIGURES	91
1. Fluorescence microscopy images of rock chips from Phase I microcosms	91
2. Fluorescence microscopy images of rock chips from Phase II microcosms	92
3. SEM images of rock chips from Phase II microcosms	93
Inoculum sediments & rock core XRD patterns overlain with standard patterns for:	
4. lizardite	94
5. actinolite	95
6. forsterite.	96
7. diopside	97
8. orthopyroxene	98

9. enstatite	99
10. magnetite(2332).....	100
11. magnetite(3536).....	101
12. hematite.....	102
13. ferrihydrite	103

Phase I microcosm XRD patterns overlain with standard patterns for:

14. actinolite	104
15. diopside	105
16. enstatite	106
17. ferrihydrite	107
18. forsterite	108
19. hematite	109
20. maghemite	110
21. magnetite(2332).....	111
22. magnetite(3536).....	112
23. orthopyroxene	113

Phase II microcosm XRD patterns overlain with standard patterns for:

24. actinolite	114
25. diopside	115
26. enstatite	116
27. ferrihydrite	117
28. forsterite	118
29. hematite	119

30. lizardite	120
31. maghemite	121
32. magnetite(2332)	122
33. magnetite(3536)	123
34. orthopyroxene	124
35. Relative abundances of genera in Phase I microcosm experiments	125
APPENDIX B. FIGURES	126
Culture XRD patterns overlain with standard patterns for:	
1. actinolite	126
2. hematite	127
3. lizardite	128
4. magnesiowuestite	129
5. magnetite(2332)	130
6. magnetite(3536)	131
7. siderite	132

LIST OF ABBREVIATIONS

OTU	Operational Taxonomic Unit
SEM	Scanning Electron Microscopy
XEDS	X-ray Energy Dispersive Spectroscopy
XPS	X-ray Photo-electron Spectroscopy
XRD	X-ray Diffraction

SUMMARY

A study of the geobiology of two serpentinizing systems in the Coast Range ophiolite, California and Zambales ophiolite, Philippines was motivated by thermodynamic calculations that predicted microbial metabolisms in these systems. Microcosms simulated surface and subsurface serpentinizing systems using samples collected from each study region, and were sampled over a period of six weeks to document microbe-mineral interactions. Iron redox in the two systems was investigated through batch culturing techniques employing ferric hydroxide as a growth substrate and sediments collected from the serpentinizing study sites as inoculum.

Microcosm experiments indicated microbial interaction with mineral surfaces, shown by visual observations of the solids in the microcosms and scanning electron micrographs of rock chips in the experiments. Cell morphologies and taxonomic assemblages of communities were identified via fluorescence microscopy and DNA sequencing, which indicated the presence of iron metabolizing microbes. Culture experiments indicated that microbes were engaging in iron redox reactions as predicted by thermodynamic modeling. Indications included visual observations of color change and magnetic attraction of precipitates, as well as scanning electron micrographs of the precipitates and oxidation states of the precipitates measured through X-ray photoelectron spectroscopy. DNA sequencing indicated the presence of iron metabolizing microbes in these experiments. A comparison of microbial communities in this study to communities in other studies from global serpentinizing systems indicated the persistence of two taxa across all systems: Firmicutes and Proteobacteria.

I. INTRODUCTION: WHY STUDY THE DEEP SUBSURFACE?

The deep subsurface is an environment that hosts microorganisms in the absence of light and presence of life-supporting chemical reactions within Earth's crust. Examples of places the deep subsurface is explored include ophiolites, sea floor spreading ridges, deep basalt aquifers, deep subsurface sediments, and black shales (Szponar et al. 2003, Schrenk et al. 2003, Stevens et al. 1995, Kormas et al. 1993, Matlakowska et al. 2012). Almost a century ago, petroleum geologists thought microbial life might exist in the deep subsurface. However, they had no means to sample the subsurface aseptically and the idea of life in the deep subsurface was not widely accepted. By the late 1970's, a growing interest in the possibility of deep subsurface life was driven by the urgent need to manage groundwater quality. By the early 1990's, technology allowed for aseptic subsurface sampling, and microbial life in the subsurface was confirmed (Frederickson et al. 1996). Once thought to be completely devoid of life, the subsurface is now understood to host microbial life at depths of over three kilometers in terrestrial rocks (Chivian et al. 2008), and it has been estimated that the subsurface hosts 4.1 billion tons of biomass (Kallmeyer et al. 2012). We now access deep subsurface habitats through wells, mines, drill holes retrofitted with observation and collection equipment, and by capturing fluids escaping the deep biosphere at Earth's surface. Life in the deep subsurface is still largely unexplored and these ecosystems are biogeochemically and astrobiologically relevant.

A. Serpentinization Reactions in Ophiolites Support Life in the Subsurface

Ophiolites are formed by tectonic emplacement of oceanic crust onto continental crust in unique compressional environments around the world (Figure 1). Stratigraphy of ophiolites show that

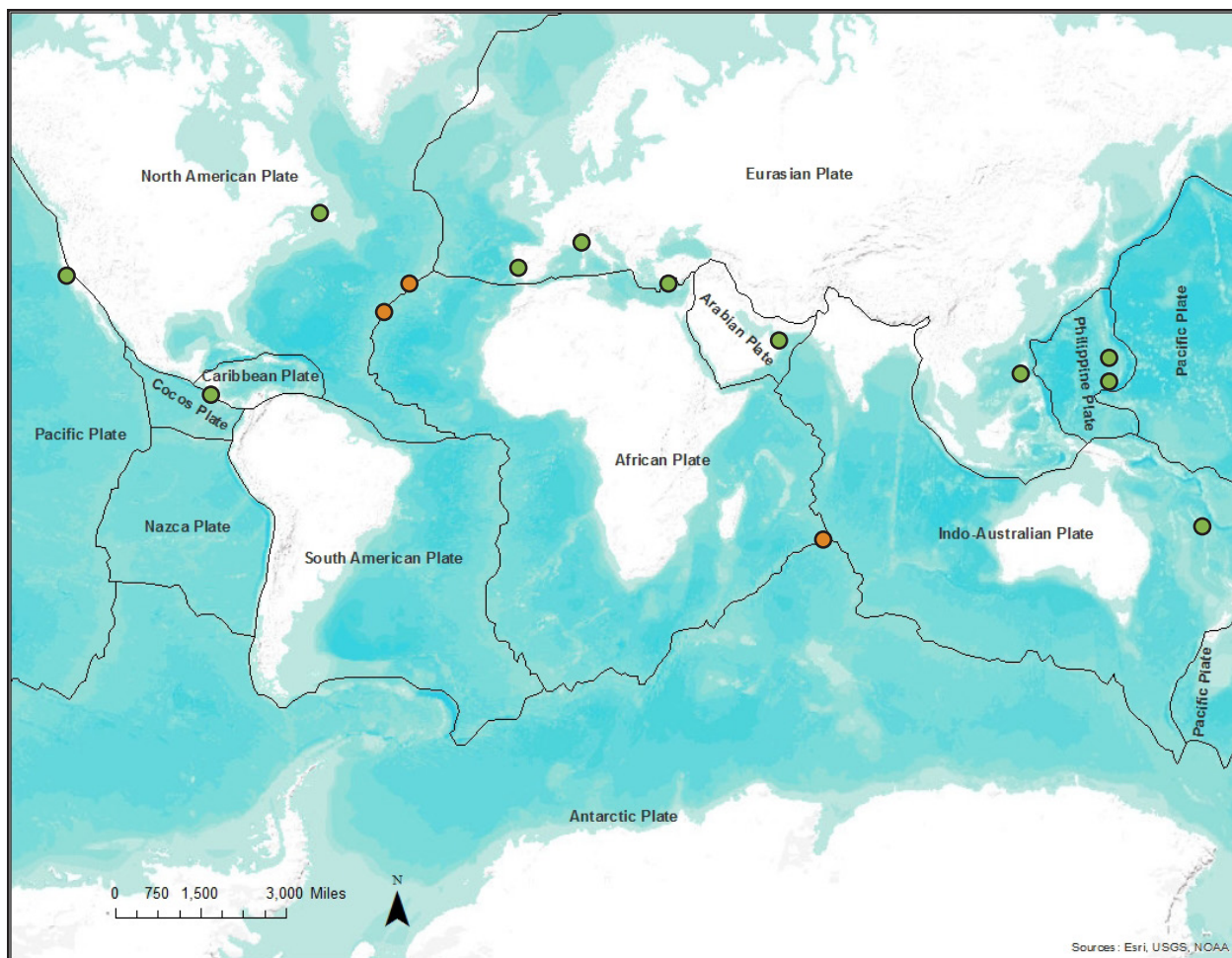
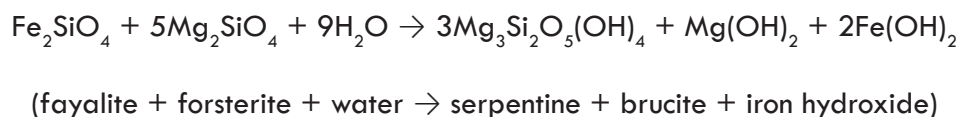


Figure 1. Global map of selected serpentinizing system locations. Green dots represent ophiolite exposures (continental systems), orange dots represent marine systems. Figure generated in ArcGIS with data from Schrenk et al. 2013. Plate boundaries downloaded from ArcGIS.com December 2014.

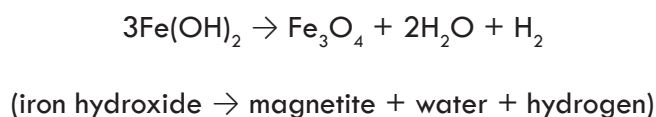
they originate at mid-ocean ridges, and typically include the entire marine sequence of carbonates overlain by mantle rocks, layered gabbros, sheeted dikes, and pillow basalts. When mantle rocks in the ophiolite are exposed to planetary surface conditions, they become unstable and weather rapidly, creating an energetic environment that is conducive to microbial life. Ophiolite rocks containing olivine react readily with water to form serpentine minerals while releasing hydrogen and methane gas in a process called serpentinization. Serpentinization reactions produce fluids with

extremely high pH at low temperatures (Schrenk et al. 2013). The following reactions outline the hydrothermal transformation of olivine to serpentine with the production of reduced iron species, hydrogen and methane gas.

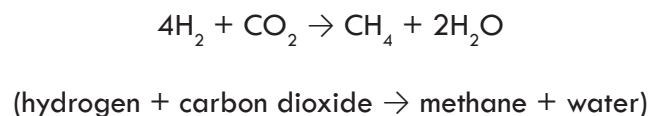
Reaction 1:



Reaction 2:



Reaction 3:



Fluids at depth in serpentinizing systems are characterized by low concentrations of dissolved inorganic carbon and oxygen and high concentrations of methane and hydrogen. Microorganisms may harness energy by coupling these gases to the reduction or oxidation of reactants such as iron. The oxidation or reduction of iron in the fluids is largely dependent on pH. Ferrous iron is not stable at a high pH, and spontaneously reacts with atmospheric oxygen to form ferric iron which is then hydrolyzed to ferrihydrite ($\text{Fe}(\text{OH})_3$). These reaction kinetics may be too rapid for microbes to harness energy for growth; however cells have been documented to act as nucleation sites for ferrihydrite precipitation in natural environments (Sawicki et al. 1995). Serpentinizing fluids travel along fault conduits in the host rock, sometimes resulting in exposure to the atmosphere. Ferrous precipitates that remain in the anaerobic subsurface may act as substrates for microbial metabolisms where microbes carry out iron oxidation and reduction (Konhauser, 1998, Posth et al. 2014).

B. Global Biogeochemical Cycling Impacts

In the deep subsurface, for example in subsurface serpentinizing systems, access to energy from the sun and products of photosynthesis is limited or nonexistent. The deep subsurface is energized by oxidation-reduction gradients that drive chemical reactions which support chemotrophic life. A flux of two billion cubic meters of hydrogen has been estimated at slow spreading ridges alone (Charlou et al. 2010). Methane fluxes were estimated to be 380 kmol per year at hydrothermal vents along the Juan de Fuca ridge (Wankel et al. 2011), and 6.7 kmol per day above a hydrocarbon seep off the coast of California (Du et al. 2014). Hydrogen and methane are abiogenically produced in a number of other subsurface environments (including serpentinizing systems) known to support chemotrophy via hydrogen or methane coupling in redox reactions. However, the flux of these gases have not been documented across many subsurface systems. Current models of biogeochemical cycles may underestimate the influence of the deep subsurface on global gas fluxes (Kotelnikova, 2002, Charlou et al. 2010) and the amount of potential biomass supported by these gases, warranting the need for further investigations of biogeochemical fluxes in deep subsurface systems.

C. Extraterrestrial Analog Environments

The deep subsurface is characterized by limited oxygen, light, nutrients, and by extreme temperatures and pressures, matching potential environments that may be found in extraterrestrial habitats. Understanding the thresholds of life on Earth and what biomarkers may be left behind will allow us to search for it elsewhere in our solar system.

Terrestrial serpentinizing environments are good analogs for potential extraterrestrial ecosystems. For example, a methane plume corresponding to serpentinized rocks was recently detected in the Martian atmosphere (Ehlmann et al. 2010). Methane and hydrogen produced in

potential Martian subsurface serpentinizing systems may support microbial life similar to life in terrestrial serpentinizing systems. Since the detection of serpentine and methane on Mars, terrestrial serpentinizing systems have been studied as analogs to understand Martian habitability as a result of methane (Etiope et al. 2013) and hydrogen production and the potential for biosignature preservation (Greenberger et al. 2015, Blank et al. 2009). A variety of other terrestrial subsurface environments useful to understanding planetary habitability have been proposed as analogs for Europa, Titan, and Enceladus including subglacial lakes (Lorenz et al. 2011), asphalt lakes (Schulze-Makuch et al. 2011) and basalt aquifers (McKay et al. 2008) . Further research on subsurface environments is critical to our understanding of the nature of potential extraterrestrial life.

D. Iron Metabolisms in Serpentinizing Systems

Microorganisms harness geochemical energy by taking advantage of redox gradients when it is energetically favorable to do so and the reaction is otherwise kinetically inhibited. To predict chemical reactions that yield energy in subsurface serpentinizing systems for chemotrophic organisms, gas and ion chemistry of fluids from serpentinizing systems were used to model microbial metabolisms by calculating the amount of energy potentially available for each reaction. The Gibbs free energy of reaction is given by:

$$\Delta G_r = \Delta G_r^\circ + RT \ln Q_r$$

where ΔG_r , ΔG_r° , R , T , and Q_r are the Gibbs free energy of reaction, standard Gibbs free energy of reaction, gas constant, temperature, and activity product of the reaction, respectively.

Utilizing this reaction, the energy availability for a given metabolism can be calculated. Cardace et al. 2013, predicted the feasibility of microbially-driven iron oxidation and reduction in global terrestrial serpentinizing systems by calculating energy availability in these systems (methods

described in Cardace et al. 2009), reported in Gibbs free energy of reaction (in kJ/mol of electrons transferred (Figure 2). These calculations showed that ferric iron reduction is energetically favorable in serpentinizing subsurface environments. A more recent study shows that both ferric iron reduction and ferrous iron oxidation are energetically favorable metabolisms in subsurface serpentinizing systems in the Philippines (Figure 3) (Cardace et al. 2015). Metagenomic studies of serpentinizing systems have indicated the presence of microbes capable of metabolizing iron (Woycheese et al. 2015; Brazelton et al. 2012, 2013; Tiago et al. 2013, Dæe et al. 2013, Suzuki et al. 2013), but to our knowledge, no studies have directly observed iron metabolisms in these systems through culture-dependent techniques. These predictions motivated the study of the geobiology of two serpentinizing systems in the Coast Range and Zambales ophiolites in order to directly observe microbe-mineral interactions and iron microbial metabolisms.

E. Ophiolite Study Sites

1. Coast Range Ophiolite, Lower Lake, California

The Coast Range ophiolite is located in the northwestern region of the United States where the Juan de Fuca plate subducts beneath the North American plate. A microbial observatory was established at the McLaughlin National Reserve in Lower Lake, California (Figure 4) to access subsurface serpentinizing fluids from monitoring wells drilled by the Homestake Mining Company (Crespo-Medina et al. 2014). The study area is characterized by steep topography and serpentine outcrops. Samples from this study area came from wells QV1,1 and QV1,3 located next to a decommissioned open-pit gold mine, which was drilled in Quarry Valley (N 38°51.724'; W 122°25.827'). QV1,1 was drilled to a depth of 21 meters, and the lithology of the well is described as magnetite-bearing clay with albite. QV1,3 was drilled to a depth of 34.6 meters, and the

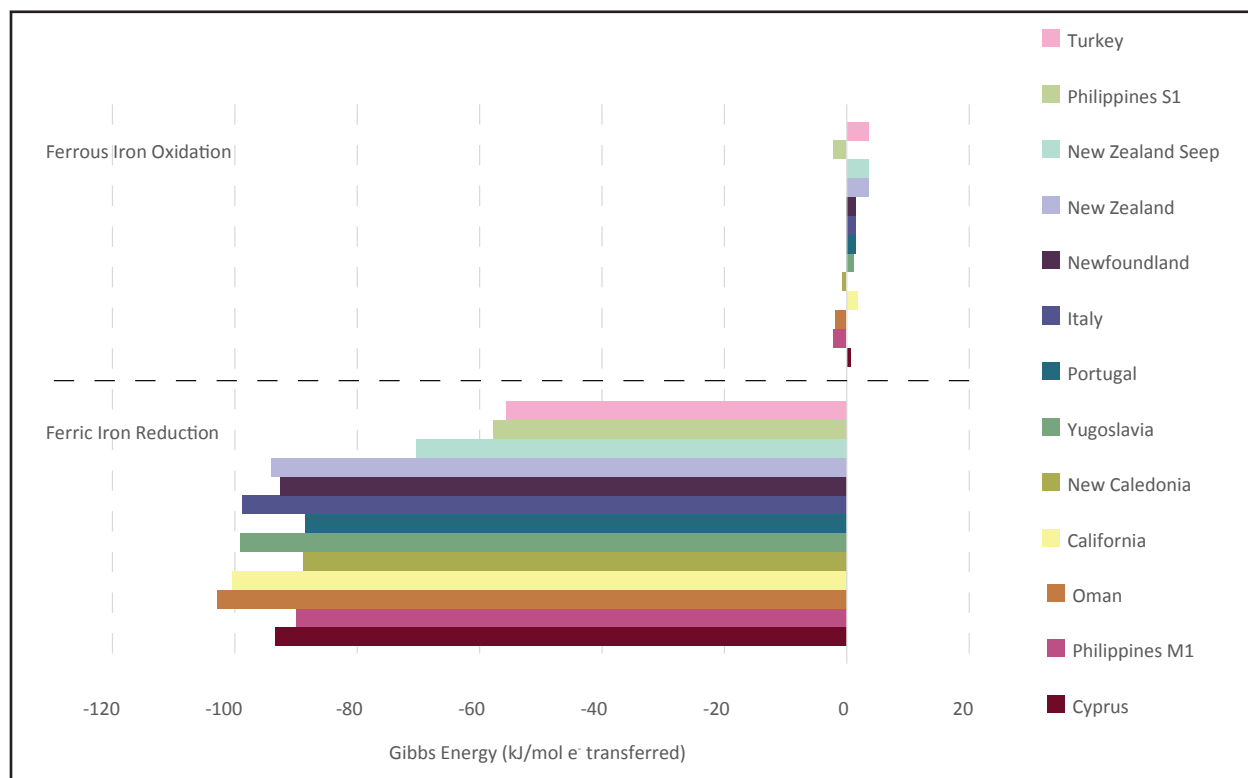


Figure 2. Predicted iron metabolisms in subsurface serpentinizing systems worldwide. Figure adapted from Cardace et al. 2013.

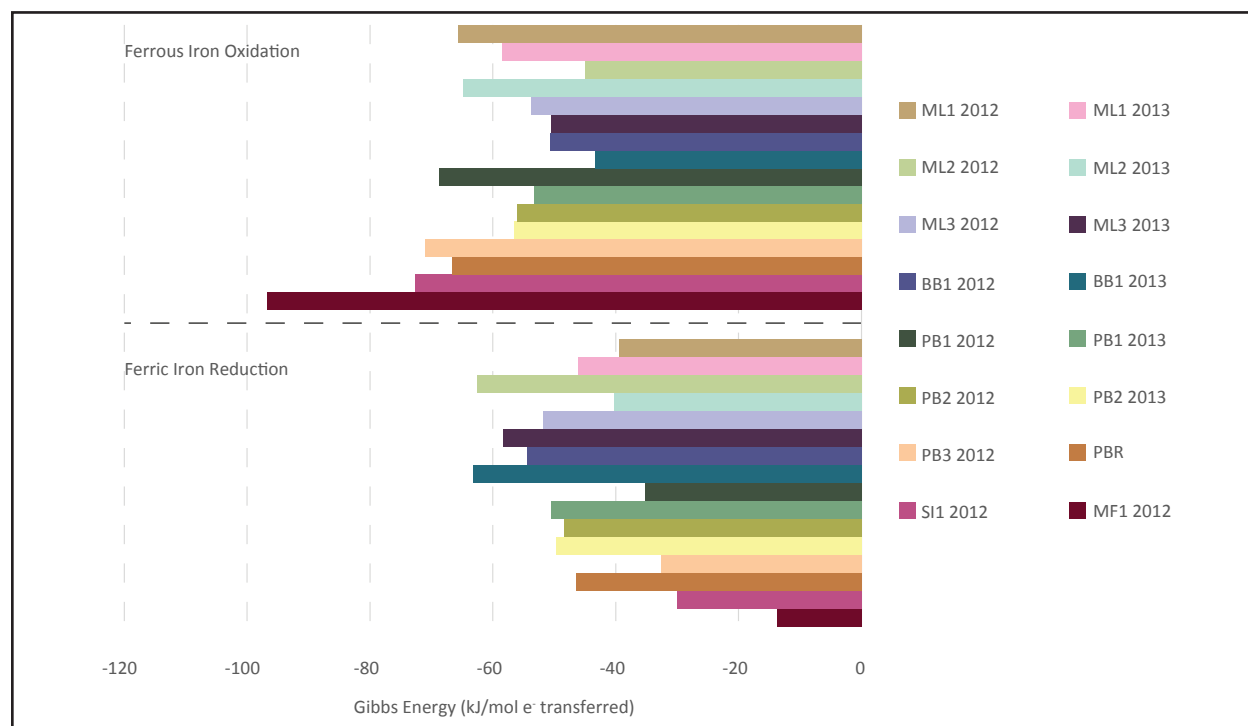


Figure 3. Predicted iron metabolisms in serpentinizing systems in the Philippines. Figure adapted from Cardace et al. 2015.

Coast Range Ophiolite | QV1,3 Study Site

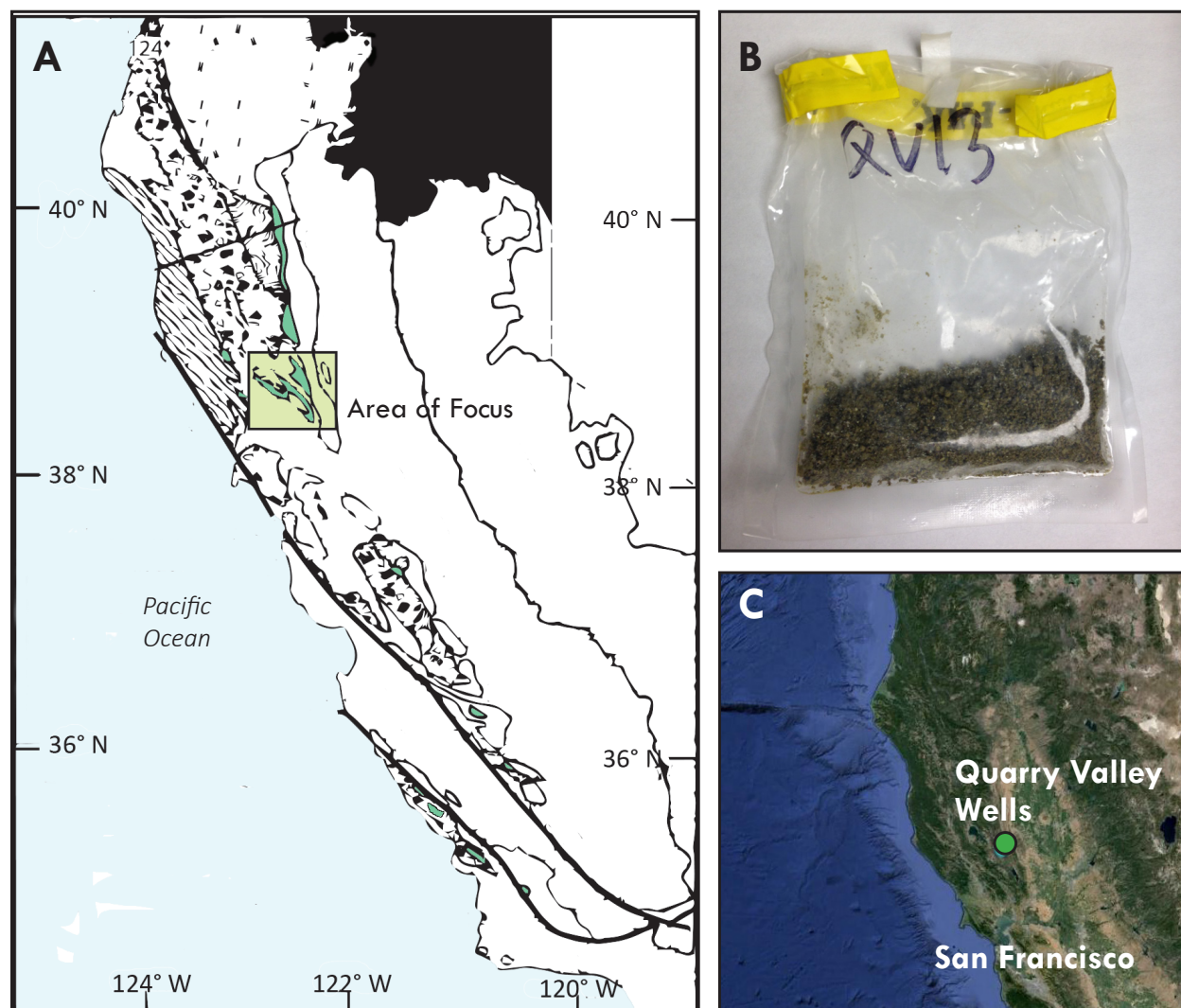


Figure 4. A) Map of the Coast Range ophiolite (symbolized in green) in California, including outlined study site region (adapted from Shervais et al. 2011). B) Sediments collected from QV1,3 drill hole. C) Quarry Valley well location at McLaughlin National Reserve (image created with Google Earth).

Table 1. Site Fluid Chemistry

Site	pH	T (°C)	ORP	H ₂ (μm)	CH ₄ (μm)	DO (%)	DIC	DOC (ppm C)	Fe ²⁺ (ppm)	SO ₄ ²⁻ (ppm)	NO ₂ ⁻ (mg/L)	NO ₃ ⁻ (mg/L)
QV1,1	11.7	12.94	-224.4	~2	~750	1.9	~100 μm	-	0	-	-	-
QV1,3	9.63	14.65	-77	~1	~1500	1.6-3.1	~550 μm	-	47	-	-	-
ML2	10.8	34.44	-424.7	496	400	0.86	0.1 ppm C	0.1	bdl	18.5	bdl	1.6
PB1	9.6	29.7	-125	161	bdl	5.5	3 ppm C	0.3	bdl	9.6	bdl	1.4

Selected fluid chemistry for Coast Range ophiolite sites QV1,1 and QV1,3 (2012) and Zambales ophiolite sites PB1 and ML2 (2013) (Cardace et al. 2012; Cardace et al. 2015; Cardace et al. 2015²).

lithology of the well is described as altered mafic rock (Cardace et al. 2013). The fluids in the QV1,3 well have a pH typical of serpentinizing fluids, whereas the relatively low pH of QV1,3 has been suggested to be due to serpentinizing fluids mixing with waters that have interacted with gabbros and basalts (Cardace et al. 2015). This region in California is arid, receiving 31.5 inches of annual rainfall. Published fluid chemistry is summarized in Table 1.

2. Zambales Ophiolite, Philippines

The Zambales ophiolite is located in the northwestern region of the Philippines (Figure 5) where the Pacific, Eurasian, and Philippine plates converge. Serpentinizing fluids are exposed at the surface as natural springs, some of which have been modified for tourism and bathing pools. The natural springs sampled for this study are located along one side of the Poon Bato River (PB1, N15°30.863'; E 120°22.891') and at Manleluag Springs (ML2, N 15°42.367'; E 120°16.935') next to a protected park. The Poon Bato country rock is serpentinite (altered mantle rock), with fluid chemistry indicative of being sourced in an actively serpentinizing host rock. The Manleluag country rock is gabbroic, with fluid chemistry indicative of serpentinizing fluids mixing with waters interacting with gabbros (Cardace et al. 2015). Both springs have developed travertine terraces along their outflow channels. Country rock was drilled for this study at a nearby location called Butili (N 15°48.013'; E 120°02.55'). This region is tropical, and receives 87.5 inches of rainfall annually. Published fluid and gas chemistry for PB1 and ML2 are summarized in Table 1.

F. Purpose of Proposed Study/Research Questions

This study investigates the geobiology of two serpentinizing systems in the Coast Range and Zambales ophiolites. Based on the predictions of possible metabolic processes by Cardace et al.

Zambales Ophiolite | ML2 Study Site

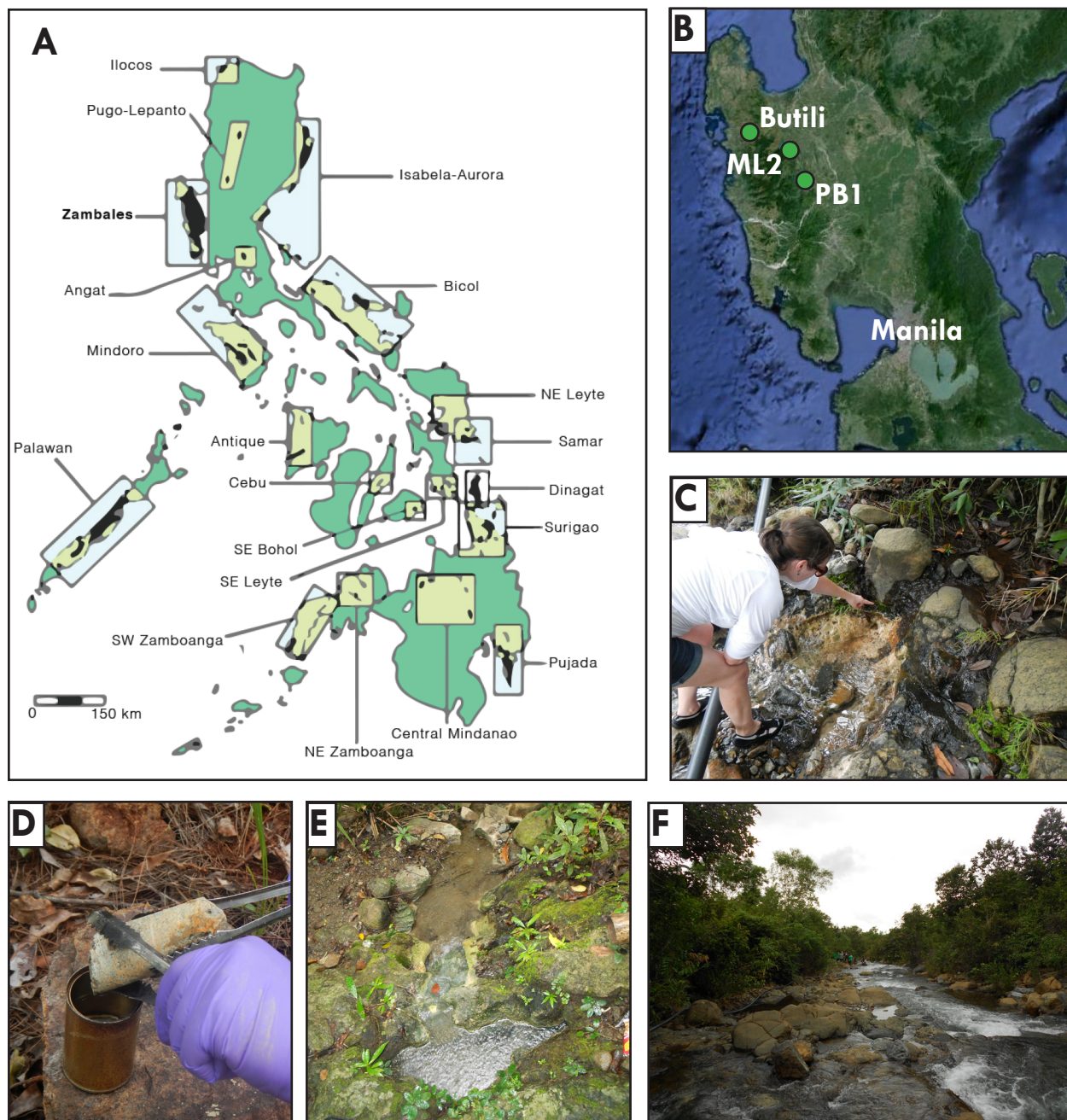


Figure 5. A) Map of major ophiolite exposures (solid black fill) in the Philippines, including study region in Zambales (adapted from Arcilla et al. 2011), B) sampling locations (image created with Google Earth), C) spring PB1, D) drilling at Butili, E) spring ML2, and F) Poon Bato River.

2015, we would expect that:

- 1) Abiotic oxidation of ferrous iron occurs in surface and near-surface environments in continental serpentinizing systems. Further, cells may supply nucleation sites for ferric iron precipitation.
- 2) Microbial reduction and oxidation of iron should be possible in the subsurface. These processes may provide secondary iron minerals to the surface system as fluids emerge.

To investigate these hypotheses, this study observed the interaction of microbial life with mineral surfaces and potential subsequent alteration of minerals in the system, with the goal of identifying the presence of iron-reducing microorganisms in a subsurface serpentinizing system based on geochemical predictions.

1. Ubiquity of Microbial Communities Among Serpentinizing Systems

Several taxa have been suggested to be ubiquitous across subsurface serpentinizing systems (Anderson et al. 2013; Crespo-Medina et al. 2014; Morrill et al. 2014; Woycheese et al. 2015). DNA sequencing results from the Coast Range and Zambales ophiolite serpentinizing systems were compared with published data from other sites. This comparison served to help identify taxa occurring across global systems, which taxa might be shared between the surface and subsurface, and which taxa may be present owing to local variables such as climate.

2. Microbial Alteration of Local Mineralogy

To address the nature of microbe-mineral interactions, fluid, sediments, and rock from the sampling region were utilized in microcosm experiments mimicking subsurface and surface conditions of natural serpentinizing environments. These microcosms experiments consider the following:

- a) Do microbes prefer solid or fluid substrates for growth?
- b) Does microbial growth alter the local mineralogy?
- c) Do the microbes engage in iron redox reactions?
- d) How might the above differ in surface vs. subsurface?

Observations of microbe-mineral interactions were documented with a suite of analyses including imaging by fluorescence microscopy to document microbial growth and morphology, scanning electron microscopy to document microbial action on mineral surfaces, X-ray diffraction to record changes in iron-bearing mineralogy, and DNA sequencing to document variations in microbial community structures and to identify possible iron metabolizing organisms.

3. Iron Redox in Continental Serpentinizing Communities

In addition to exploring microbe-mineral interactions, closer investigation of the metabolism of iron was carried out with batch culturing. These experiments sought to determine if it is possible to enrich for iron metabolizing microbes from these environments, as suggested by the modeling of energy availability. Further, experiments may determine if microbes can transform the redox state of iron minerals in surface or subsurface environments. The predicted metabolism in the subsurface was investigated through batch culturing techniques using ferric hydroxide as a growth substrate, subsequent analysis of iron oxidation states by X-ray photoelectron spectroscopy, scanning electron microscopy to document microbe-mineral interactions, and DNA sequencing to document variations in microbial community structure and identify iron-metabolizing microorganisms.

II. METHODS

A. Sample Collection

Sediment samples from a drill core at well QV1,3 at the Coast Range Ophiolite Microbial Observatory (CROMO) in Lower Lake, California were collected by Dr. Matt Schrenk and shipped on ice to the University of Illinois at Chicago (UIC) in September 2012. Fluids collected from the well placed in the QV1,1 drill hole were collected by Dr. Dawn Cardace and shipped to UIC in December, 2013.

Samples from the Zambales ophiolite region in the Philippines were collected in September 2013. Fluids were sampled from serpentinizing spring PB1, sediments were sampled from spring ML2, and country rock was drilled from Butili at a depth of 8 meters. Samples were collected and stored using sterile instruments and containers to minimize microbial contamination. Samples were kept on ice in the field and shipped on ice to UIC for storage at 4°C until experiments and analysis.

B. Documenting Microbe-Mineral Interactions

1. Microcosm Setup

Time series Phase I microcosms were set up in serum bottles, including a) live sediments as the inoculum, b) pulverized rock and polished chips of rock, c) serpentinizing fluids, and d) two types of headspace (air and H₂ to simulate near surface and subsurface environments, respectively) (Figure 6a). These experiments were replicated with an additional set of microcosms. Phase I microcosms observed both sediment and rock core communities. Phase II microcosms were set up set up in serum bottles, including a) autoclave-sterilized sediments as the inoculum, b) pulverized rock and polished chips of rock, c) serpentinizing fluids, and d) two types of headspace (air and H₂ to simulate near

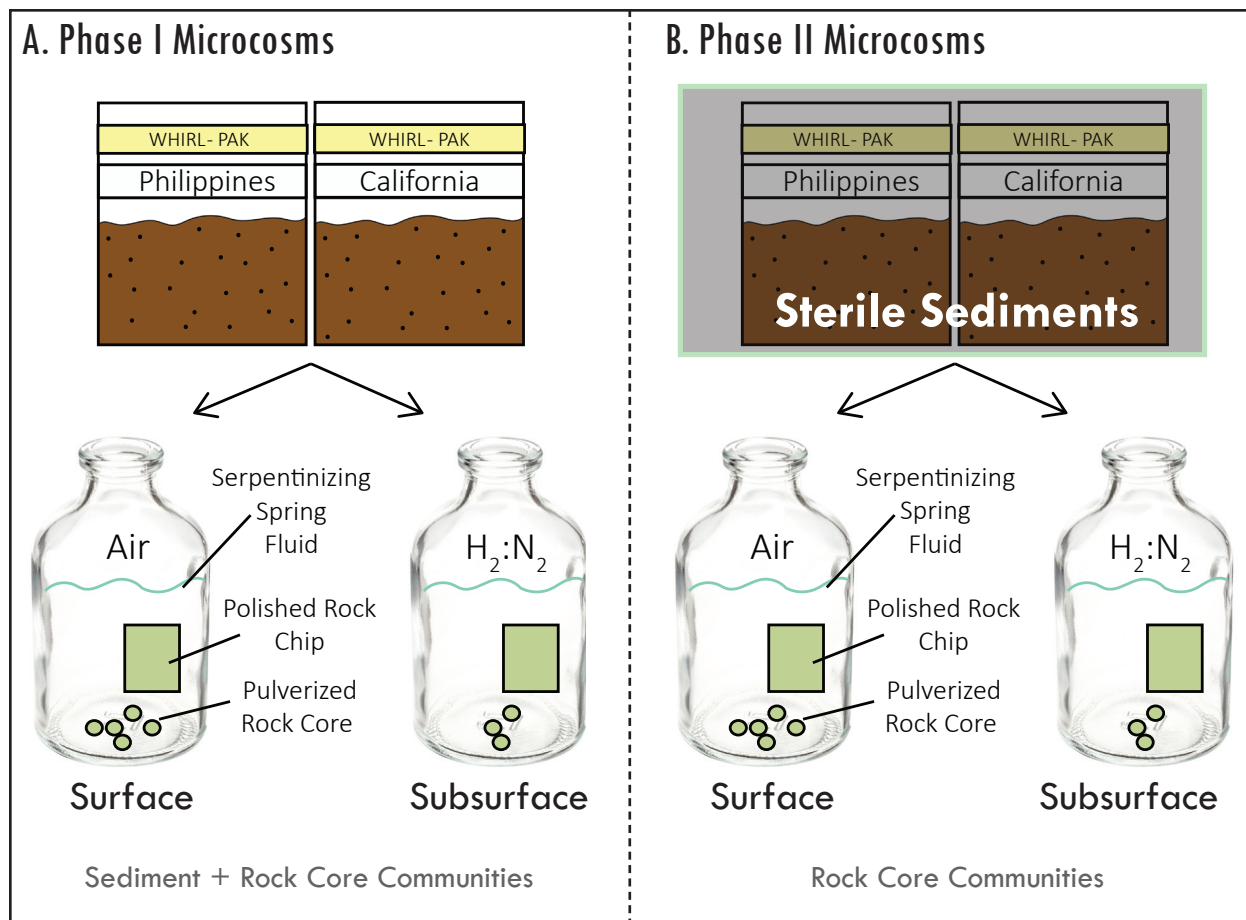


Figure 6. Microcosm experiment set up including rock chips and pulverized rock from Butili, fluids from QV11 and PB1, and sediments from QV1,3 and ML2. A) Phase I microcosms including live inoculum sediments. B) Phase II microcosms including autoclaved inoculum sediments.

surface and subsurface environments, respectively) (Figure 6b). Phase II microcosms observed only rock core communities. The rock core was cut into ~2mm-thick slices, sectioned into ~1x1cm chips, and polished on one side. Slices of core were rinsed with ethanol and sterilized in a 100°C oven for one hour. Oven sterilization was chosen over autoclaving to minimize geochemical changes to the rock in the presence of heat and water. Additional samples of core were pulverized with a percussion mortar and sieved into size fractions of 38-45 μ m, 45-75 μ m, and >75 μ m, and each of these fractions were weighed to determine how much went into each microcosm. The pulverized rock

was then recombined and homogenized before addition to microcosms. Each microcosm contained 1g of homogenized sediment, 5ml of pH 11 yeast-peptone growth media solution (5g/L yeast, 5g/L peptone), 5g of pulverized, oven-sterilized rock, and 25ml of 0.2 μ m filter-sterilized serpentinizing fluid. Initially the subsurface microcosms were prepared in a Coy chamber filled with 5% H₂:N₂. Microcosm headspace was flushed weekly with 0.2 μ m filtered air and 99.999% pure hydrogen to maintain surface and subsurface conditions, respectively. The pulverized rock provided large surface areas for microbe attachment, and the polished chip provided a surface for examining microbe-mineral associations. At intervals of three and six weeks, the microcosms were removed from incubators and stored at 4°C. Samples from microcosms were examined via fluorescence microscopy, SEM imaging, XRD analysis, and DNA sequencing.

2. Experiment Observations

Photos of the microcosms were taken daily for the duration of the project to document large-scale visible changes such as biofilm formation, relative turbidity, and color change of the sediments. The magnetism of the solid particles was tested with a neodymium magnet and the pH of the fluids was measured with a Fischer Scientific Accumet Basic AB15 pH meter after three and six weeks.

3. Fluorescence Microscopy

Samples were fixed in 4% paraformaldehyde/phosphate buffer solution overnight before imaging. Rock chips were rinsed with fluids from the microcosm and stained with DAPI (4',6'-diamidino-2-phenylindole, Sigma) and surface-viewed by fluorescence microscopy. Fluids were stained with a 1 μ l/mL solution of DAPI for ten minutes, vacuum-dried, and mounted on 0.2 μ m Whatman polycarbonate filters on glass slides in preparation for microscopy. Fluorescence microscopy was

performed using a Leica DM5500 B microscope (spectral cube absorbance peak 365 nm), and images were taken using ImagePro software.

4. Scanning Electron Microscopy (SEM) and X-ray Energy Dispersive Spectroscopy (XEDS)

Rock chips were prepared for SEM via gradual drying with increasing ratios of phosphate buffer:ethanol mixes and hexamethyldisilazane (HDMS) to prevent shrinking and crushing of cells (Nation, 1983). Chips were mounted on aluminum stubs with adhesive and sputter-coated with platinum/palladium vapor to a thickness of 7.5 nm. Imaging was performed at the University of Illinois at Chicago on a Hitachi 3000N variable pressure scanning electron microscope and a JEOL JSM-6320F field emission scanning electron microscope. Operating conditions of the electron beam were 3 kV at a working distance of approximately 10mm. Bulk mineralogy was analyzed with an Oxford Inca EDX system with a light element X-ray detector attached to the Hitachi SEM. Samples were scanned at an elevation of 35° and an accelerating voltage of 15Kv for a duration of 60 seconds.

5. X-ray Diffraction (XRD)

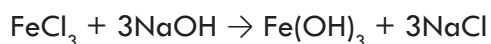
The initial and final mineralogical compositions of the crushed rock in the microcosms were identified via XRD. Samples were suspended in deionized water, ground with a mortar and pestle, then poured in a fluid slurry onto background-less quartz plates in an anaerobic Coy chamber filled with 5% H₂:N₂ gas to dry to prevent oxidation of the samples. The samples were analyzed at the University of Illinois at Chicago on a Siemens (Bruker) D5000 XRD with copper radiation (1.5418 Å) at a 2theta range of 2-60° with a 0.02 step size and dwell time of one second. Operating

conditions of the X-ray beam were 40 kV at 25 mA. Diffraction peaks were analyzed with three kinds of software: Match! software using the Precipitate Lography Open Database; MDI Jade software using the 2015 ICDD Powder Diffraction File; X Powder software using the 2015 ICDD Powder Diffraction File.

C. Verifying Fe-Metabolisms

1. Fe-Enrichment Cultures

To demonstrate iron cycling metabolisms in communities from the Coast Range and Zambales serpentinizing systems, sediments from each system were suspended in growth media enriched with yeast, peptone, and ferric hydroxide and incubated at 35°C (Figure 7). Fe(OH)₃ was precipitated by buffering a 60g/L FeCl solution with 1M NaOH to a pH of 8.5 by the following reaction:



Precipitates were stored at room temperature overnight in the dark, then autoclaved for 30 minutes the following day. The Fe(OH)₃ solution was then centrifuged at 2000rpm for 5 minutes, decanted, resuspended in 400ml pH 11 yeast-peptone growth media for a final pH of 9.8 and stored at 4°C. The yeast-peptone growth media was prepared by buffering a solution of 2.5g yeast and 2.5g peptone in 450 ml to pH 8.5, then adding 50ml 1M NaOH solution after autoclaving. Each culture contained 5ml Fe-enriched media solution, 10ml yeast-peptone media solution, and 1ml sonicated live sediment suspended in phosphate buffer solution. Culture headspace was composed of air and 5% H₂:N₂ to simulate surface and subsurface conditions, respectively. These experiments were replicated with an additional set of cultures. Replicates with no Fe(OH)₃ were also incubated to differentiate between iron metabolic activity and heterotrophy, and sterilized controls were incubated to differentiate between biotic and abiotic processes.

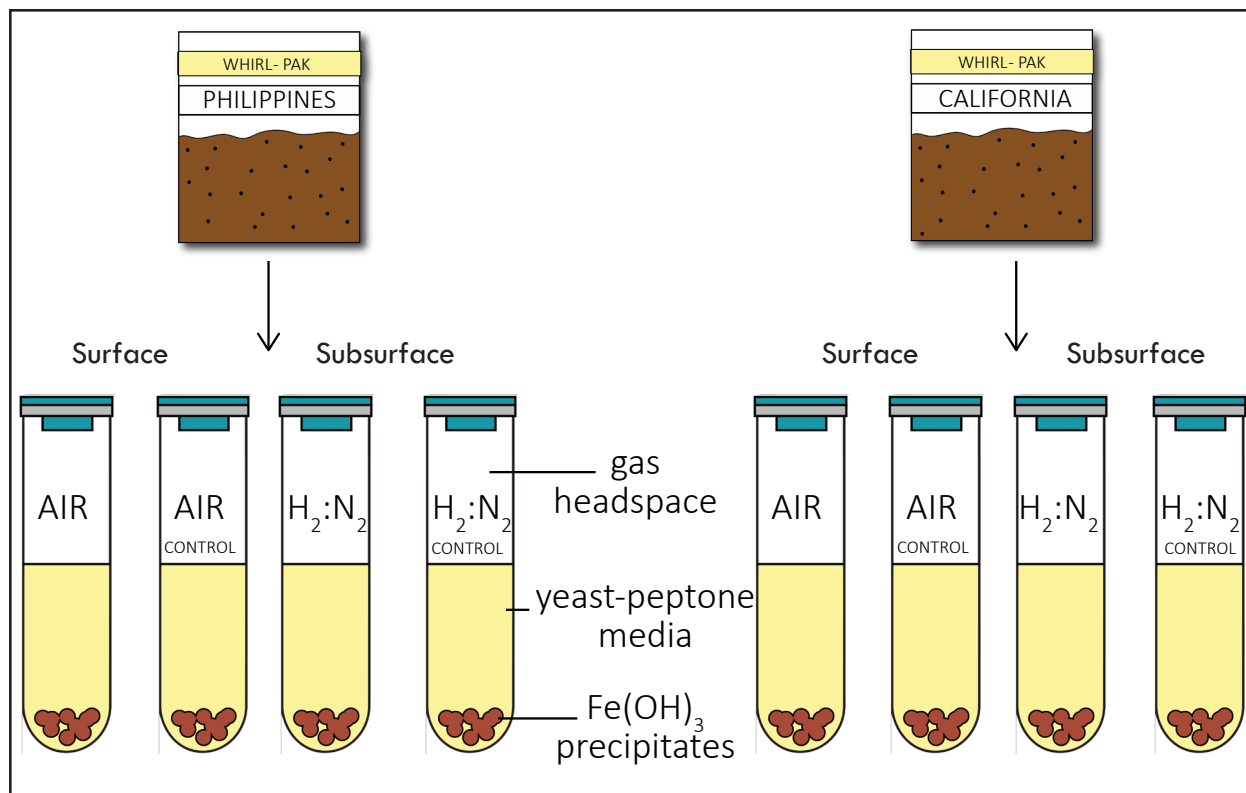


Figure 7. Iron enrichment culture set up including inoculum sediments collected from California (QV1,3) and the Philippines (ML2).

To determine possible anaerobic iron oxidation coupled to nitrate reduction, 1ml of 1M NaNO_3 was added to a transfer set of QV1,3 and ML2 aerobic and anaerobic cultures with the iron enrichment media containing yeast and peptone at a pH of 9.8 after three days of incubation.

2. Experiment Observations

Photos of the microcosms were taken daily for the duration of the project to document large-scale visible changes such as biofilm formation, relative turbidity, and color change in sediments. The magnetism of the solids was tested with a neodymium magnet and the pH of the fluids was measured with a Fischer Scientific Accumet Basic AB15 pH meter after three and six weeks.

3. Fluorescence Microscopy

Cultures were sampled for microscopy at intervals of 3 and 6 weeks to document relative cell densities and morphologies. Fluids were fixed with 8% paraformaldehyde and stained with a 1 μ L/mL DAPI solution for ten minutes, vacuum-dried, and mounted on 0.2 μ m Whatman polycarbonate filters on glass slides in preparation for microscopy. Fluorescence microscopy was performed using a Leica DM5500 B microscope (spectral cube abs peak 365 nm), and images were taken using ImagePro software.

4. Scanning Electron Microscopy (SEM) and X-ray Energy Dispersive Spectroscopy (XEDS)

All cultures were shaken in their tubes and extracted through the rubber stopper with a needle inside an anaerobic Coy chamber (filled with 5% H₂:N₂). Samples were fixed with 8% paraformaldehyde and left overnight to mitigate cell wall collapsing by making the cells more rigid. To minimize exposure to oxygen, samples were transferred to a freeze-dryer in an air-tight container filled with 5% H₂:N₂ before removal. Each sample was poured onto a glass slide in a petri dish and quickly put under vacuum. After freeze-drying, the samples were returned to a container with 5% H₂:N₂ to be transferred to the SEM/EDS for coating and imaging of the dried sample on the glass slide. Samples were mounted on aluminum stubs with adhesive and sputter-coated with platinum/palladium vapor to a thickness of 7.5 nm. Imaging was performed at the University of Illinois at Chicago on a Hitachi 3000N variable pressure scanning electron microscope and a JEOL JSM-6320F field emission scanning electron microscope. Operating conditions of the electron beam were 3 kV at a working distance of approximately 10mm. Bulk mineralogy was analyzed with an Oxford Inca EDX system with a light element X-ray detector attached to the Hitachi SEM. Samples

were scanned at an elevation of 35° and an accelerating voltage of 15Kv for a duration of 60 seconds.

5. X-ray Diffraction (XRD)

Samples were shaken to suspend iron particles, extracted through the rubber stopper with a syringe and deposited onto background-less quartz plates in an anaerobic Coy chamber filled with 5% $\text{H}_2:\text{N}_2$ gas to dry. The samples were analyzed at the University of Illinois at Chicago on a Siemens (Bruker) D5000 XRD with copper radiation (1.5418 Å) at a 2theta range of $2-60^\circ$ with a 0.02 step size and dwell time of one second. Operating conditions of the X-ray beam were 40 kV at 25 mA. Pattern peaks were analyzed with three kinds of software: Match! software, Precipitate Lography Open Database; Jade software, Powder Diffraction File 2015; X Powder software, ICDD Powder Diffraction File 2015.

6. X-ray Photoelectron Spectroscopy (XPS)

To demonstrate the change in oxidation state in the Fe-enrichment cultures, the solids from the cultures were analyzed via XPS. Samples were vacuum filtered onto a $0.2\mu\text{m}$ polycarbonate filter and dried in a Coy chamber filled with 5% $\text{H}_2:\text{N}_2$. Precipitate surfaces were analyzed with a Kratos AXIS-165 XPS at the UIC RRC facility. An incident monochromated X-ray beam from an aluminum (12 Kv, 10 mA) was focused on a $0.7\text{mm} \times 0.3\text{mm}$ area of the sample surface at 45° to the surface at a step size of 0.1 eV.

D. DNA Sequencing/Analyses

DNA was extracted from microcosm experiments (pulverized rock/sediment and from

the fluids) and culture experiments after three weeks using the MO BIO FastDNA for Soils Spin Kit following the kit-suggested protocol. DNA was amplified via PCR using 515F/806R primers, and extracted DNA was analyzed at UIC DNA Services for 16S rRNA sequencing for microbial identification. Paired-end FASTQ files were merged with PEAR (paired-end read merger) (<http://www.exelixis-lab.org/pear>), then imported to CLCBio (<http://www.clcbio.com>) for quality and length trimming. A Q20 quality trim was performed with QTrim (<http://omictools.com/qtrim-s1549.html>) and anything <250bp was discarded and the 515F/806R primer sequences were removed. The data was analyzed via QIIME (<http://qiime.org>) to remove Chimeras, cluster and taxonomically classify the sequences, and perform alpha and beta diversity statistical analyses. Taxon included in reports of relative abundances are those with a threshold value of 2,000 sequence reads or greater in at least one sample.

16S rRNA sequences were aligned to Greengenes (<http://greengenes.lbl.gov/cgi-bin/nph-index.cgi>) with PYNAST (Python Nearest Alignment Space Termination tool) and clustered into OTU's at 97% similarity with UCLUST (centroid-based algorithm). Alpha diversity was performed on family and species-level rarefactions sampled to a depth of 5,000-25,000 sequence reads at intervals of 5,000 and ten iterations per step. The iterations were averaged for each step and rarefaction plots were generated with Microsoft Excel. A jackknifed beta diversity analysis was performed on rarefied species-level OTU tables to an even depth of 25,000 sequence reads. Maximum-likelihood phylogenetic trees were constructed with FastTree using weighted and unweighted unfrac metrics on the representative set of sequences. Both trees are UPGMA (UPGMA (Unweighted Pair Group Method with Arithmetic Mean) consensus trees.

E. Expected Results of Analyses

1. Documenting Microbe-Mineral Interactions

In microcosms simulating surface conditions, biofilm formation was expected to occur uniformly, with no preference for substrate based on mineral composition during heterotrophic growth. Abiotic oxidation of ferrous iron within the pulverized rock, rock chips, and sediments was expected to occur, with cells acting as nucleation sites for ferric iron precipitation. No ferric iron reduction was anticipated. Uniform distribution of precipitates would have indicated no preference for microbial nucleation sites, whereas preferential precipitation on/around microorganisms would have indicated nucleation sites encouraged precipitation. DNA sequencing was expected to confirm the presence of organotrophs.

In microcosms simulating subsurface conditions, microbial reduction of ferric iron was expected to occur as predicted, and physical signs of microbial action on mineral surfaces (pitting and attachment of microbes to the minerals) would be present. Iron precipitates were expected to form around cells with microbes preferentially forming biofilms on mineral surfaces containing iron. DNA sequencing was expected to indicate the presence of iron-metabolizing microorganisms.

2. Verifying Fe Metabolisms

Iron redox states were observed both visually and analytically. Initially, the $\text{Fe}(\text{OH})_3$ in the aerobic cultures was orange-red, and was expected to turn black under anaerobic conditions where microbial iron reduction could occur. With increased growth and consumption of oxygen in the aerobic culture, a metabolic shift to anaerobic iron reduction was expected to occur. The anaerobic cultures were expected to show the same change from red to black iron precipitates over a shorter period of time, with ferric iron reduction occurring. XPS results were expected to show differences

in iron redox states between anaerobic and aerobic iron cultures. DNA sequencing results were expected to indicate metabolisms consistent with these predictions.

III. RESULTS

A. Documenting Microbe-Mineral Interactions

The results from microcosm experiments observing microbe-mineral interactions in the California and Philippines serpentinizing systems are reported here for each analysis performed on the samples. These analyses include experiment observations, fluorescence microscopy, scanning-electron microscopy (SEM), X-ray diffraction (XRD), and DNA sequencing. A flowchart of analyses performed with corresponding section numbers and headings is shown in Figure 8.

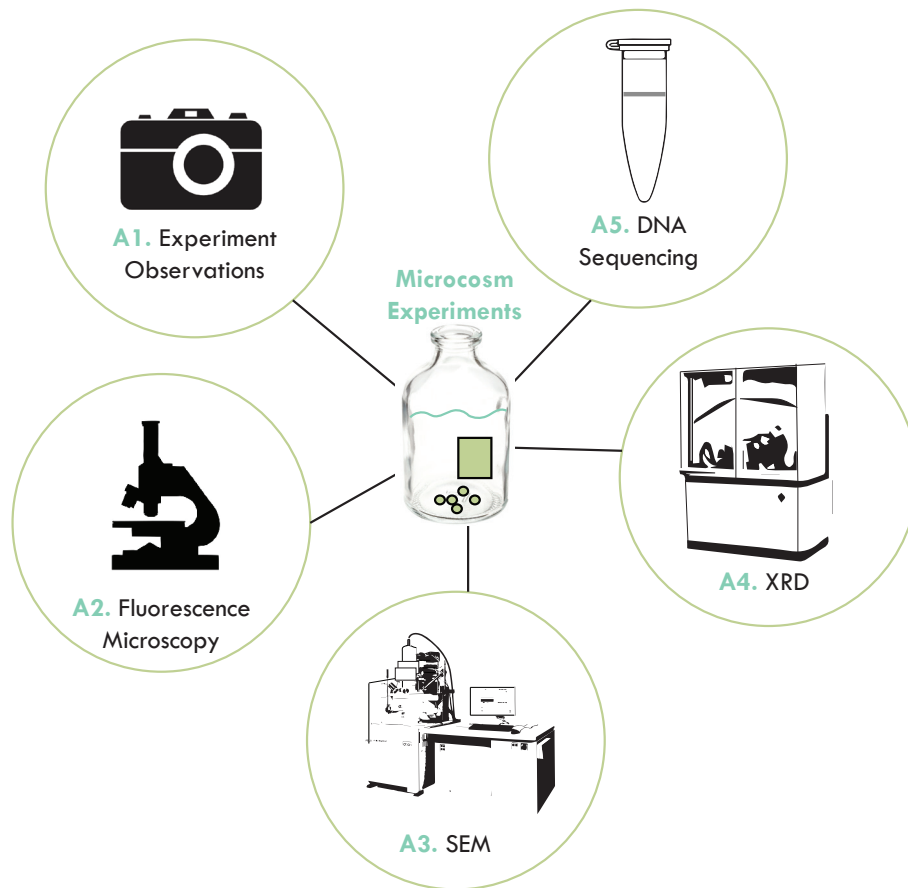


Figure 8. Documenting Microbe-Mineral Interactions: Flowchart of analyses of microcosm experiments with their corresponding section numbers in the results section.

1. Experiment Observations

Visual observations of the microcosm experiment included daily photos to document relative turbidity, biofilm formation, and color changes in sediments, and pH measurements were recorded after three and six weeks. Phase I microcosms included live sediment inoculum and surface-sterilized rock core, and Phase II microcosms included autoclaved sediments and surface-sterilized rock core, effectively isolating the community within the rock pore spaces. Images of California (QV1,3) and Philippines (ML2) surface (aerobic) and subsurface (anaerobic) simulations are shown in Figure 9, and the results for the visual observations are reported here.

i. QV1,3

Phase I aerobic microcosms became turbid after 1-2 days. The final pH of the microcosms after 3 and 6 weeks was 8.36 and 7.84, respectively. Phase I anaerobic microcosms became turbid after 4-14 days and the final pH after 3 and 6 weeks was 8.23 and 8.72, respectively, decreasing from an initial pH of 9.8. Phase II aerobic and anaerobic microcosms became turbid after 1-2 days. The final pH of the aerobic microcosms after 3 and 6 weeks was 8.39 and 7.9, respectively. The final pH of the anaerobic microcosms after 3 and 6 weeks was 8.56 and 8.3, respectively. None of the microcosms formed biofilms that were visible to the unaided eye for the duration of the experiments, and sediments in the microcosms did not change color.

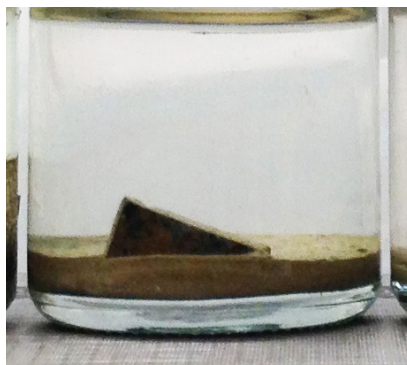
ii. ML2

Phase I aerobic and anaerobic microcosms became turbid after 1 day. The final pH of the aerobic microcosms after 3 and 6 weeks was 8.55 and 7.86, respectively. The final pH of the anaerobic microcosms after 3 and 6 weeks was 8.53 and 8.59, respectively, decreasing from an initial pH of 9.8. Both aerobic and anaerobic microcosms formed biofilms visible to the unaided eye. Sediments in live aerobic and anaerobic microcosms were initially brown, but became grey. The

California Microcosms (QV1,3)

Surface
(Aerobic)

Day 7



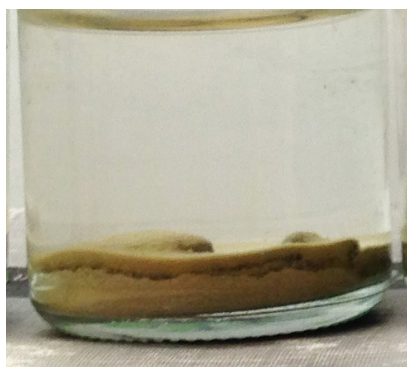
Subsurface
(Anaerobic)

Day 7



Surface
(Aerobic)

Day 42



Subsurface
(Anaerobic)

Day 42



Philippines Microcosms (ML2)

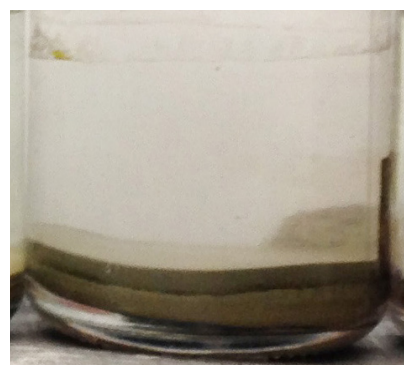
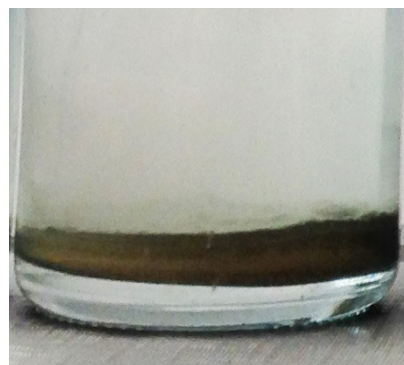


Figure 9. Images of Phase I California (left) and Philippines (right) microcosm sediments after 7 (top) and 42 (bottom) days of growth.

sediments returned to their original color after flushing the headspace with air in aerobic microcosms, and repeatedly became grey again until flushing. The anaerobic microcosm sediments remained grey after flushing the headspace with hydrogen. Phase II aerobic and anaerobic microcosms became turbid after 1 day. The final pH of the aerobic microcosms after 3 and 6 weeks was 8.44 and 7.94, respectively. The final pH of the anaerobic microcosms after 3 and 6 weeks was 8.76 and 8.26, respectively. Phase II microcosm sediments did not change colors.

2. Fluorescence Microscopy

Fluorescence microscopy was employed to document relative cell abundances and morphologies in fluids from California (QV1,3) and Philippines (ML2) surface (aerobic) and subsurface (anaerobic) microcosm experiments. Fluorescence microscopy images are shown in Figure 10.

i. QV1,3

After sixteen days, the Phase I aerobic microcosm exhibited round-shaped cells $\sim 1\mu\text{m}$ in diameter, and rod-shaped cells after six weeks measuring $\sim 1\mu\text{m} \times 5\mu\text{m}$. The Phase I anaerobic microcosm exhibited round (ranging from $1\text{-}3\mu\text{m}$) and rod-shaped cells measuring $1\text{-}3\mu\text{m} \times 5\mu\text{m}$ after sixteen days, and $1\text{-}3\mu\text{m} \times 10\mu\text{m}$ rod-shaped cells after six weeks. After six weeks, the Phase III aerobic microcosm exhibited rod-shaped cells measuring $2\mu\text{m} \times 20\mu\text{m}$. No cells were observed after six weeks in the Phase II anaerobic microcosm.

ii. ML2

After sixteen days, the Phase I aerobic microcosm exhibited round ($1\text{-}10\mu\text{m}$) and rod-shaped cells measuring $1\text{-}5\mu\text{m} \times 10\mu\text{m}$, and $10\mu\text{m}$ round-shaped cells after six weeks. After sixteen days, the Phase I anaerobic microcosms exhibited round (ranging from $1\text{-}3\mu\text{m}$) and rod-shaped

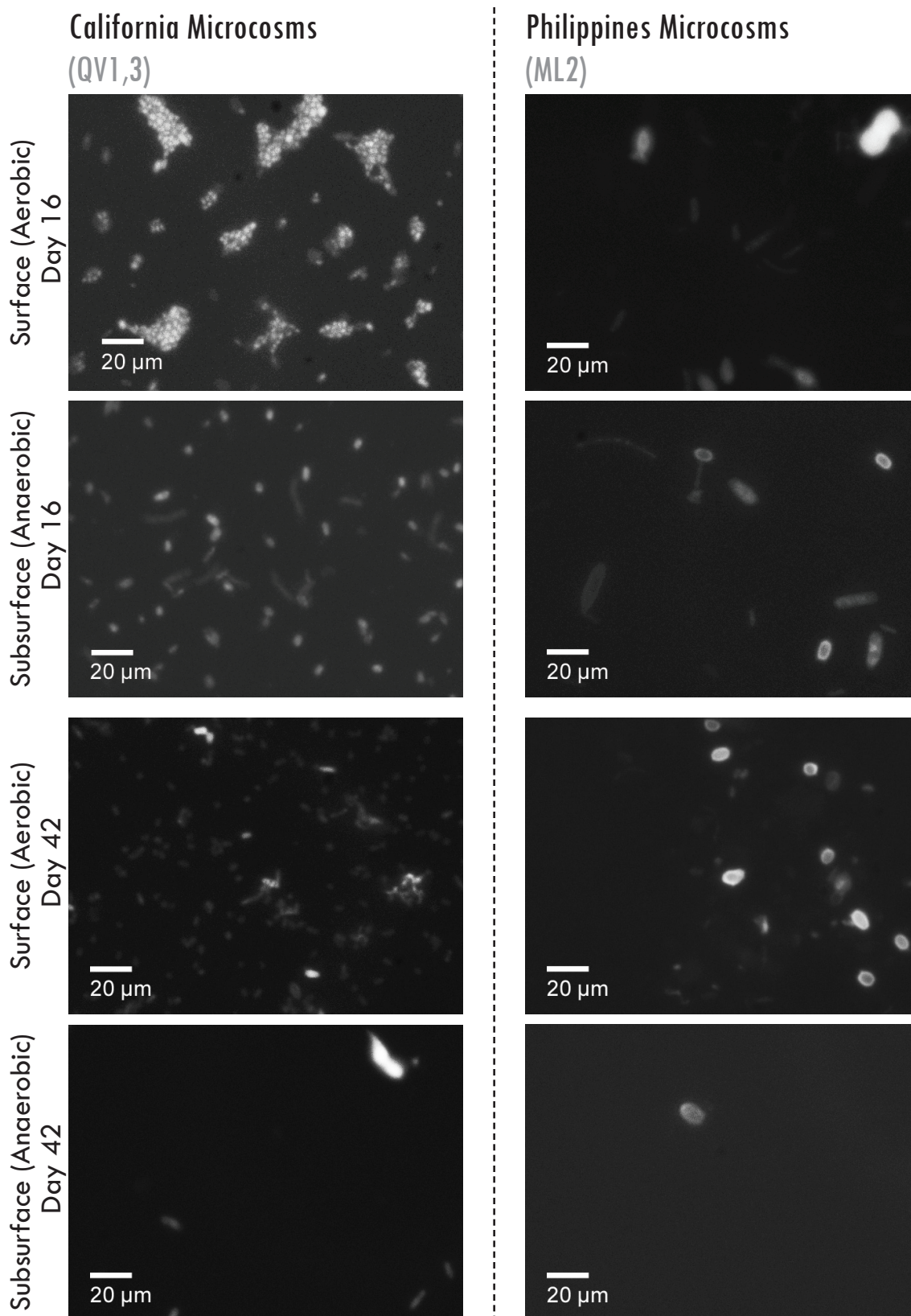


Figure 10. Fluorescence microscopy images of cells in Phase I California (QV1,3) and Philippines (ML2) microcosms after 16 and 42 days of growth.

cells, measuring 1-3 μm x 10 μm . After six weeks, cells in the Phase I anaerobic microcosm were 10 μm cocci. The cocci appear hollow in the center, possibly indicating a toga formation or cell encapsulation. After six weeks, the Phase II aerobic microcosm exhibited rod-shaped cells measuring 1 μm x 5 μm . No cells were observed after six weeks in the Phase II anaerobic microcosm.

iii. Relative Cell Observations

Overall, cell densities were relatively higher in QV1,3 microcosms than in ML2 microcosms, and all aerobic microcosm cell densities were higher than anaerobic microcosm cell densities. Cells in QV1,3 microcosms were much smaller in diameter than in ML2 microcosms. Cells in all microcosms did not stain as well after six weeks as they did after three weeks, and some cells appeared hollow after six weeks. Positive growth was documented in Phase II microcosms in relatively lower abundances than their Phase I counterparts.

iv. Rock Chips

Attempts were made to observe distributions of biofilms across rock chip surfaces by staining chips with fluorescent dye. However, differences between images of a stained unreacted chip and a stained reacted chip could not be distinguished. The fluorescence of the unreacted chip may be due to fluorescent minerals present in the rock chips. Fluorescence microscopy images of the unreacted and reacted chips are shown in Appendix A, Figures 1 and 2.

3. Scanning Electron Microscopy and X-ray Energy Dispersive Spectroscopy (SEM & XEDS)

Scanning electron microscopy and XEDS were employed to document microbial action on mineral surfaces and identify the chemistry of rock chips and secondary precipitates in California (QV1,3) and Philippines (ML2) surface (aerobic) and subsurface (anaerobic) microcosm experiments.

All Phase I microcosm rock chip SEM images are shown in Figure 11, and Phase II microcosm rock chip images are shown in Appendix A, Figure 3. Initially, the unreacted rock chip surface had large empty pits and angular platy material along the surface. One elongated needle-like precipitate was observed, measuring $0.1\mu\text{m}$ thick x $1\mu\text{m}$ long. The bulk element composition (reported as averaged values of multiple scans) of the unreacted rock chip detected by XEDS was 46.04% O, 28.57% Si, 26.93% Mg, and 5.34% Fe. Chemistries of secondary precipitates could not be determined via XEDS.

i. QV1,3

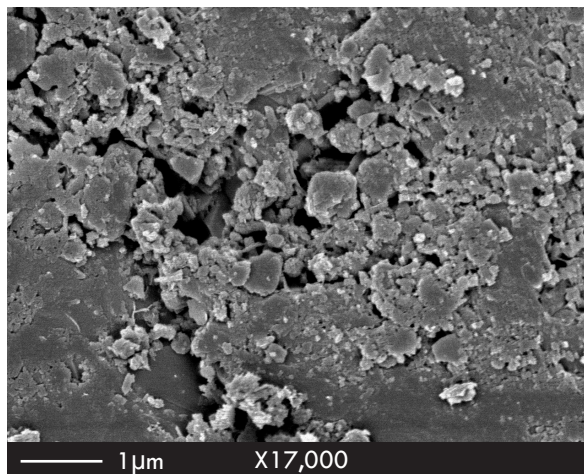
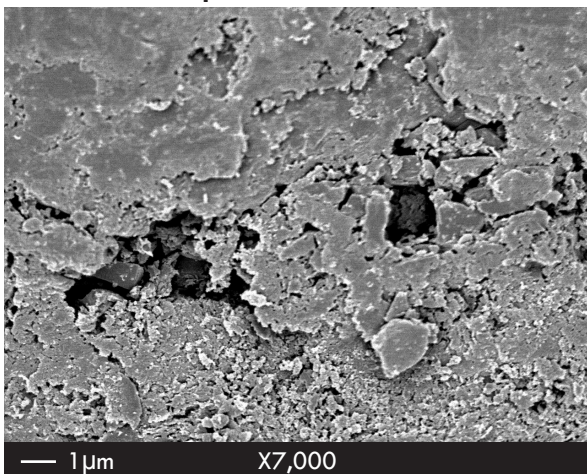
Secondary mineral formation was observed in crevasses on the rock chip from the Phase I aerobic microcosm. These randomly stacked precipitates were thin, straight, and $0.1\mu\text{m}$ thick x $0.5\text{-}2\mu\text{m}$ long. A randomly occurring structure was observed that appeared filamentous (Figure 11A). Platy material with soft edges coated with film was observed beneath the long precipitates. The aerobic Phase II chip surface had platy material with hard edges and straight, $0.1\mu\text{m}$ thick x $1\text{-}2\mu\text{m}$ long needle-like precipitates precipitated within pits and crevasses.

The rock chip from the Phase I anaerobic microcosm had dense stacks of short, randomly oriented precipitates completely filling pits on the chip surface (Figure 11C). The precipitates measured $0.1\text{-}0.2\mu\text{m}$ thick x $0.5\text{-}3\mu\text{m}$ long. These precipitates were not observed elsewhere on the chip surface. The anaerobic Phase II chip surface had angular platy material and long, thin, draping wire-like precipitates measuring $0.1\mu\text{m}$ thick x $2\text{-}10\mu\text{m}$ long occurring in pits but not filling them.

ii. ML2

Secondary mineral precipitation was observed on the rock chip from the aerobic Phase I microcosm. Singular twinned, curved and straight straw-like precipitates resembling straws measuring

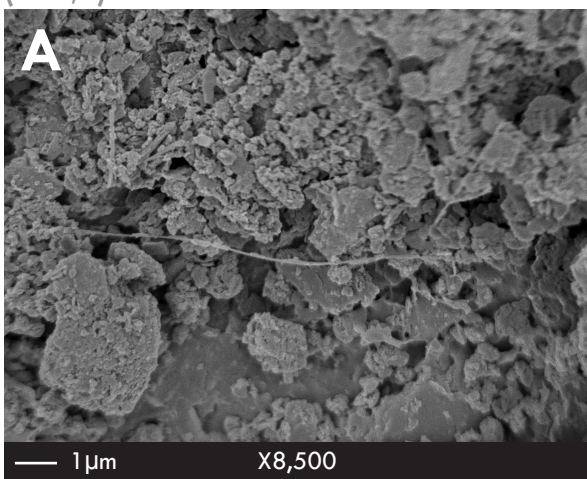
Unreacted Chip



California Microcosms

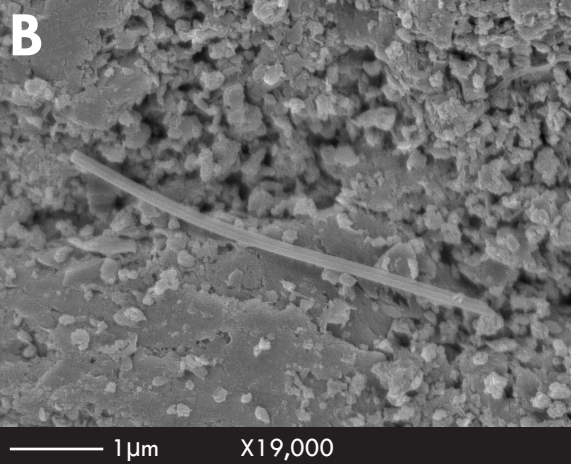
(QV1,3)

Surface (Aerobic) | Day 21



Philippines Microcosms

(ML2)



Subsurface (Anaerobic) | Day 21

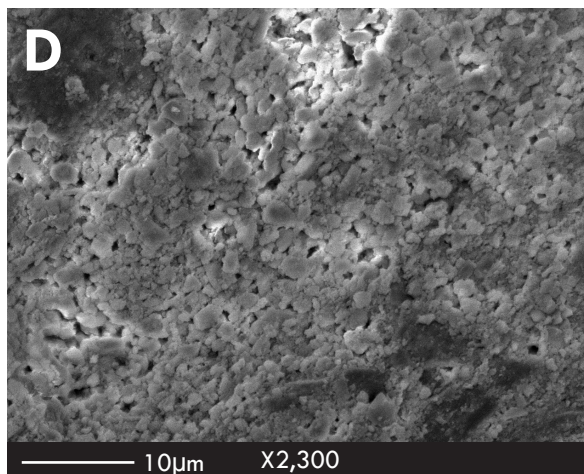
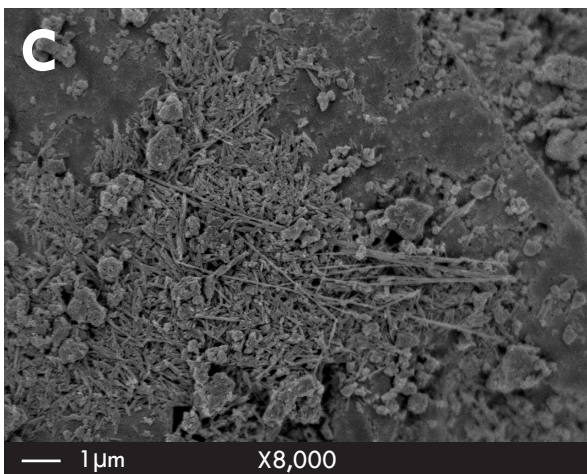


Figure 11. SEM images of an unreacted rock chip (top) and rock chips in Phase I microcosms after 21 days of growth (bottom) showing A) wire-like, B) straw-like, C) needle, and D) platy precipitates.

0.1 μm thick x 2-3 μm long occurred in random orientations across the chip surface. Pits on the chip were lined with platy material with soft edges coated with film (Figure 11B). The aerobic Phase II chip had a flat, angular surfaces and one observed needle-like precipitate measuring 1 μm wide x 10 μm long.

The anaerobic Phase I rock chip had platy material both lining the pits as well as occurring on the chip surface. Plates were \sim 2 μm wide and coated with film (Figure 11D). The anaerobic Phase II chip had smaller, less extensive platy material than the chip in the anaerobic Phase I microcosm. One elongate precipitate was observed, measuring 0.1 μm thick x 1 μm long.

4. X-ray Diffraction (XRD)

X-ray diffraction was employed to document mineralogical compositions of materials from California (QV1,3) and Philippines (ML2) surface (aerobic) and subsurface (anaerobic) microcosm experiments. XRD patterns of all Phase I microcosm experiments overlain with the standard pattern for lizardite are shown in Figure 12. Inoculum sediments and rock core XRD patterns overlain with standard patterns for lizardite, actinolite, forsterite, diopside, orthopyroxene, enstatite, magnetite, hematite, and ferrihydrite are shown in Appendix A, Figures 4-13. Phase I and Phase II microcosm patterns overlain with standard patterns for forsterite, ferrihydrite, enstatite, magnetite, wuestite, maghemite, diopside, hematite, actinolite, and orthopyroxene are shown in Appendix A, Figures 14-23 and Figures 24-34, respectively. Peak positions are reported here as 2θ . Inoculum sediments, rock core, and Phase I microcosm sediment mineralogies are summarized in Table 2. Strong diffraction peaks were observed in the rock core at 12.1, 19.3, 22.9, 24.35, 28.1, 31.1, 32.3, 35.5, 36.5, 40, 42, 52.3, and 56.1 ($^{\circ}$). These peak positions agree with standard pattern for diopside, lizardite, forsterite, enstatite, hematite, magnetite, orthopyroxene, and ferrihydrite. Strong

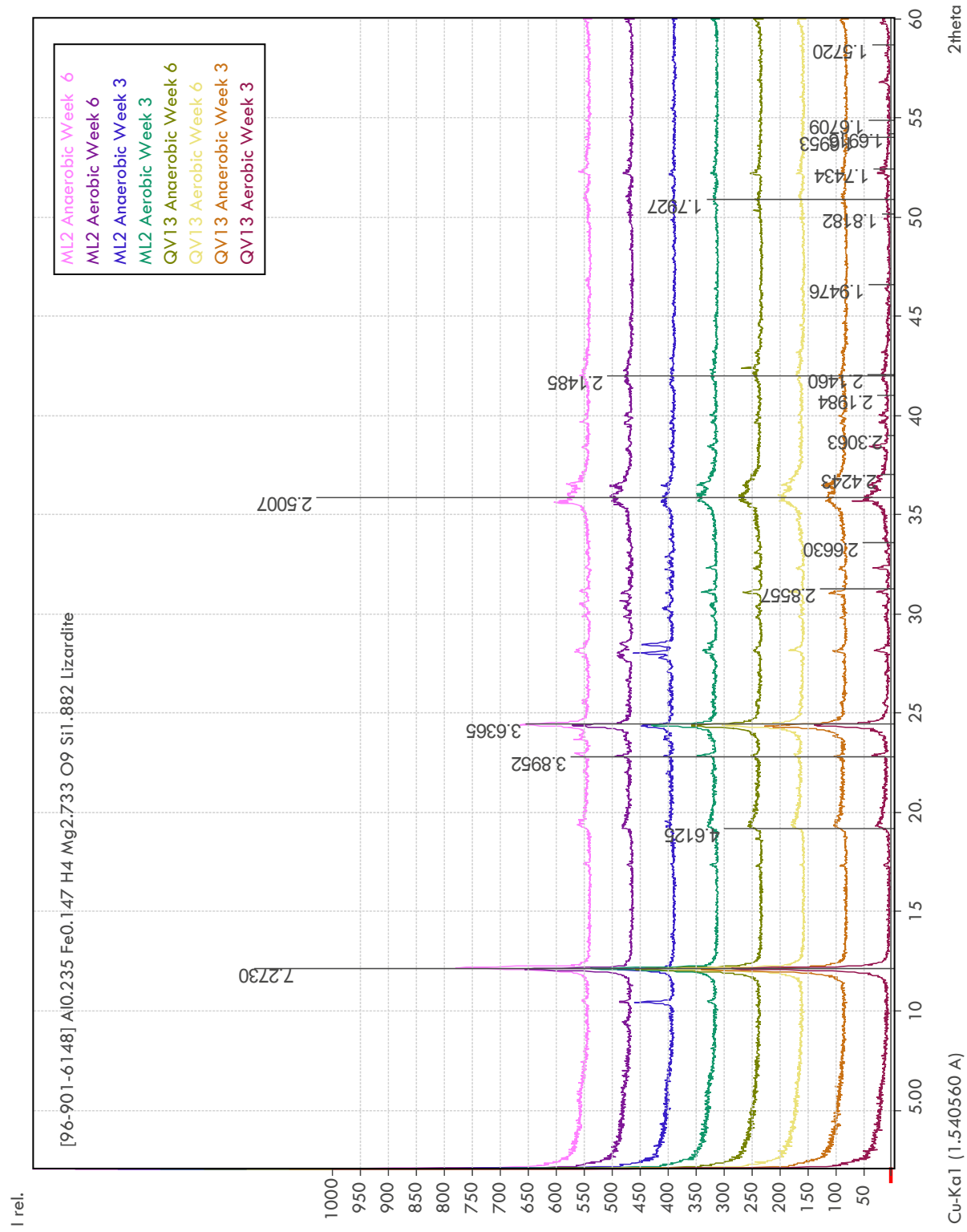


Figure 12. Phase I microcosm XRD patterns overlain with the standard pattern for lizardite (shown with d-values).

Table 2. Phase I Microcosm Mineralogy (XRD)

Microcosm	Lizardite	Forst	Diops	Orthopx	Enst	Maghemite	Magnetite	Hematite	Ferrihydrite	Actinolite
QV1,3 Aerobic (wk 3)	X	X	***	***	***	***	X			
QV1,3 Aerobic (wk 6)	X	X	***	***	***	***	X			
QV1,3 Anaerobic (wk 3)	X	X	***	***	***	***	X			
QV1,3 Anaerobic (wk 6)	X	X	***	***	***	***	X			
ML2 Aerobic (wk 3)	X	X	***	***	***	***	X			**
ML2 Aerobic (wk 6)	X	X	***	***	***	***	X			**
ML2 Anaerobic (wk 3)	X	X	***	***	***	***	X			**
ML2 Anaerobic (wk 6)	X	X	***	***	***	***	X			**
QV1,3 Inodulum Sed (T0)	X	X	***	***	***					
ML2 Inoculum Sed (T0)	X	X	***	***	***					*
Rock Core (T0)	X	X	***	***	***		**	**	***	

Magnetite was detected via XRD and with a neodymium magnet.

X = confident match

* = 1 Peak match

** = 1-3 peak matches

*** = more than 3 peak matches

peaks were observed in the QV1,3 inoculum sediments at 12.1, 19.8, 24.4, 30.1, 35.5, 36.6, and 43.2(°). These peak positions agree with standard pattern for orthopyroxene, enstatite, forsterite, lizardite. Peak intensities were relatively low for the ML2 inoculum sediment, and the strongest peaks were observed at 10.65, 22.25, 24, 24.6, 28.3, 28.6, 30.6, 31.8, and 37(°). These peak positions agree with standard pattern for lizardite, forsterite, orthopyroxene, enstatite, diopside, and actinolite.

i. QV1,3

In the Phase I QV1,3 microcosm sediment pattern, the strongest peaks were observed at 12.1, 17.35, 19.3, 22.9, 24.5, 28.1, 31.1, 32.3, 36, 39.5, 40, 51, and 52.2(°). Two peaks are present only in the aerobic week 3 microcosm at 38.4 and 56.8(°), and two peaks are present only in the anaerobic week 6 microcosm at 18.7 and 42.5(°). All Phase I microcosm patterns agree with standard patterns for lizardite, forsterite, enstatite, diopside, orthopyroxene, magnetite, and maghemite.

ii. ML2

In Phase I ML2 microcosm sediment pattern, the strongest peaks were observed at 10.5, 12.1, 17.5, 19.4, 22, 23, 24.4, 28.1, 28.5, 29.9, 30.5, 31.2, 32.1, 35.7, 36.6, 38.5, 42, and 52.3(°). All microcosm patterns agree with standard patterns for lizardite, enstatite, forsterite, diopside, actinolite, maghemite, magnetite, and orthopyroxene.

5. DNA Sequencing

Taxonomic relative abundances of inoculum sediment, Phase I, and Phase II microcosm communities are reported here in order from most abundant to least abundant. Dominant taxa were not identifiable to a species level for all experiments, therefore taxa are reported here at the genus level (Figure 13). Relative abundances of taxa in Phase II microcosms are shown in Appendix A, Figure 35. The dominant genera in the QV1,3 inoculum sediments were Zoogloea, Dechloromonas, Hydrogenophaga, and Pseudomonas; 60% of the genera were not identifiable using the available databases. The dominant genera in the ML2 inoculum sediments were Hydrogenophaga, Hylemonella, Pseudomonas, Sphingopyxis, Zoogloea, and Phyllobacterium; 45% of the genera were unidentified.

i. QV1,3 Microcosm Fluids

The dominant genera in the Phase I aerobic microcosm were Phyllobacterium, Hydrogenophaga, Desulfotomaculum, and Zoogloea; 11% of the genera were unidentified. The dominant genus in the aerobic Phase II microcosm was Sphingopyxis; less than 1% of the genera were unidentified.

The dominant genera in the Phase I anaerobic microcosm were Phyllobacterium, Hydrogenophaga, Zoogloea, and Dechloromonas; 15% of the genera were unidentified. The dominant genera in the anaerobic Phase II microcosm were Zoogloea, Dechloromonas, and

Taxonomic Identification of Phase I Microcosms | Genus Level

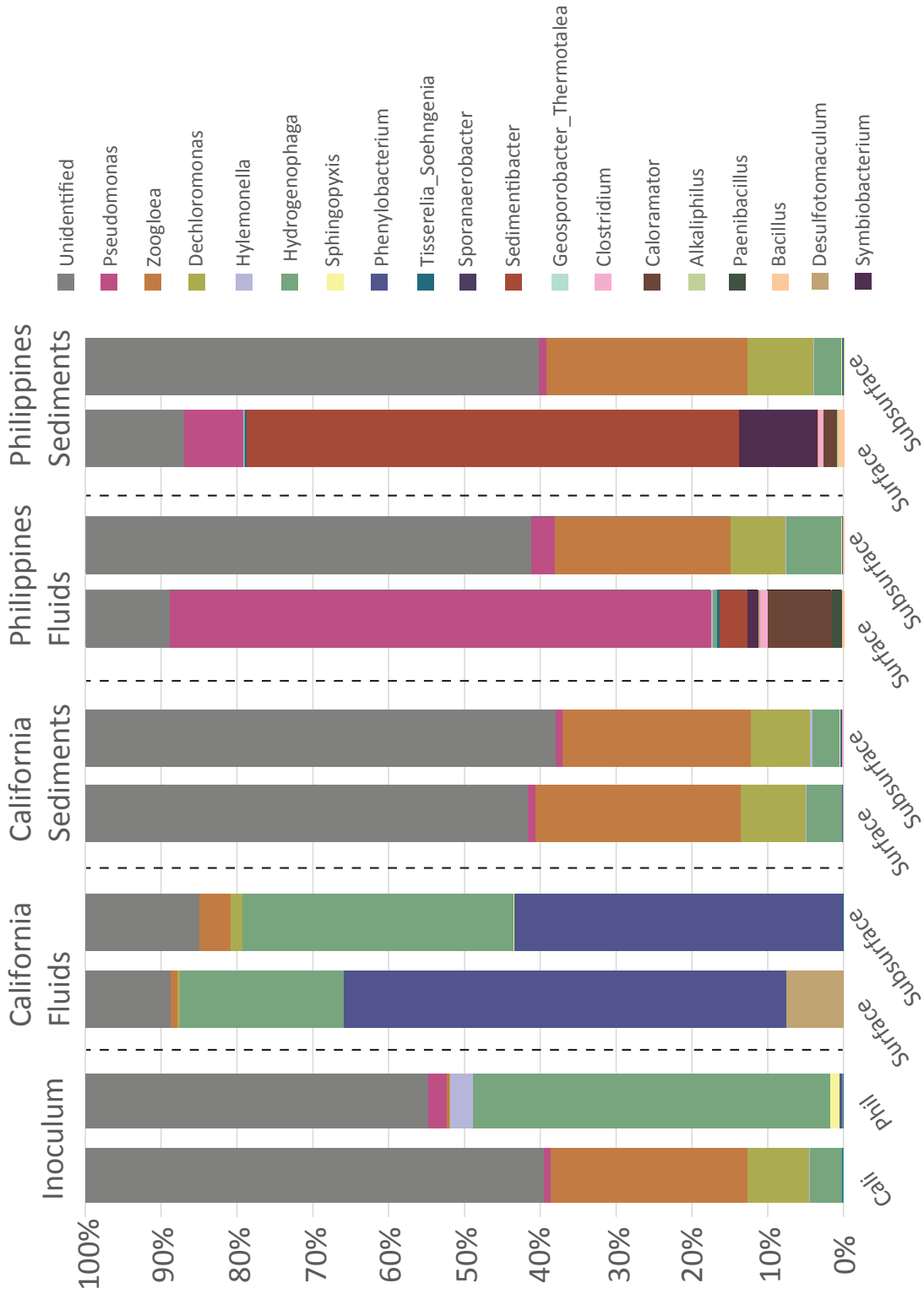


Figure 13. Relative abundances of genera in Phase I California (QV1_3) and Philippines (ML2) microcosm fluids and sediments after three weeks of growth.

Hydrogenophaga; 63% of the genera were unidentified.

ii. QV1,3 Microcosm Sediments

The dominant genera in the Phase I aerobic microcosm were Zoogloea, Dechloromonas, Hydrogenophaga, and Pseudomonas; 58% of the genera were unidentified. The dominant genera in the Phase II aerobic microcosm were Zoogloea, Dechloromonas, Hydrogenophaga, Sphingopyxis, and Pseudomonas; 59% of the genera were unidentified.

The dominant genera in both the Phase I and Phase II anaerobic microcosms were Zoogloea, Dechloromonas, Hydrogenophaga, and Pseudomonas; 62% and 63% of the genera were unidentified, respectively.

iii. ML2 Microcosm Fluids

The dominant genera in the Phase I aerobic microcosm were Pseudomonas, Caloramator, Sedimentibacter, Symbiobacterium, Paenibacillus, and Clostridium; 11% of the genera were unidentified. The dominant genera in the Phase II aerobic microcosm were Hylemonella, Zoogloea, Dechloromonas, and Hydrogenophaga; 29% were unidentified.

The dominant genera in the Phase I anaerobic microcosm were Zoogloea, Dechloromonas, Hydrogenophaga, and Pseudomonas; 59% of the genera were unidentified. The Phase II anaerobic microcosm maximum number of sequence reads was 7, which corresponded to unidentified taxa, therefore the genera are not reported here.

iv. ML2 Microcosm Sediments

The dominant genera in the Phase I aerobic microcosm were Sedimentibacter, Symbiobacterium, Pseudomonas, Caloramator, Clostridium, and Bacillus; 13% of the genera were unidentified. The dominant genera in the aerobic Phase II microcosm were Zoogloea, Dechloromonas, and Hydrogenophaga; 60% of the genera were unidentified.

The dominant genera in the Phase I and Phase II anaerobic microcosms were Zoogloea, Dechloromonas, Hydrogenophaga, and Pseudomonas; 60% and 64% of the genera were unidentified, respectively.

B. Verifying Fe-Metabolisms

The results from culturing experiments observing microbial iron metabolisms in the California and Philippines serpentinizing systems are reported here for each analysis performed on the samples. These analyses include experiment observations, fluorescence microscopy, scanning-electron microscopy (SEM), X-ray photoelectron spectroscopy (XPS), X-ray diffraction (XRD), and DNA sequencing. A flowchart of analyses performed with corresponding section numbers and headings is shown in Figure 14.

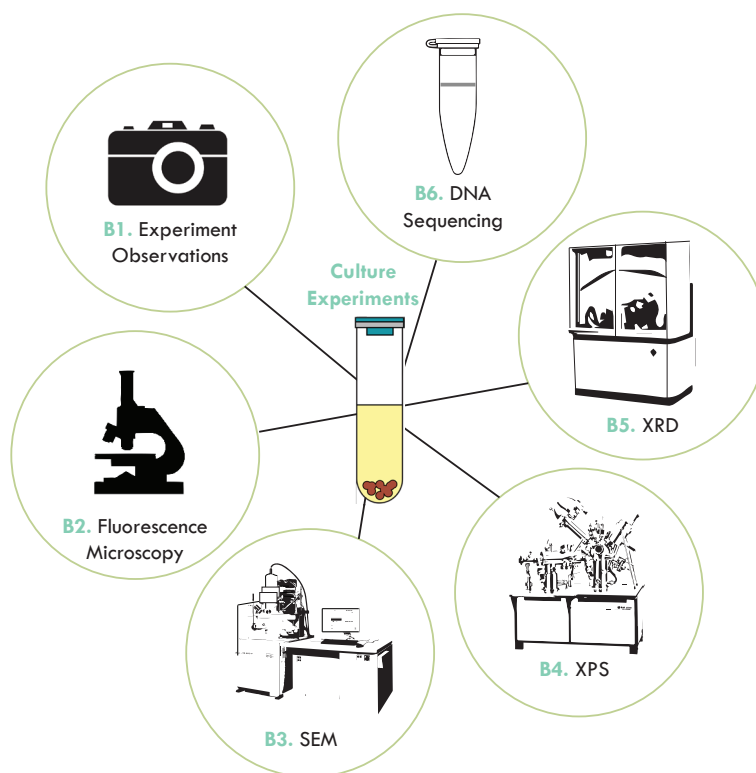


Figure 14. Verifying Fe-Metabolisms: Flowchart of analyses of culture experiments with their corresponding section numbers in the results section.

1. Experiment Observations

Visual observations of the microcosm experiment included daily photos to document relative turbidity, biofilm formation, and color changes in culture precipitates, and pH measurements were recorded after three and six weeks. Images of California (QV1,3) and Philippines (ML2) surface (aerobic) and subsurface (anaerobic) cultures are shown in Figures 15-18, and the results for the visual observations are reported here.

No growth occurred in the sterile control cultures for the duration of the project. The solids in the controls with iron were not magnetic, and no color change occurred.

i. QV1,3

Aerobic cultures became turbid after 3 days (Figure 15). The final pH of the aerobic cultures with iron after 3 and 6 weeks were 9.17 and 9.32, respectively. The final pH of the aerobic cultures without iron after 3 and 6 weeks were 9.22 and 9.18, respectively. Anaerobic cultures with iron became turbid after 5 days, and cultures without iron became turbid after 3-4 days. The anaerobic cultures without iron produced gas bubbles from the settled precipitates at the bottom of the tubes by the eighth day. The final pH of anaerobic cultures with iron after 3 and 6 weeks were 9.18 and 9.43, respectively. The final pH of anaerobic cultures without iron after 3 and 6 weeks were 9.61 and 9.48, respectively. All cultures formed biofilms visible to the unaided eye, and none exhibited any color change in the iron precipitates. The solids in all cultures containing iron were weakly magnetic compared to ML2 culture solids (described below).

ii. ML2

Aerobic cultures became turbid after 1 day (Figure 16), and gas was observed bubbling from precipitates settled on the bottom of the tubes after 2 days. Bubbles were not observed by the fourth day. The final pH of aerobic cultures with iron after 3 and 6 weeks were 7.69 and 8,

California Cultures (QV1,3)

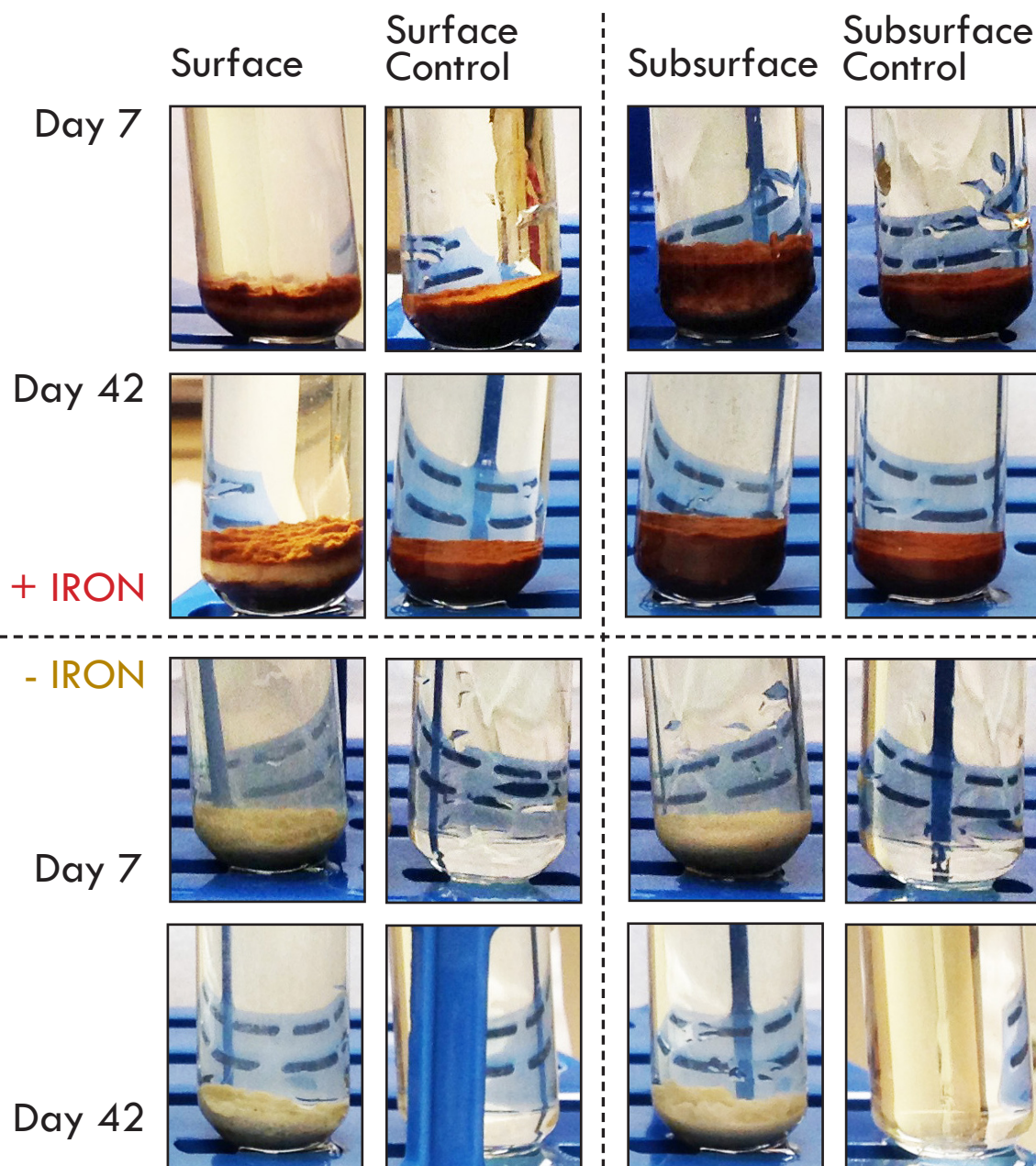


Figure 15. Images of California (QV1,3) cultures with iron (top) and without iron (bottom) after 7 and 42 days of growth under surface (aerobic, left) and subsurface (anaerobic, right) conditions.

Philippines Cultures (ML2)

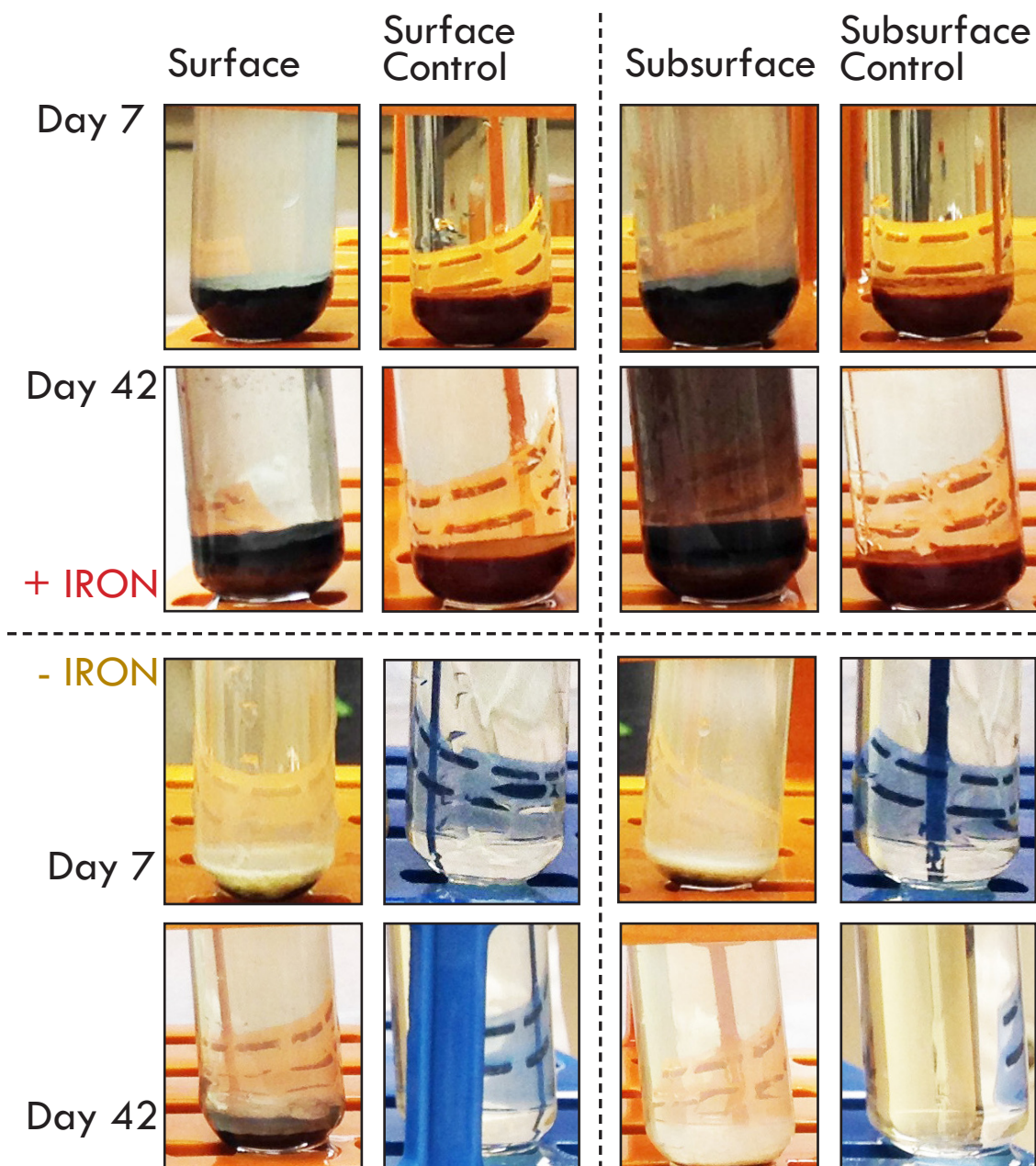
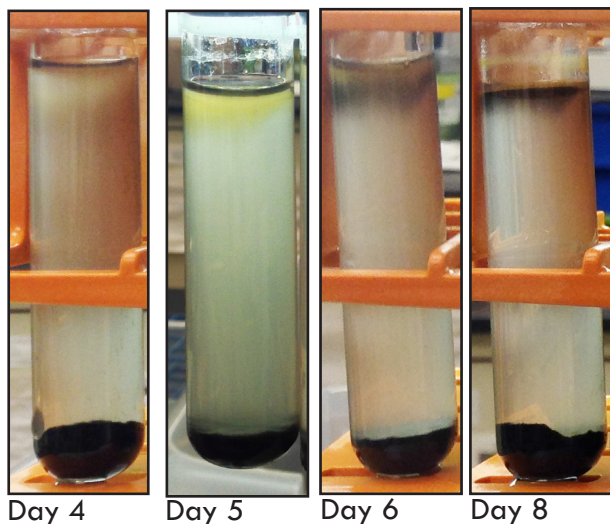


Figure 16. Images of Philippines (ML2) cultures with iron (top) and without iron (bottom) after 7 and 42 days of growth under surface (aerobic, left) and subsurface (anaerobic, right) conditions.

A. Orange Precipitates in Philippines Surface Cultures +Fe



Day 4

Day 5

Day 6

Day 8

B. Black Precipitates in Philippines Cultures +Fe

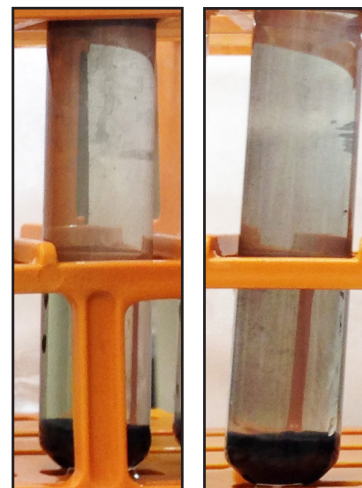
Surface
(Aerobic)
Day 12Subsurface
(Anaerobic)
Day 12

Figure 17. A) Philippines (ML2) surface cultures with iron showing formation of fluid-gas interface films and orange precipitates after 5 days of growth, and color change of precipitates from orange to black after 8 days of growth, becoming darker after 8 days of growth. B) Philippines (ML2) surface and subsurface cultures with iron showing formation of black precipitates along the length of the glass tubes after 12 days of growth.

respectively. The final pH of aerobic cultures without iron after 3 and 6 weeks were 7.85 and 7.43, respectively. Anaerobic cultures became turbid after 2-3 days, and gas was observed bubbling from precipitates settled on the bottom of tubes after 3 days. Bubbles were not observed by the fourth day. The final pH of anaerobic cultures with iron after 3 and 6 weeks were 7.99 and 8.46, respectively. The final pH of anaerobic cultures without iron after 3 and 6 weeks were 7.6 and 7.65, respectively. All cultures formed biofilms visible to the unaided eye. Cultures with iron formed strongly magnetic black precipitates after three days. By the fifth day, aerobic cultures formed iridescent orange films across the fluid-gas interface surface, and orange precipitates extended 1/4" down the side walls of the glass tubes (Figure 17). By the sixth day, the orange precipitates

along the side of the tube became black. After 12 days, aerobic and anaerobic cultures formed black precipitates along the full length of the glass tube walls. Solid material in one anaerobic culture without iron became grey, otherwise no color change was observed in cultures without iron.

iii. NaNO_3 Experiment

Nitrate as a possible electron acceptor for anaerobic iron oxidation was investigated through the addition of NaNO_3 to iron enrichment cultures after three days of growth. Before the addition of NaNO_3 , the QV1,3 aerobic culture became turbid after three days and showed no change in precipitate color, the QV1,3 anaerobic culture showed no growth and no change in precipitate color, and both ML2 cultures became turbid and formed black magnetic precipitates after one day. Cultures were amended with NaNO_3 three days after inoculation. No changes in turbidity or precipitate color occurred in the QV1,3 aerobic culture or the ML2 cultures after the addition of NaNO_3 . Five days after the addition of NaNO_3 , the QV1,3 anaerobic culture became turbid and formed black, strongly magnetic precipitates (Figure 18).

NaNO_3 Experiments

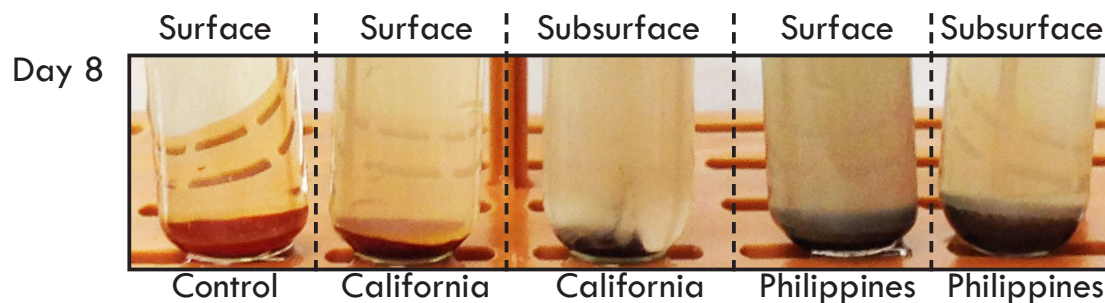


Figure 18. Images of QV1,3 and ML2 cultures 5 days after nitrate addition showing 8 days of total growth and black precipitates in the California (QV1,3) subsurface culture and Philippines (ML2) cultures. Surface conditions were simulated using an aerobic headspace, and subsurface conditions were simulated with an anaerobic headspace.

2. Fluorescence Microscopy

Fluorescence microscopy was employed to document relative cell abundances and morphologies in fluids from California (QV1,3) and Philippines (ML2) surface (aerobic) and subsurface (anaerobic) culture experiments. Fluorescence microscopy images are shown in Figures 19-21.

i. QV1,3

Aerobic cultures with iron exhibited round and rod-shaped cells measuring $1\mu\text{m} \times 1.5\mu\text{m}$ after three weeks. After six weeks, the morphology and size of the cells was unchanged, but had relatively lower densities after six weeks. The aerobic cultures without iron exhibited round and rod-shaped cells measuring $1\mu\text{m} \times 1.5\mu\text{m}$ after three weeks. After six weeks, the morphology and size of the cells was unchanged, but had relatively higher densities after six weeks.

Anaerobic cultures with iron exhibited rod-shaped cells measuring $1\mu\text{m} \times 1.5\mu\text{m}$ after three weeks. After six weeks, the cells were rod-shaped, measuring $1\mu\text{m} \times 3\mu\text{m}$. Anaerobic cultures without iron exhibited round and rod-shaped cells measuring $1\mu\text{m} \times 1.5\mu\text{m}$ after three weeks. After six weeks, the cell size, morphology, and relative densities were unchanged (Figure 19).

ii. ML2

Aerobic cultures with iron exhibited cells with terminal endospores measuring $1\mu\text{m} \times 20\mu\text{m}$ after three days. After three weeks, aerobic cultures with iron exhibited cells measuring $1\mu\text{m} \times 10\mu\text{m}$. After six weeks, cultures exhibited rod-shaped cells measuring $3\mu\text{m} \times 5\mu\text{m}$ and filaments measuring $1\mu\text{m} \times 50\mu\text{m}$. Aerobic cultures without iron exhibited round and rod-shaped cells and filaments measuring $3\mu\text{m} \times 3\mu\text{m}$, $3\mu\text{m} \times 6\mu\text{m}$, and $1\mu\text{m} \times 30\mu\text{m}$, respectively, after three weeks. After six weeks, the size and morphologies of cells were the same, however the relative proportion of filaments to rods was higher after six weeks.

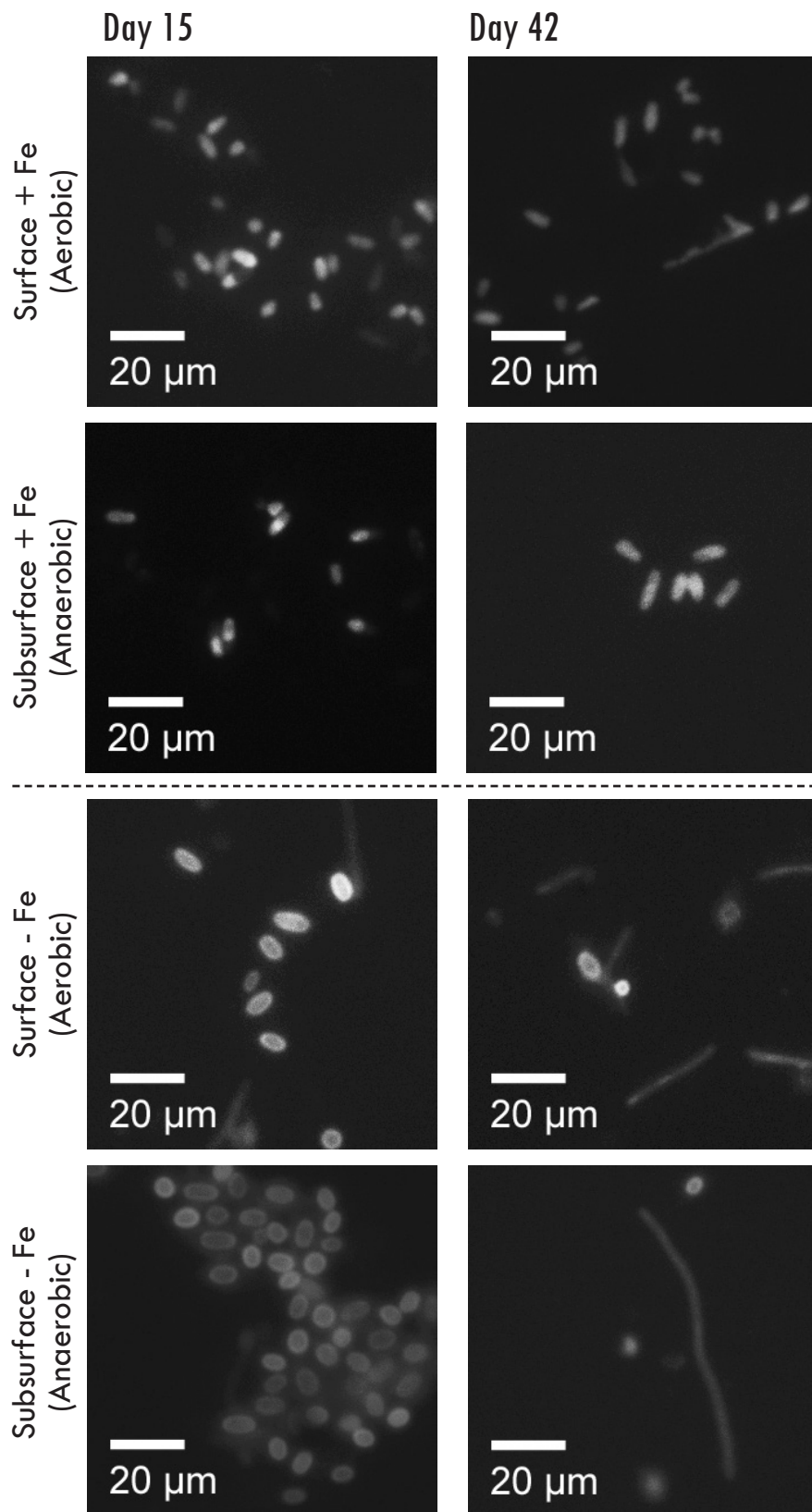


Figure 19. Fluorescence microscopy images of California (QV1,3) cultures with iron (top) and without iron (bottom) after 7 (left) and 42 (right) days of growth.

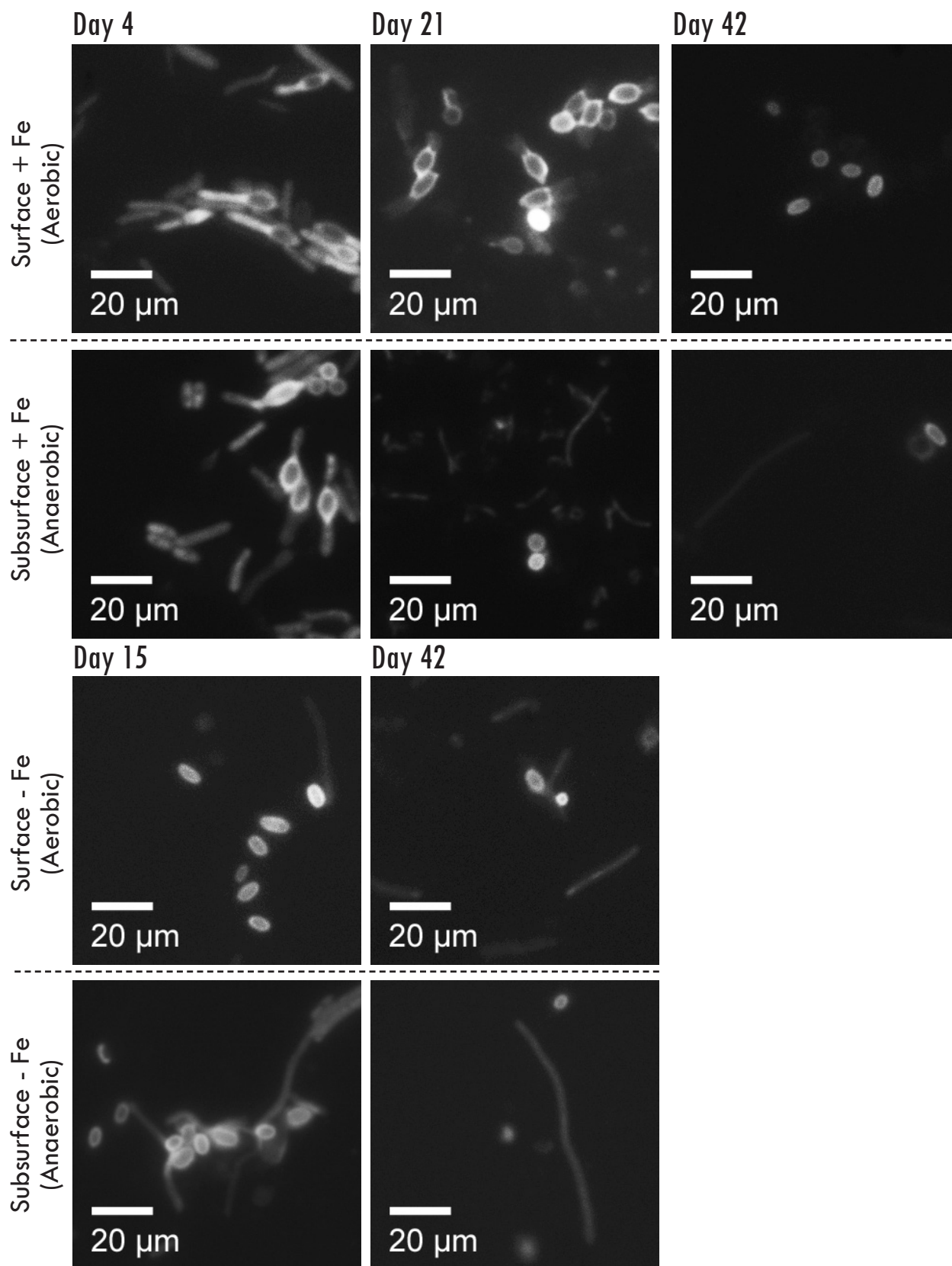


Figure 20. Fluorescence microscopy images of ML2 cultures with iron (top) and without iron (bottom) after 4-42 days of growth.

Anaerobic cultures with iron exhibited cells with terminal endospores measuring $1\ \mu\text{m} \times 20\ \mu\text{m}$ after three days. After six weeks, cultures exhibited round and rod-shaped cells and filaments measuring $2\ \mu\text{m} \times 2\ \mu\text{m}$, $2\ \mu\text{m} \times 4\ \mu\text{m}$, and $1\ \mu\text{m} \times 50\ \mu\text{m}$, respectively. Anaerobic cultures without iron exhibited rod-shaped cells and filaments measuring $3\ \mu\text{m} \times 5\ \mu\text{m}$ and $1\ \mu\text{m} \times 20\text{-}60\ \mu\text{m}$, respectively, after three weeks. After six weeks, cell morphology and size was unchanged, however relative cell densities were lower after six weeks (Figure 20).

iii. NaNO_3 Enrichment Experiment

No changes in cell morphologies were observed in the QV1,3 aerobic culture after the addition of nitrate. Five days after the addition of nitrate, the QV1,3 anaerobic culture exhibited cells with terminal endospores measuring $1\ \mu\text{m} \times 20\ \mu\text{m}$. No changes in cell morphologies were observed in the ML2 cultures after the addition of nitrate (Figure 21).

3. Scanning Electron Microscopy and X-ray Energy Dispersive Spectroscopy (SEM & XEDS)

Scanning electron microscopy and XEDS were employed to document microbe-precipitate interactions and identify the chemistry of secondary precipitates in California (QV1,3) and Philippines (ML2) surface (aerobic) and subsurface (anaerobic) iron enrichment culture experiments. All iron enrichment culture SEM images are shown in Figure 22.

i. QV1,3

The aerobic culture had rod-shaped cells measuring $0.5\ \mu\text{m}$ thick \times $1\ \mu\text{m}$ long within the matrix of iron, as well as needle-like precipitates protruding between desiccation cracks measuring $0.1\ \mu\text{m} \times 1\text{-}2\ \mu\text{m}$ after three days. After three weeks, microbial cells were not apparent in the matrix, however many needle-like precipitates were visible in the matrix, measuring $0.1\ \mu\text{m} \times 1\text{-}3\ \mu\text{m}$.

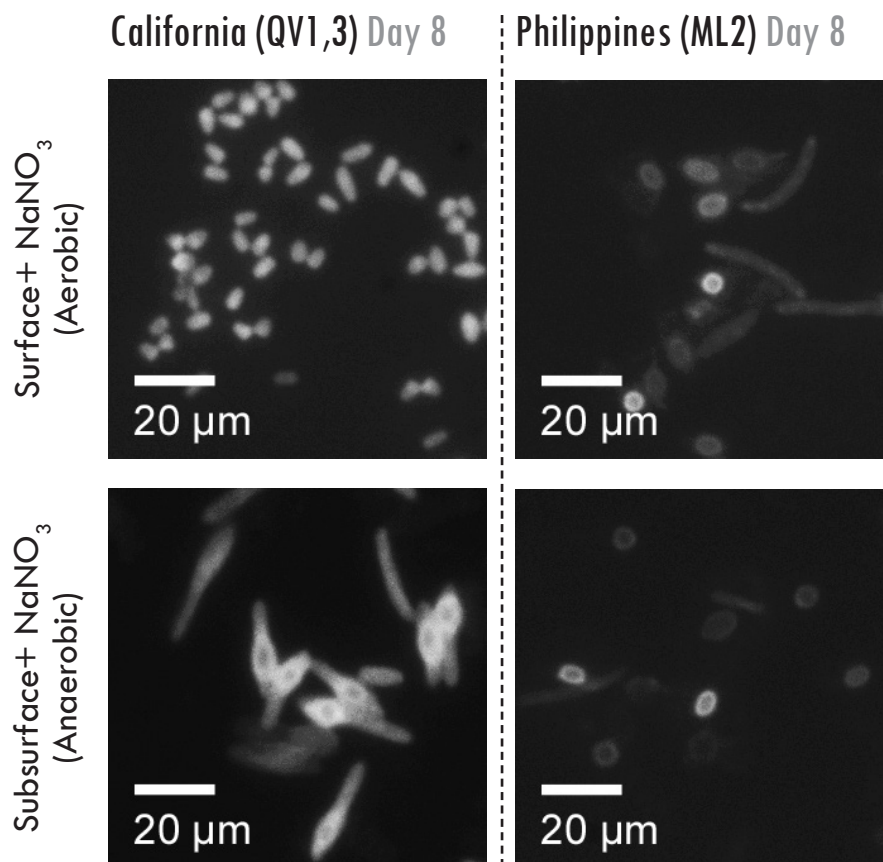


Figure 21. Fluorescence microscopy images of California (QV1,3, left) and Philippines (ML2, right) cultures five days after the addition of NaNO_3 under surface (aerobic, top) and subsurface (anaerobic, bottom) conditions.

Structures bridging desiccation cracks measured $0.5\mu\text{m} \times 5\mu\text{m}$. One filamentous structure with seven nodes was observed, measuring $0.1 - 0.3\mu\text{m} \times 3\mu\text{m}$.

Anaerobic cultures had needle-like precipitates within the matrix of iron, with needles measuring $0.1\mu\text{m}$ wide \times $1-5\mu\text{m}$ long protruding between desiccation cracks. After three weeks, the anaerobic culture had cells measuring $0.5\mu\text{m}$ wide \times $1\mu\text{m}$ thick within the matrix of iron, as well as needle-like precipitates protruding between desiccation cracks measuring $0.1-0.5\mu\text{m} \times 1-2\mu\text{m}$. Filamentous structures with several nodes were observed, measuring $0.1-0.3\mu\text{m} \times 10\mu\text{m}$.

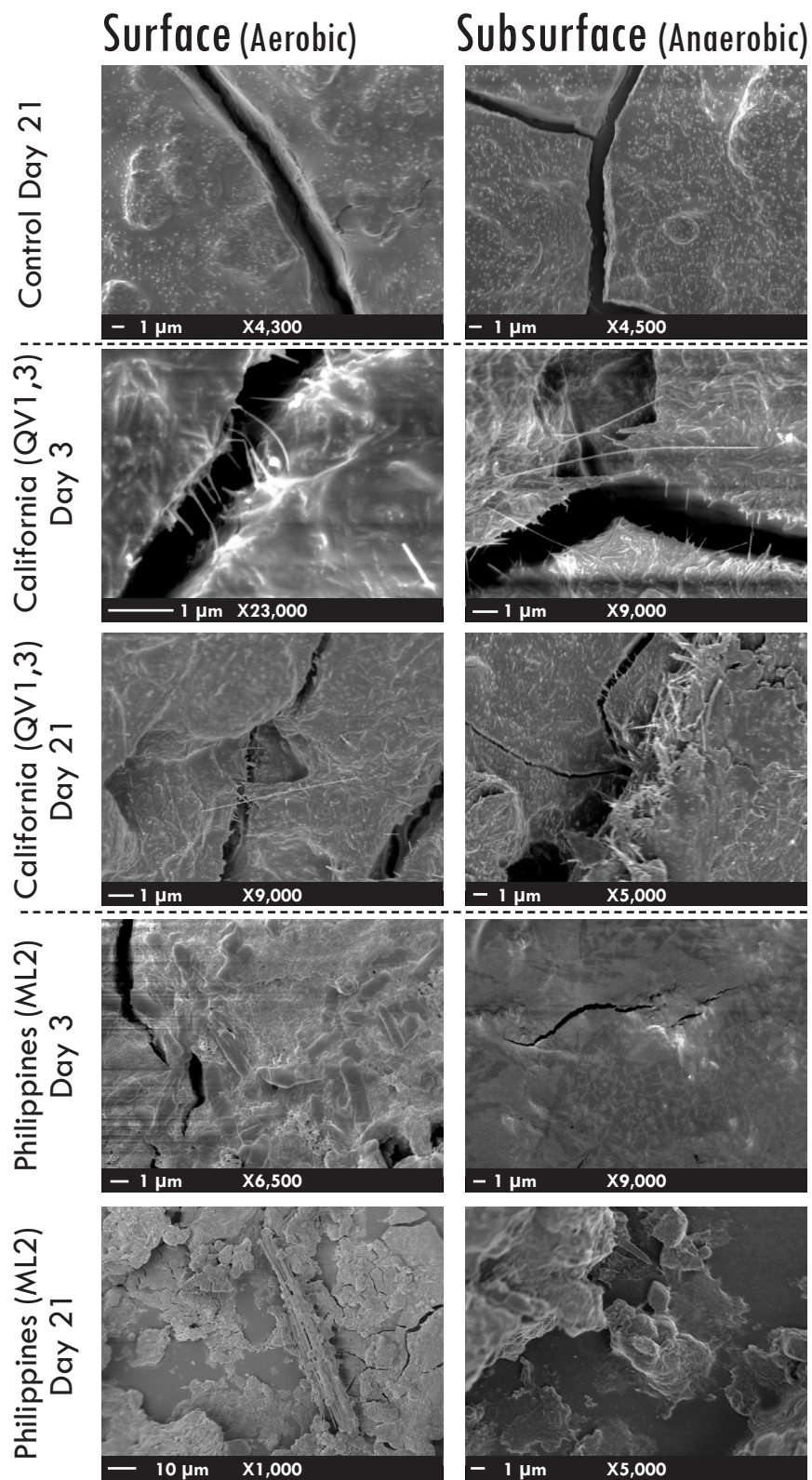


Figure 22. SEM images of iron enrichment culture sterile control precipitates (top) and live California (QV1,3, middle) and Philippines (ML2, bottom) culture precipitates after three days and three weeks of growth under surface (aerobic, left) and subsurface (anaerobic, right) conditions.

ii. ML2

Aerobic cultures had cells measuring $1\ \mu\text{m} \times 1\text{-}4\ \mu\text{m}$ within the matrix of iron after three days. After three weeks, the iron particles appeared to be flocculated platy material coated with film. One elongated structure composed of several thinner structures measuring $1\ \mu\text{m} \times 50\ \mu\text{m}$ with round-shaped cells ($1\ \mu\text{m} \times 1\ \mu\text{m}$) attached along its length was observed.

Anaerobic cultures had no visible cells after three days, but had thin, curved structures measuring $0.5\ \mu\text{m} \times 3\ \mu\text{m}$ within the matrix of iron. After three weeks, cultures had flocculated platy material coated with film and rod-shaped cells measuring $1\ \mu\text{m} \times 3\ \mu\text{m}$. One elongated precipitate structure was observed, measuring $0.2\ \mu\text{m} \times 4\ \mu\text{m}$.

The aerobic and anaerobic controls had no needle or cell structures after three weeks.

iii. X-ray Energy Dispersive Spectroscopy (XEDS)

The following elements were detected via X-ray Energy Dispersive Spectroscopy (XEDS) across all culture precipitates scanned, reported here as averages of multiple scans (summarized in Table 3): oxygen, silicon, iron, carbon, sodium, chlorine, and potassium. The experimental QV1,3 aerobic culture precipitates also contained titanium, and the experimental QV1,3 aerobic and anaerobic cultures both contained magnesium.

Table 3. Culture and Inoculum Sediment Bulk Elemental Chemistry (Wt%) (XEDS)

Culture	O%	Mg%	Si%	Fe%	C%	Na%	Cl%	Ti%	K%	Ca%
QV1,3 Aerobic	21.928	12.243	21.8	6.57	34.47	6.385	8.91	5.19	5.0533	nd
QV1,3 Anaerobic	11.265	6.355	15.545	21	9.66	8.175	14.29	nd	5.18	nd
ML2 Aerobic	8.25	nd	1.82	33.445	17.605	13.765	10.95	nd	5.64	nd
ML2 Anaerobic	17.72	nd	1.2	4.7233	44.7	16.28	6.6633	nd	3.25	nd
Aerobic Control	5.175	nd	nd	60.635	12.53	6.06	6.75	nd	3.265	nd
Anaerobic Control	7.155	nd	2.83	40.995	12.565	7.79	11.565	nd	5.285	nd
QV1,3 Inoculum Sed	14.54	17.7	22.46	20.68	nd	nd	nd	nd	nd	nd
ML2 Inoculum Sed	12.567	2.1133	22.863	38.303	8.6733	nd	nd	nd	nd	7.8467

nd = not detected

4. X-ray Photoelectron Spectroscopy (XPS)

X-ray photoelectron spectroscopy was employed to document the oxidation states of the iron precipitates in the California (QV1,3) and Philippines (ML2) surface (aerobic) and subsurface (anaerobic) iron enrichment cultures. Three peak maxima were characteristic of the element iron in the sample spectra. Relative to the sterile control (Fe-enriched yeast-peptone growth media), all culture iron peaks except the aerobic QV1,3 iron peaks were shifted to a lower binding energy, indicative of the iron being reduced relative to the control (Figure 23).

XPS | Iron Oxidation States of Culture Precipitates

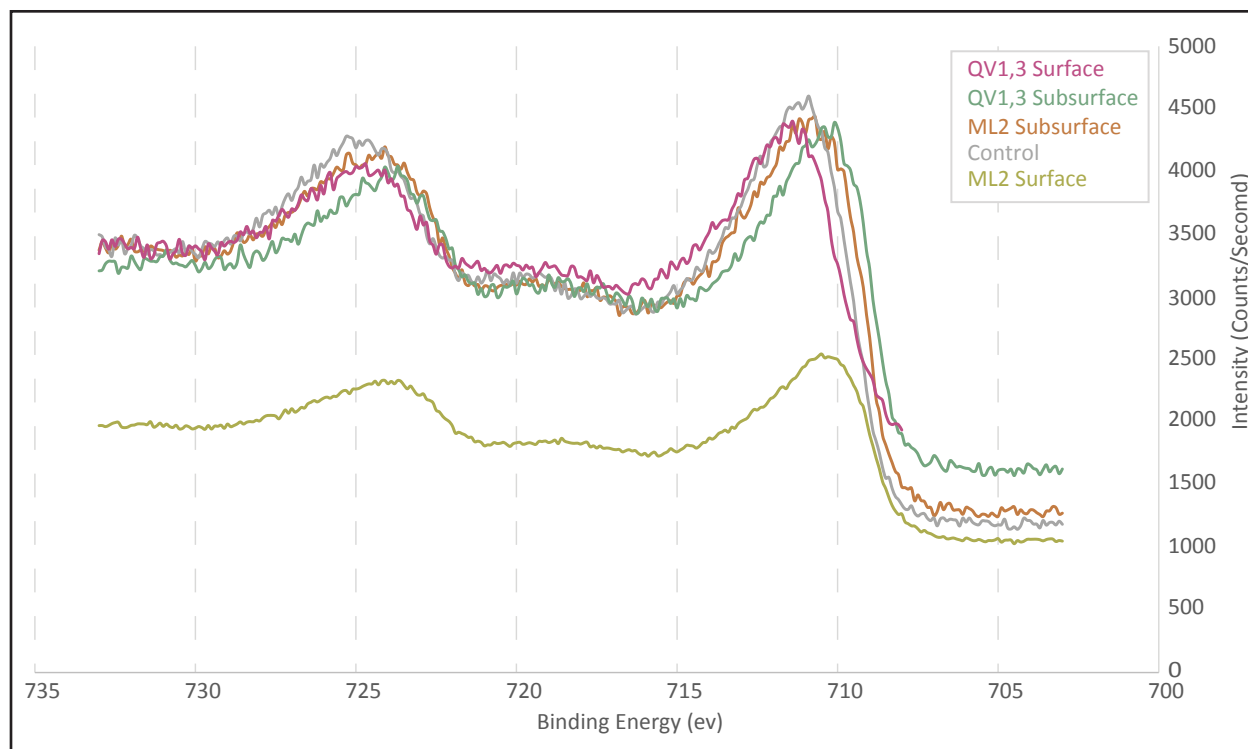


Figure 23. XPS spectra of precipitates from sterile control and live California (QV1,3) and Philippines (ML2) cultures after three weeks of growth under surface (aerobic) and subsurface (anaerobic) conditions.

The control peaks occurred at binding energies of approximately 724.7, 719.4, and 710.9(eV). The peaks for the aerobic QV1,3 culture occurred at 724.7, 719.6, and 711.4(eV). The peaks for the anaerobic QV1,3 culture occurred at 723.7, 718.4, and 710.1(eV). The peaks for the aerobic ML2 culture occurred at 723.7, 718.2, and 710.1(eV). The peaks for the anaerobic ML2 culture occurred at 724.2, 718.6, and 710.7(eV). The intensities of all peaks were relatively equal, except for the peak intensities for the aerobic ML2 culture. The lower intensity for that sample is due to the patchiness of iron solids on the filter that was analyzed.

5. X-ray Diffraction (XRD)

X-ray diffraction was employed to document mineralogical compositions of the solids in the California (QV1,3) and Philippines (ML2) surface (aerobic) and subsurface (anaerobic) cultures. Culture XRD patterns overlain with the standard patterns for halite are shown in Figure 24, culture patterns overlain with standard patterns for lizardite, actinolite, magnetite, magnesiowuestite, siderite, and hematite are shown in Appendix B, Figures 1-7, and peak positions are reported here as 2θ . Mineralogy is summarized in Table 4. A strong diffraction peak at 31.7° and a second weaker peak at 45.4° was observed in all culture patterns. A strong peak at 31.7° and weak peaks at 45.4° and 56.5° was observed in the QV1,3 and ML2 aerobic week 3 control patterns, ML2 anaerobic week 3 pattern, and ML2 aerobic week 6 pattern. All peak positions listed here agree with the standard pattern for halite.

i. QV1,3

Strong peaks were observed in all experimental patterns and not observed in control patterns at 12.1 and 24.4 ($^\circ$). These peak positions agree with standard patterns for lizardite and hematite.

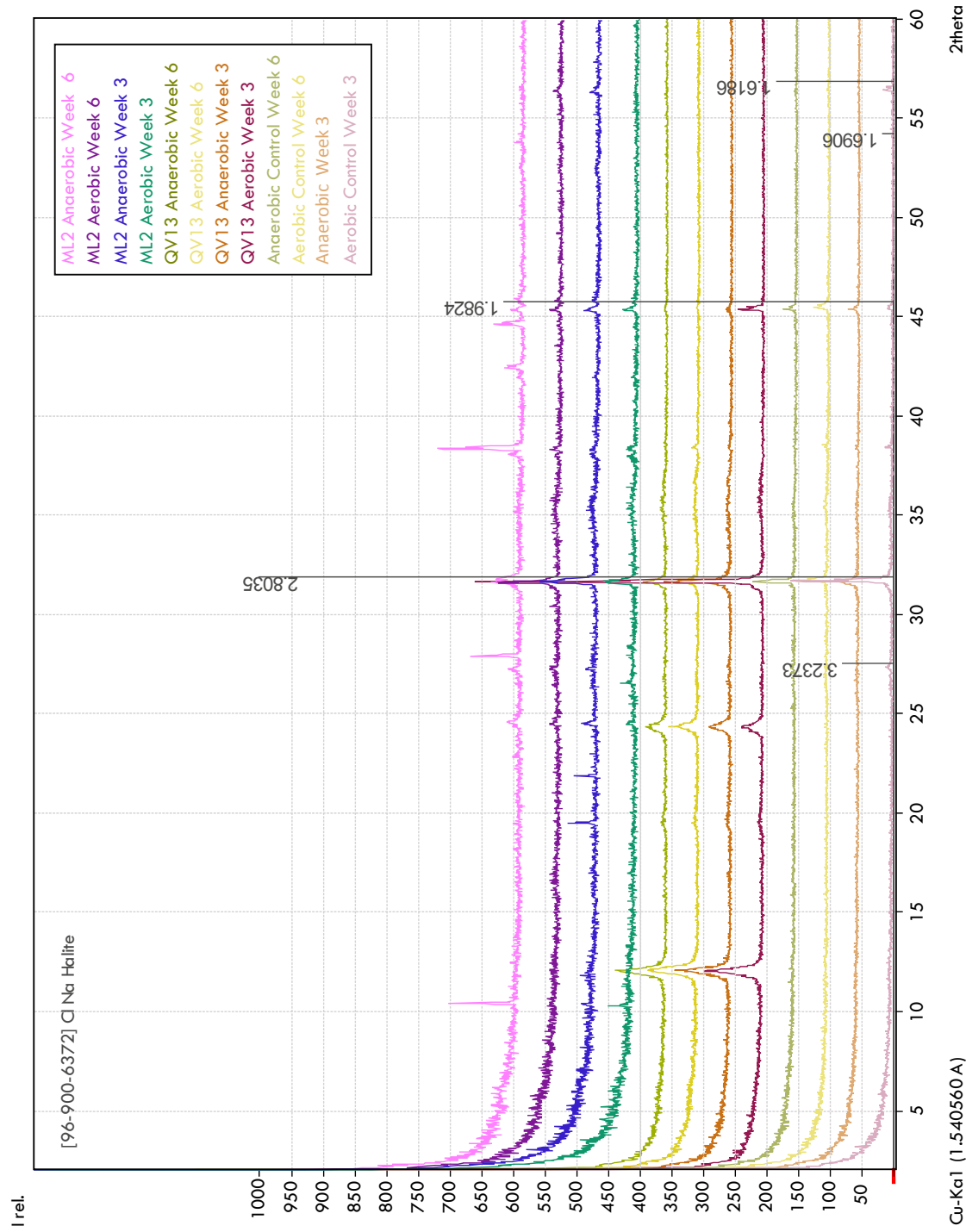


Figure 24. Live California (QV1,3) and Philippines (ML2) cultures and sterile control culture XRD patterns overlain with the standard pattern for halite (shown with d-values). Surface cultures were incubated under aerobic conditions, and subsurface cultures were incubated under anaerobic conditions.

Table 4. Culture Mineralogy (XRD)

Culture	halite	lizardite	actinolite	magnetite	magnesiowuestite	siderite	hematite
QV1,3 Aerobic (wk 3)	X	X				*	*
QV1,3 Aerobic (wk 6)	X	X				*	*
QV1,3 Anaerobic (wk 3)	X	X				*	*
QV1,3 Anaerobic (wk 6)	X	X				*	*
ML2 Aerobic (wk 3)	X		***	X	*	*	*
ML2 Aerobic (wk 6)	X		***	X	*	*	*
ML2 Anaerobic (wk 3)	X		***	X	*	*	*
ML2 Anaerobic (wk 6)	X		***	X	*	*	*
Aerobic Control (wk3)	X					*	
Aerobic Control (wk 6)	X					*	
Anaerobic Control (wk 3)	X					*	
Anaerobic Control (wk 6)	X					*	

Magnetite was detected via XRD and with a neodymium magnet.

X = confident match

* = 1 Peak match

** = 1-3 peak matches

*** = more than 3 peak matches

ii. ML2

Strong peaks occur in the aerobic week 6 pattern at 19.6, 22, 24.6 ($^{\circ}$), these peaks were unidentified. Strong peaks occur in the anaerobic week 6 pattern at 10.6, 24.6, 28, 38.5, 42.6, and 44.5 ($^{\circ}$). These peak positions agree with standard patterns for magnetite, magnesiowuestite and siderite.

6. DNA Sequencing

Taxonomic relative abundances are reported here for the California (QV1,3) and Philippines (ML2) surface (aerobic) and subsurface (anaerobic) iron enrichment culture communities in order from most abundant to least abundant (Figure 25).

i. QV1,3

The dominant genera in the aerobic culture with iron were Zoogloea, Dechloromonas, Hydrogenophaga, Phyllobacterium, and Pseudomonas; 60% of the genera were unidentified.

The dominant genera in the aerobic culture without iron were Zoogloea, Phyllobacterium, Dechloromonas, Hydrogenophaga, and Pseudomonas; 53% of the genera were unidentified.

The dominant genera in the anaerobic culture with iron were Zoogloea, Dechloromonas, Hydrogenophaga, and Pseudomonas; 60% of the genera were unidentified. The dominant genera in the anaerobic culture without iron were Zoogloea, Dechloromonas, Hydrogenophaga, Phyllobacterium, and Pseudomonas; 60% of the genera were unidentified.

ii. ML2

The dominant genera in the aerobic culture with iron were Tisserelia/Soehngenia, Alkaliphilus, Clostridium, Bacillus, Pseudomonas, and Paenibacillus; 10% of the genera were unidentified. The dominant genera in the aerobic culture without iron were Tisserelia/Soehngenia, Clostridium, Sporanaerobacter, Bacillus, Alkaliphilus, Paenibacillus, Sedimentibacter, Caloramator, and Hydrogenophaga; 35% of the genera were unidentified.

The dominant genera in the anaerobic culture with iron were Tisserelia/Soehngenia, Clostridium, Alkaliphilus, Bacillus, Paenibacillus, Geosporobacter/Thermotalea, Pseudomonas, and Hydrogenophaga; 13% of the genera were unidentified. The dominant genera in the anaerobic culture with no iron were Tisserelia/Soehngenia, Clostridium, Sedimentibacter, Alkaliphilus, and Bacillus; 12% of the genera were unidentified.

iii. NaNO₃ Enrichment Experiment

The dominant genus in the QV1,3 anaerobic culture was Clostridium. Less than 1% of the genera were unidentified.

Taxonomic Identification of Inoculum Sediments and Enrichment Cultures | Genus Level

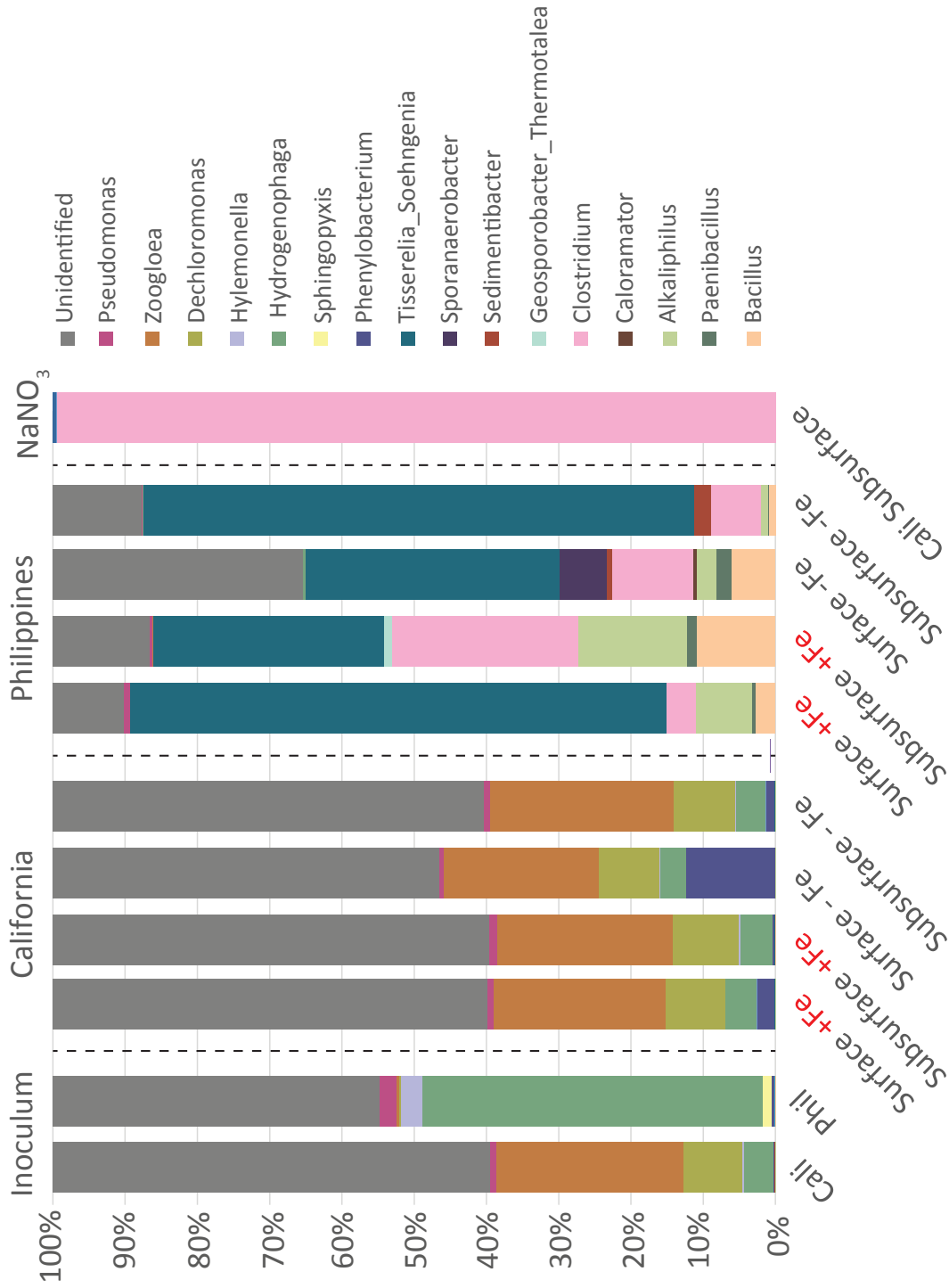


Figure 25. Relative abundances of genera in inoculum sediments from California (QV1,3) and Philippines (ML2) and cultures after three weeks of growth under surface (aerobic) and subsurface (anaerobic) conditions.

C. DNA Sequence Analyses

The maximum and minimum number of sequence reads per sample after chimera removal were 246,440 and 28,488, respectively, with the exception of the ML2 anaerobic Phase II microcosm fluid sample, which had 20 sequence reads. The average chimera removal for each sample was 8.47% of the total number of sequences (Table 5).

Table 5. DNA Sequence Summary

Sample ID	# Reads After Trim	Avg. Read Length	%Chimeras removed
QV1,3 Aer. Mic. Fluids	60,712	292.9	4.5
QV1,3 Aer. Mic. Fluids Phase II	77,228	292.8	0.12
QV1,3 Anaer. Mic. Fluids	62,469	293	5.99
QV1,3 Anaer. Mic. Fluids Phase II	40,938	292.9	13.76
ML2 Aer. Mic. Fluids	62,598	292.9	11.17
ML2 Aer. Mic. Fluids Phase II	42,972	292.9	3.52
ML2 Anaer. Mic. Fluids	48,666	292.7	13.82
ML2 Anaer. Mic. Fluids Phase II	20	333.5	0
QV1,3 Aer. Mic. Sediments	32,134	292.6	12.92
QV1,3 Aer. Mic. Sediments Phase II	49,748	292.7	13.45
QV1,3 Anaer. Mic. Sediments	46,417	292.8	13.4
QV1,3 Anaer. Mic. Sediments Phase II	55,972	293	12.85
ML2 Aer. Mic. Sediments	47,389	292.1	1.37
ML2 Aer. Mic. Sediments Phase II	32,575	292.8	14.78
ML2 Anaer Mic. Sediments	55,788	292.6	13.66
ML2 Anaer Mic Sediments Phase II	69,472	293.1	13.94
QV1,3 Aer. Culture +Fe	40,516	293	13.72
QV1,3 Aer. Culture -Fe	67,709	293	13.48
QV1,3 Anaer. Culture +Fe	28,488	292.8	13.77
QV1,3 Anaer. Culture -Fe	41,139	292.8	14.21
ML2 Aer. Culture +Fe	71,719	292	7.82
ML2 Aer. Culture -Fe	60,188	292.3	16.23
ML2 Anaer. Culture +Fe	246,440	292.4	3.28
ML2 Anaer. Culture -Fe	60988	292.2	12.34
QV1,3 Anaer. Culture +Fe +NaNO ₃	63317	292.9	0.09
QV1,3 Inoculum Sediments	48,920	292.8	13.28
ML2 Inoculum Sediments	65,807	293.1	8.32

D. Summary of Results

The experiments in this study investigated microbe-mineral interactions through microcosm experiments simulating serpentinizing surface and subsurface conditions from two serpentinizing systems located in the Philippines and Zambales ophiolites. A second set of experiments investigated microbial iron metabolisms through batch culturing with ferric hydroxide. The results of these experiments are summarized here (Figures 26-27).

1. Documenting Microbe-Mineral Interactions

Microcosm experiments investigated microbial influence on mineralogy, evidence of microbial engagement in redox reactions, and microbial preference for solid or fluid substrates. Visual observations of California microcosms did not indicate chemical changes by color changes in the sediments, whereas visual observations of Philippines microcosms did indicate chemical changes by color changes in the sediments. Under oxic conditions in Philippines microcosms, sediments were light brown, and under anoxic conditions, sediments were grey. Putative nanowires were observed on rock chips from California microcosms, but they were not observed on Philippines microcosm rock chip surfaces. Iron metabolizing microbes were sequenced from both the California and Philippines serpentinizing systems under surface and subsurface microcosm simulations. Optimal growth in Phase I microcosms from the California system under surface and subsurface conditions occurred in the sediments and fluid, and optimal growth in Phase II microcosms from the same system under surface conditions occurred in sediments, and under subsurface conditions occurred in fluids and sediments. Optimal growth in Phase I microcosms from the Philippines system under surface conditions occurred in the sediments and fluid, and under subsurface conditions growth was not optimal. Optimal growth in Phase II microcosms from the Philippines system under surface and subsurface conditions occurred

in sediments.

2. Verifying Fe-Metabolisms

Culturing experiments investigated the potential for enrichment of iron-metabolizing microbes from the California and Philippines serpentinizing systems and microbial transformation of iron redox states. Visual observations did not indicate chemical changes by color changes in the iron precipitates, whereas visual observations of Philippines cultures did indicate chemical changes by color changes in the precipitates. Under oxic conditions in Philippines cultures, precipitates were red, and under anoxic conditions, precipitates were black. Putative nanowires were observed in iron precipitates from California cultures under surface and subsurface simulations, and were not observed in precipitates from Philippines cultures. A neodymium magnet weakly attracted iron precipitates from California cultures, and strongly attracted precipitates from Philippines cultures, indicating biomagnetite in Philippines cultures. If the putative nanowires were not truly nanowires in California cultures, then they are considered secondary precipitates. XPS data indicated that the California surface culture precipitates were oxidized, and subsurface precipitates were reduced, whereas Philippines surface and subsurface culture precipitates were reduced. Iron-metabolizing microbes were sequenced from California and Philippines cultures.

Summarized Results | Documenting Microbe-Mineral Interactions

	CALIFORNIA				PHILIPPINES			
	Phase I		Phase II		Phase I		Phase II	
	Surface	Subsurface	Surface	Subsurface	Surface	Subsurface	Surface	Subsurface
Sediment color change	no	no	no	no	yes	yes	yes	yes
Putative nanowires	yes	yes	yes	yes	no	no	no	no
Fe-metabolizing microbes	yes	yes	yes	yes	yes	yes	yes	yes
Optimal growth substrate	fluids and sediments	fluids and sediments	sediments	fluids and sediments	fluids and sediments	not optimal	sediments	sediments

Figure 26. Summarized results from Phase I and Phase II microcosm experiments simulating surface and subsurface conditions from the California and Philippines serpentinizing systems.

Summarized Results | Verifying Fe-Metabolisms

	CALIFORNIA		PHILIPPINES	
	Surface	Subsurface	Surface	Subsurface
Fe oxidation state	Oxidized	Reduced	Reduced	Reduced
Precipitate color change	no	no	yes (red to black)	yes (red to black)
Putative nanowires	yes	yes	no	no
Magnetic	weak	weak	strong	strong
Fe-metabolizing microbes	yes	yes	yes	yes
Iron transformation	secondary precipitates	secondary precipitates	biomagnetite	biomagnetite

Figure 27. Summarized results from culture experiments simulating surface and subsurface conditions from the California and Philippines serpentinizing systems.

IV. DISCUSSION

This study examined microbial iron metabolism in the Coast Range and Zambales serpentinizing systems by investigating two main hypotheses:

- 1) redox reactions with iron occur abiotically at the surface, with biomineralization occurring passively with cells acting as nucleation sites, and
- 2) both microbial iron oxidation and reduction are possible in the subsurface, where biomineralization can be actively controlled by iron metabolizing bacteria.

First, the microbial communities from experiments in this study were compared to communities from global serpentinizing systems to determine whether the deep subsurface harbors a distinct assemblage of microorganisms. Then, the hypotheses were tested through microcosm experiments to examine the interactions between microbes and mineral surfaces, while culturing experiments probed for the enrichment of iron metabolizing bacteria from serpentinizing systems and investigated their effect on iron. The findings of these experiments are discussed here.

A. Ubiquity of Microbial Communities Among Serpentinizing Systems

A ubiquitous serpentinizing subsurface community was proposed by Anderson et al. 2013; Crespo-Medina et al. 2014; Morrill et al. 2014; and Woycheese et al. 2015. Results from DNA sequencing of the inoculum sediments and experiment fluids and sediments in this study have been compared to published microbial community data from other serpentinizing systems around the world (Figure 28).

A background subsurface signature was apparent in these experiments, as shown by a common community in Phase I QV1,3 microcosms, Phase I ML2 anaerobic microcosm, Phase II

Taxonomic Comparison of Serpentinizing Communities | Phylum Level

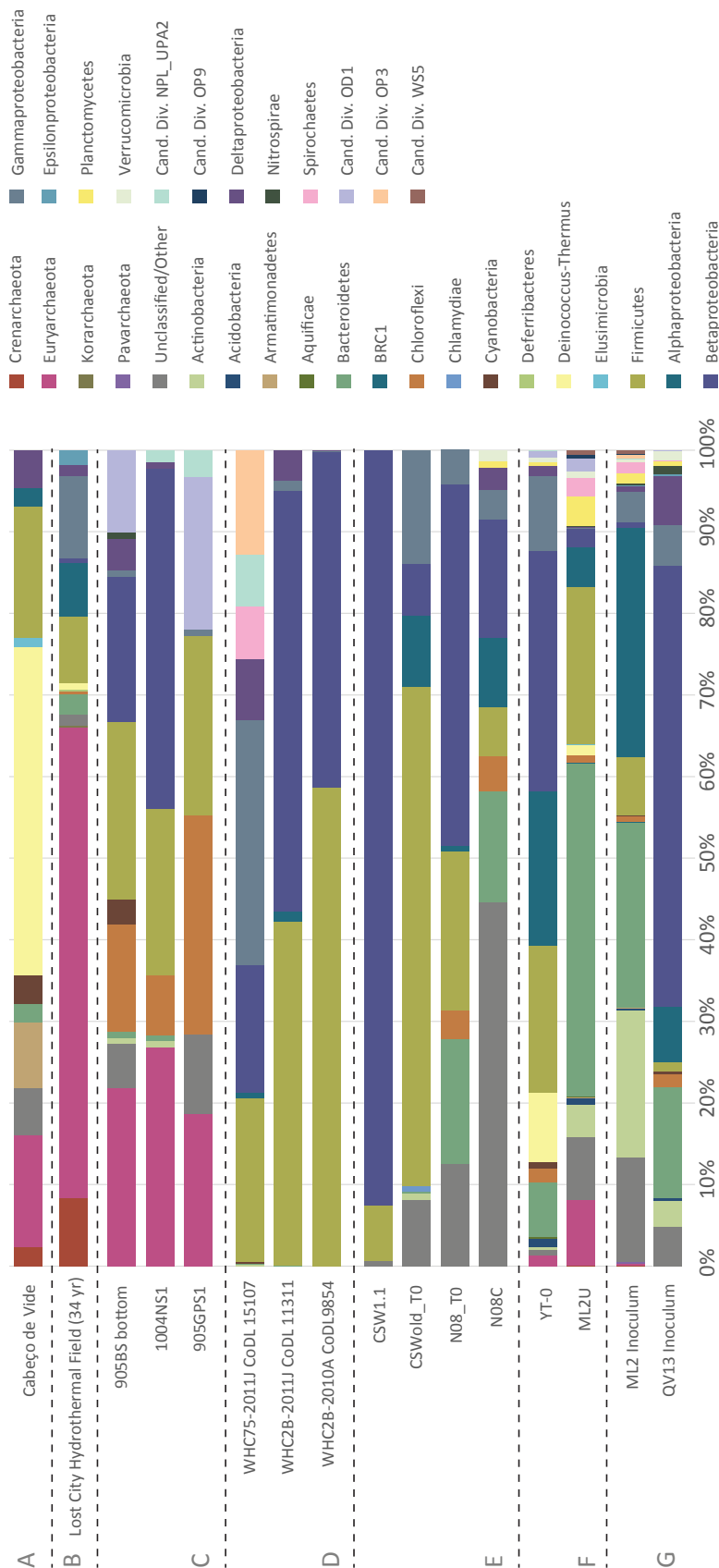


Figure 28. Phylum-level comparison of microbial communities sequenced from various serpentinizing systems, showing that several taxa are shared among systems in a subsurface aquifer (A; Tiago and Verissimo, 2012), a marine seep (B; Brazelton et al. 2010), the Cedars (C; Suzuki et al. 2014), Tablelands (D; Brazelton et al. 2013), CROMO (E; Crespo-Medina et al. 2014), Yanartas and Zambales (F; Woycheese et al. 2015), and Zambales and CROMO (G; this study).

microcosm sediments, and QV1,3 inoculum sediments (Figure 13 and Appendix A, Figure x). This is interpreted to be a true signal of the subsurface because QV1,3 inoculum sediments and the Butili rock core used in the microcosms were both drilled at depth, whereas ML2 inoculum sediments were collected at the surface. The communities present in the Phase II microcosms are attributed to the rock core because the core material was not sterilized in an autoclave. Oven-sterilization of the rock core sampled from Zambales effectively removed surface contamination (and chemical changes that may have occurred in an autoclave under wet conditions at high temperatures and pressures were avoided), but microbial inhabitants of rock pore spaces were most likely protected from the heat and survived the sterilization process (Fajardo-Cavazos et al. 2006).

Comparison of the subsurface community from this study to communities in other studies shows that the ubiquitous phyla in microbial communities in serpentinizing systems across the world are Proteobacteria and Firmicutes (Suzuki et al. 2014; Crespo-Medina et al. 2014; Woycheese et al. 2015; Schrenk et al. 2013; Brazelton et al. 2013; Brazelton et al. 2010; Tiago and Verissimo, 2012). In particular, Clostridiales of the phylum Firmicutes has been commonly sequenced in continental serpentinizing systems (Crespo-Medina et al. 2014). Other phyla present in continental and marine serpentinizing systems include Bacteroidetes, Alphaproteobacteria, Gammaproteobacteria, and Deltaproteobacteria. Three of the sites compared (Figure 28) were sequenced with the same set of primers - Quarry Valley, Manleluag, and Yanartas, and have the following additional phyla in common: Actinobacteria, Acidobacteria, Chloroflexi, Planctomycetes, Verrucomicrobia, and Cand. Div. OD1. Common microbial communities across different serpentinizing systems may suggest deep subsurface biosphere connectivity or selection of communities by environmental controls common to all. Variations in community structures across sites may be controlled by variables such as climate, fluid chemistry, and depth of sampling.

B. Microbial Alteration of Mineralogy

Microcosm experiments examining the interaction between microbes and mineral surfaces showed differences between surface and subsurface simulations, and differences between microcosms inoculated with sediments from the Coast Range and the Zambales ophiolite complexes.

1. Mineralogy of Microcosm Sediments

The mineralogy of the microcosm sediments examined after three and six weeks was largely unchanged from the starting materials, as analyzed by XRD. The inoculum sediments from ML2 contained mafic and ultramafic minerals, such as actinolite, characteristic of the gabbroic country rock in the region of sampling, and these minerals were present in ML2 microcosm sediments after three and six weeks. The QV1,3 microcosm sediments, however, were dominantly lizardite at both the beginning and end of the experiment (reflective of their serpentine inoculum sediments). XRD diffractograms were compared against standard patterns for several iron oxides characteristic of iron biomineralization. Standard patterns for iron oxides overlap with other diffraction patterns in the microcosm sediments, complicating the detection of iron oxides. The amorphous nature of iron biominerals further complicates their detection via XRD. A neodymium magnet attracted magnetic particles in all microcosm sediments, therefore the presence of magnetite is likely. Microcosm sediments from ML2 displayed a color change from brown to grey under anoxic conditions (assumed to indicate reduction of the sediments), and these sediments returned to their original light brown color when the microcosms were re-oxygenated (assumed to indicate oxidation of the sediments).

2. Secondary Precipitation on Microcosm Rock Chip Surfaces

Scanning electron microscopy images of the rock chips after three weeks indicate four general

precipitate morphologies on the reacted chip surfaces: needles, wires, straws, and plates (Figure 29). The absence of needle, wire, and straw precipitates on the unreacted chip surface suggest that secondary mineral precipitation in the experiments was driven or facilitated by microbial growth. Differences in precipitate structures on chip surfaces in QV1,3 and ML2 experiments suggest an influence on secondary precipitation by aqueous chemistry or microbial metabolisms.

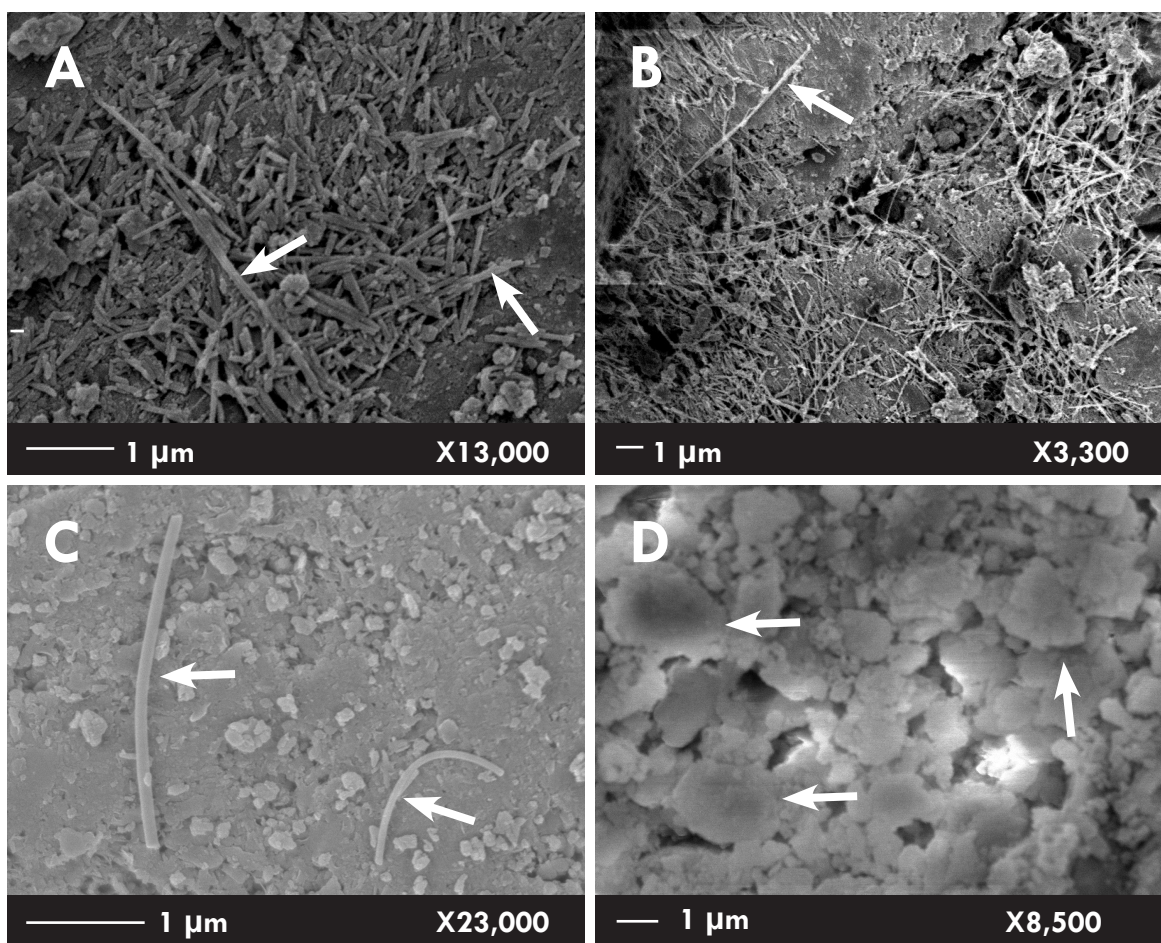


Figure 29. SEM images of secondary precipitates with four general morphologies observed on rock chip surfaces after three weeks in microcosms, arrows indicate A) needles, B) wires, C) straws, and D) plates. Chips came from a) Phase I California Subsurface (QV1,3 anaerobic), b) Phase II California Subsurface (QV1,3 anaerobic), C) Phase I Philippines Surface (ML2 aerobic), and D) Phase I Philippines Subsurface (ML2 anaerobic). Phase I microcosms included live inoculum sediments and surface-sterilized rock core, Phase II microcosms included sterilized sediments and surface-sterilized rock core.

QV1,3 rock chip surfaces had secondary precipitates occurring in voids on the chip surfaces (Figure 11C, Figure 29B), possibly due to concentration of microorganisms in these pits. The wiry precipitates are too thin to be interpreted as microbial sheaths like those associated with *Leptothrix* (Hashimoto et al. 2006), however they fall in the acceptable range of diameter (3-5nm) and length (20 μ m) for nanowires (Reguera et al. 2005, Reguera et al. 2006). The insolubility of iron at a pH4-9 (Liu et al. 1999) creates the need for electron-shuttling strategies for iron-metabolizing bacteria, including the formation of conductive pili (nanowires) such as those seen in *Shewanella* and *Geobacter* (Lovley et al. 2015; Schadler et al. 2009; Weber et al. 2006). If these structures are microbially produced and composed of iron, then the observation that there are denser occurrences of the putative nanowires on chip surfaces from microcosms representing the subsurface suggests their formation may aid in microbial iron reduction. Some precipitate morphologies on QV1,3 chip surfaces are similar to goethite morphologies precipitated in ferrihydrite enrichment experiments with *Shewanella* (Hansel et al. 2003), which may be a product of microbial iron oxidation. These precipitates may also have been formed by abiotic oxidation of microbially reduced iron precipitates upon weekly flushing of aerobic microcosm headspaces with air.

ML2 rock chip surfaces had straw-like and platy precipitates occurring across the entire surface of the chips (Figure 11 B and D, Figure 29 C and D). The straws were isolated and far less abundant than the wires on QV1,3 chip surfaces, and platy precipitates were similar to those observed on the unreacted chip surface except that they appeared to be coated in biofilm, suggesting that the precipitate surfaces may have provided a substrate for microbial attachment and promoted biofilm formation.

Attempts were made to stain and image the biofilm distributions with fluorescence microscopy as well as to determine precipitate chemistry via XEDS, however the presence of fluorescent minerals

in the chips and indistinguishable precipitate chemistry from background chip chemistry prevented successful analysis.

C. Iron Redox in Continental Serpentinizing Systems

Energy availability in the Coast Range and Zambales ophiolite serpentinizing subsurfaces was previously modeled using fluid and gas geochemical data to determine the feasibility of microbial metabolisms (Cardace et al. 2015). The modeling suggests that microbial iron reduction is feasible in the Coast Range system, and that microbial iron reduction and oxidation are both possible in the Zambales system. Iron enrichment cultures were employed to select for iron metabolizing bacteria in an effort to determine their presence in these systems. The results of this study suggest that the predictions made by geochemical modeling were accurate.

1. Visual Indications of Redox Reactions

Relative growth monitoring of the cultures via visual observation of turbidity and optical observation via fluorescence microscopy indicated that positive growth occurred in all experimental cultures, and that no growth occurred in sterile controls. Therefore, biotic and abiotic processes that may have occurred were distinguishable. All experimental QV1,3 culture precipitates remained red throughout the duration of the project, and precipitates were weakly magnetic relative to ML2 culture precipitates. A color change in iron precipitates occurred in all experimental ML2 cultures with iron, as well as in one experimental ML2 culture without iron. The ML2 precipitates were originally orange-red, became black after three days, and were strongly magnetic. Precipitates in sterile control cultures were not magnetic. These results suggest that microbial iron reduction of ferric hydroxide to biomagnetite (or another magnetic, reduced iron mineral) occurred in the experimental

cultures with iron, more efficiently in the ML2 cultures than in the QV1,3 cultures.

One aerobic ML2 culture formed a layer of orange precipitate at the fluid-gas interface, indicating oxidation of the biomagnetite at the fluid surface, though it is unclear whether this was microbially mediated. The weak magnetism of the precipitates in the QV1,3 cultures, compared to the ML2 cultures, may indicate a mixture of oxidized and reduced iron. Microbial iron oxidation was not predicted in the Coast Range serpentinizing system by Cardace et al. 2013, however more accurate future measurements of fluid chemistry in Quarry Valley wells might indicate otherwise.

2. Oxidation States of Iron Precipitates in Cultures

We were unable to determine the mineralogy of the culture precipitates by XRD, likely due to an amorphous nature which requires different techniques. X-ray photoelectron spectroscopy was employed to further investigate the oxidation state of the iron in the cultures where oxidation of the precipitates was indicated by a peak shift to a higher binding energy relative to the control, and reduction was indicated by a peak shift to a lower binding energy relative to the control. The spectra are consistent with visual observations of color change and magnetism in the cultures, in that the aerobic QV1,3 precipitates were oxidized (Figure 30A) and the anaerobic QV1,3 precipitates were reduced (Figure 30B) relative to the control, and the ML2 culture precipitates were reduced (Figure 30 C and D). Interestingly, the spectra indicate that the aerobic ML2 precipitates and QV1,3 precipitates were reduced the most, more than the ML2 anaerobic precipitates. This could be interpreted in several ways:

1. It is possible that the initial concentrations of oxygen and abundances of iron-metabolizing bacteria in all cultures were not equal, therefore the end results of the experiments are not directly comparable.

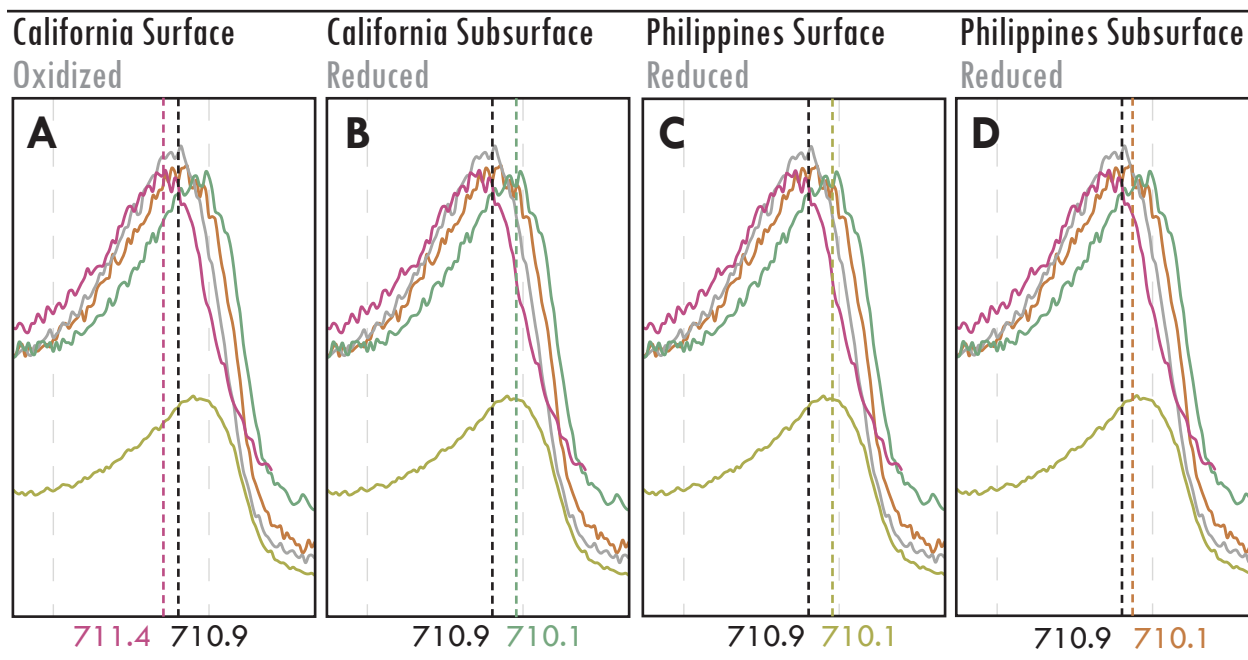


Figure 30. Close-up of right set of peaks from XPS plot (Figure 24) indicating iron peak shifts (colored dashed lines) relative to the control (black dashed line), binding energy is indicated below the dashed lines. A) California surface culture (oxidized). B) California subsurface culture (reduced). C) Philippines surface culture (reduced). D) Philippines subsurface culture (reduced).

2. The formation of endospores in ML2 cultures may be a sign of a stress response to the initial high pH (9.8). All ML2 cultures exhibited a decrease in pH, more-so in aerobic cultures. The presence of oxygen may have initially stimulated growth of aerobic microbes that respired carbon dioxide, resulting in a drop in pH (7.69 after three weeks of growth). Once conditions became completely anoxic in the aerobic cultures after exhaustion of the oxygen, microbial iron reduction could take place. The reduced pH of these cultures may have increased iron solubility (Liu et al. 1999). Therefore, conditions may have been more conducive to iron-reduction in the ML2 cultures where iron was more bioavailable, or where microbes could tolerate pH conditions, resulting in an increased reduction of available iron that matched iron reduction in the anaerobic QV1,3 culture. Remnant dissolved oxygen in

the anaerobic cultures may have supported some aerobic growth, somewhat reducing the pH in anaerobic cultures, but not to the optimal pH for iron reduction for that community. This is complemented by the higher abundance of *Alkaliphilus* in anaerobic ML2 cultures, which are bacteria that grow optimally at a high pH (Ye et al. 2004).

The fluorescence images of cell morphologies indicate a stark difference between the ML2 communities in cultures with and without iron (Figure 20). Endospore morphologies were present only in cultures with iron, indicating that the presence of iron affected the community structure in ML2 cultures. No cell morphological differences were observed when comparing ML2 aerobic to anaerobic culture communities. The reduction of iron with and without the presence of hydrogen as an electron donor suggests that hydrogen may not have played a role in microbial iron reduction in ML2 cultures. No clear difference was observed when comparing QV1,3 aerobic to anaerobic cell morphologies, and no endospores were observed (Figure 19), indicating that iron metabolisms were not inhibited by the alkaline conditions. The reduced nature of the iron in the anaerobic QV1,3 culture (and oxidized nature of the aerobic culture) relative to the control indicates microbial communities had an effect on iron oxidation states, and that hydrogen may have played a role in microbial iron reduction in the QV1,3 communities.

2. Putative Nanowires and Iron Redox in Iron Enrichment Cultures

Scanning electron microscopy images of iron precipitates from cultures (Figure 22) resemble the SEM images of precipitates on microcosm rock chip surfaces (Figure 11). Both aerobic and anaerobic QV1,3 culture precipitates exhibited dense putative nanowire precipitate structures after three days of growth, which appear similar in structure to nanowires formed in iron culture experiments with *Shewanella* (Gross 2006), although no cells were directly visible. The potential

for both iron oxidation and reduction in these cultures, suggested by the weak magnetism and lack of color change in the solids, is supported by the observation of putative nanowires as potential mechanisms for electron transport for redox reactions.

i. Iron Redox in QV1,3 Aerobic Culture

Presumably after six weeks, the oxygen in the aerobic cultures was exhausted, and conditions became anoxic and therefore suitable for iron reduction. However, the reduction of iron was not observed. The oxidation state of the iron in the aerobic culture detected by XPS showed that it was oxidized relative to the control, which may be explained by the lack of hydrogen as an electron donor for ferric iron reduction. If hydrogen was necessary as an electron donor, then anoxic conditions of the surface cultures after the oxygen was exhausted would have been unsuitable for microbial iron reduction. However, the presence of putative nanowires in the aerobic culture solids may indicate an interaction between microbes and iron precipitates. This could be explained in several ways:

- 1) Nanowire formation has been suggested as a method for preventing encrustation of the cell by precipitating ferric iron on the pili instead (Schadler et al. 2009). Any small amount of reduced iron (perhaps in the settled precipitates at the bottom of the culture tube where anoxia could be achieved) could then be reoxidized by agitation and incorporation of dissolved oxygen in the media, followed by controlled precipitation on putative nanowire nucleation sites. A mixed valence state of ferrihydrite in the media or microbially-reduced iron could also provide a source of available iron to become oxidized and precipitate on nucleation sites.
- 2) Nanowires have been documented to serve as conduits for electron transport between cells and insoluble forms of iron, which has only been described for microbial iron reduction,

but has been suggested as a possible electron transport mechanism by iron oxidizing bacteria (Weber et al. 2006). If a mixture of oxidized and reduced iron was present in the QV1,3 aerobic culture, then putative nanowires could have been utilized for either microbial iron reduction or oxidation.

- 3) Abiotic reduction of iron coupled to oxidation of organic compounds in the media may have occurred in the aerobic control culture (Ionescu et al. 2015), resulting in the reduced state of the iron precipitates relative to the oxidized QV1,3 aerobic culture. Putative nanowire formations in the aerobic QV1,3 culture may indicate cells passively acting as nucleation sites for iron precipitation.

ii. Iron redox in QV1,3 Anaerobic Culture

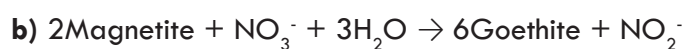
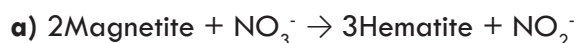
Analysis of the precipitates in the cultures indicated that the redox state of the iron in the QV1,3 anaerobic culture was reduced relative to the control, although these precipitates were red which typically indicates oxidized iron. The degree of reduction of the iron in the anaerobic QV1,3 cultures was comparable to the degree of reduction of iron in the anaerobic ML2 culture, and the QV1,3 precipitates were weakly magnetic, suggesting that the red precipitates in the QV1,3 culture may have contained reduced biominerals other than biomagnetite. Microbial reduction of iron to a red mineral such as siderite (or a mixture of red and black minerals such as siderite and biomagnetite) may explain the reduced nature of the precipitates that are not strongly magnetic in the QV1,3 anaerobic cultures (Dong, et al, 2000). Electron transport mechanisms for iron reduction of insoluble ferric iron have been relatively well described (Lovley et al. 2015), and the putative nanowire structures in the QV1,3 anaerobic cultures could provide an advantageous electron transport mechanisms for iron.

iii. Iron Redox in ML2 Cultures

Putative nanowires were not observed in ML2 cultures, potentially indicating a chemical method of accessing the insoluble iron, such as siderophores. SEM images show that after three days, aerobic ML2 culture cells were visible in a matrix of solids, whereas no cells in anaerobic cultures were observed. The absence of visible cells in anaerobic culture solids may be a function of the charging effects on the specimen surface, making imaging of the sample difficult, or the cells may have been obscured by thick biofilms and mineral precipitates. After three weeks, cells from both aerobic and anaerobic cultures appeared to be completely encrusted in precipitates.

3. Nitrate as an Electron Acceptor for Anaerobic Iron Oxidation

The potential for anaerobic iron oxidation was investigated through the addition of nitrate to cultures which would serve as an electron acceptor. Metabolic predictions in reference to nitrogen pathways for Coast Range and Philippines fluid chemistry indicate that the energetically favorable metabolisms were denitrification and nitrification, respectively (Cardace et al. 2012; Cardace et al. 2015). If iron oxidation coupled to nitrate reduction is metabolically possible, it is expected that microbial communities would reflect microbes capable of this metabolism, and the reduced precipitates in the cultures would become oxidized (Weber et al. 2006). This could be visually indicated by a change in color from black to red precipitates by one of the following reactions:



The results of the experiment did not visually indicate nitrate-dependent iron(II)oxidation. Instead, red precipitates in the anaerobic QV1,3 culture became black and magnetic, indicating that iron reduction occurred anaerobically in the presence of nitrate. Fluorescence microscopy images of the cells showed a dominance of endospore morphologies, very similar to those seen in ML2 cultures

after three days. DNA sequencing revealed that the dominant genus in the culture was *Clostridium*, a genus that is also dominant in ML2 cultures. Here, two possibilities are presented.

1) The result may indicate that the QV1,3 anaerobic culture was contaminated with sample from an ML2 culture during the addition of NaNO_3 . The similarities in biomagnetite production, cell morphologies, and enrichment for *Clostridium* and the expectation for nitrification only in ML2 fluids support the potential for contamination.

2) A metabolic pathway is possible where ammonia oxidation is coupled to the reduction of iron in a pathway known as *feammox*. This has been described in anaerobic environments (Huang et al. 2015), but is not well understood (Groenigen et al. 2015). Although *Clostridia* was not a dominant taxa in QV1,3 culture communities without nitrate, *Clostridia* was present in low abundances, and was cultured in microcosm experiments from neighboring wells at the CROMO field site (Crespo-Medina et al. 2014). An alternative to the idea that the *Clostridia* may have been a sign of contamination from an ML2 culture is the possibility of nitrate as a limiting nutrient for the *feammox* pathway by *Clostridia* in QV1,3 cultures. Replicate experiments and direct measurements of iron and ammonia concentrations are necessary to further explore the possibility of *feammox* in these cultures.

Nitrate-dependent solid-phase iron(II) oxidation products are not limited to red mineral precipitates, but include maghemite, lepidocrocite, arsenopyrite and pyrite (Weber et al. 2001; Weber et al. 2006). Sample fluid and sediment chemistries included arsenic and sulfur, making precipitation of the previously listed alternative minerals a possibility. Therefore, it is possible that anaerobic iron oxidation occurred in the ML2 cultures but could not be identified visually because a change in color could not be observed, and further analysis by XPS may be necessary to document

changes in precipitate oxidation states.

D. Comparison of Taxa in this Study

1. Alpha Diversity

Alpha diversity, which analyzes the diversity within a single sample, calculated at the family level (Figure 31) shows that the ML2 inoculum sediments were more diverse, followed by the QV1,3 experiments and inoculum sediments, and most ML2 experiments were less diverse. The QV1,3 anaerobic culture with added NaNO_3 was least diverse. The maximum and minimum number of observed families at a depth of 25000 sequence reads was 257.3 and 61.6, respectively.

Alpha diversity calculated at the species level (Figure 32) showed a similar trend as that calculated at the family level, with the majority of QV1,3 experiments being more diverse and ML2 experiments being less diverse. The most diverse was the anaerobic ML2 microcosm Phase II sediment community, and least diverse was the QV1,3 anaerobic culture with added NaNO_3 . The maximum and minimum number of observed species at a depth of 25000 sequence reads was 448.9 and 85.9, respectively.

The difference in diversity observed between the ML2 inoculum and the culture experiments indicates that the cultures enriched for a select few taxa that were able to tolerate the culture conditions. This suggests that the ML2 community is composed of many specialists, of which a few were able to thrive under culturing conditions. In contrast, the diversity of the QV1,3 communities are similar to the inoculum sediment communities, except for the aerobic microcosm fluid communities. This suggests that the QV1,3 communities are more generalist and can cope with multiple conditions as a group.

Alpha Diversity | Family Level

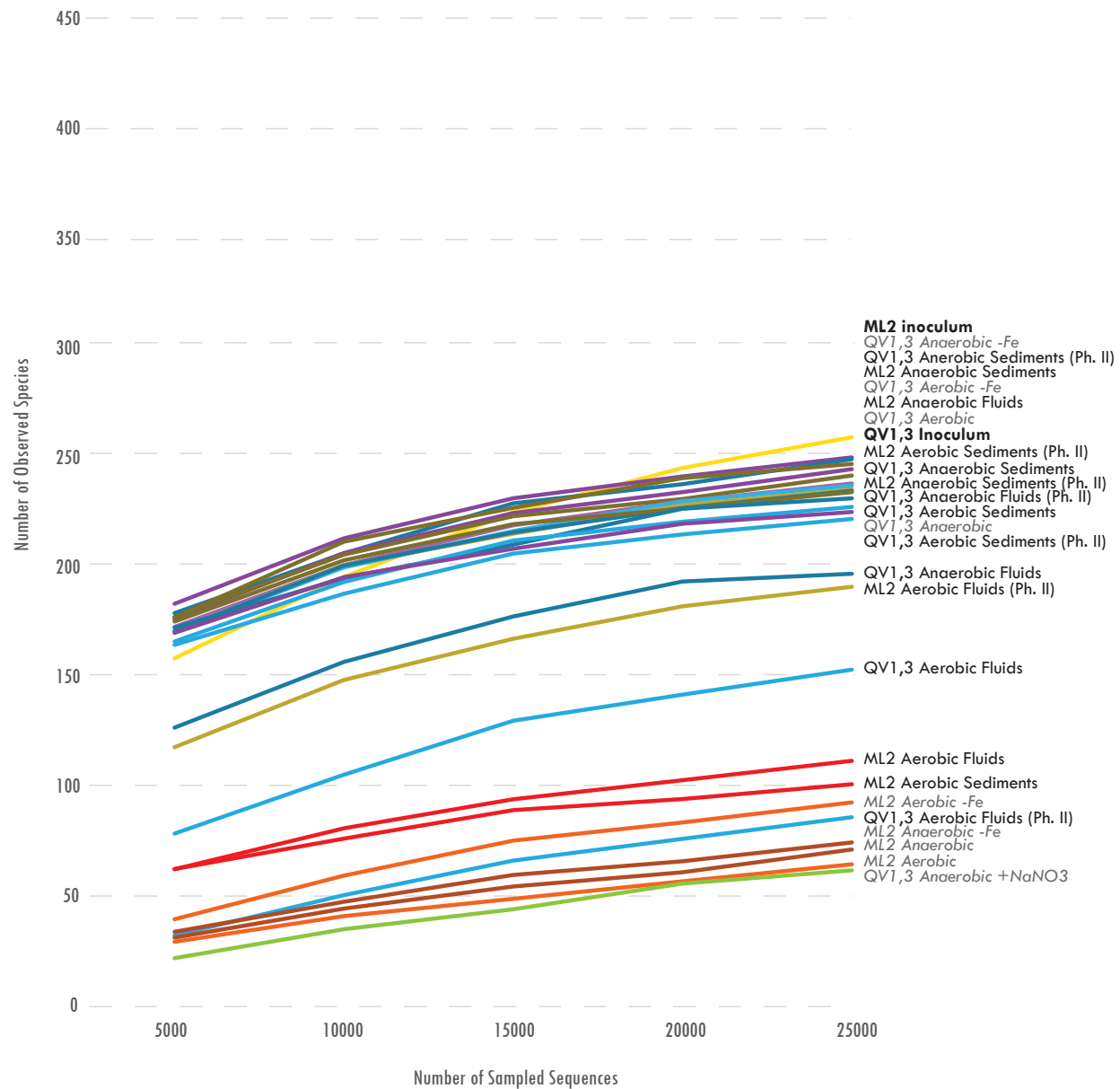


Figure 31. Alpha diversity of inoculum sediments, microcosms, and cultures (grey italic font) at the family level. Cool colors (blue and purple) indicate QV1,3 communities. Warm colors (red, orange, and yellow) indicate ML2 communities. The QV1,3 NaNO₃ community is symbolized in green. Phase II microcosm experiments are denoted as “Ph.II”.

Alpha Diversity | Species Level

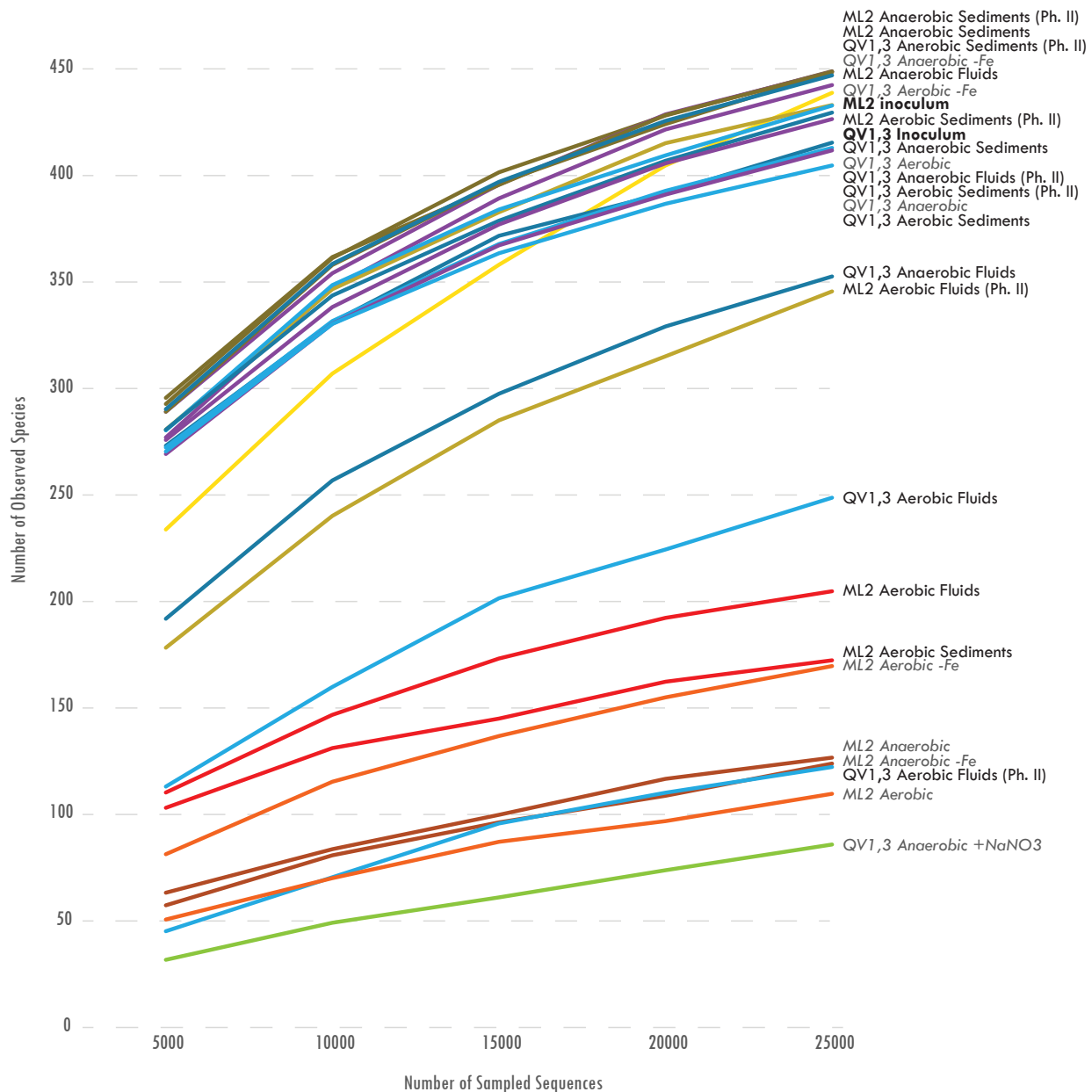


Figure 32. Alpha diversity of inoculum sediments, microcosms, and cultures (grey italic font) at the species level. Cool colors (blue and purple) indicate QV1,3 communities. Warm colors (red, orange, and yellow) indicate ML2 communities. The QV1,3 NaNO₃ community is symbolized in green. Phase II microcosm experiments are denoted as "Ph.II".

2. Beta Diversity

Beta diversity encompasses the diversity between multiple samples. The weighted beta diversity dendrogram (Figure 33), which accounts for abundances of observed species, indicates that the aerobic ML2 microcosm sediment community is an outlier, not grouping with any other community. This indicates that the conditions in the sediments of the aerobic ML2 microcosm supported a unique community among the experiments. The ML2 culture experiments form a single clade ('A' in Figure 33), indicating that the culture conditions enriched for similar communities in ML2 with only slight

Beta Diversity | Weighted Unifrac

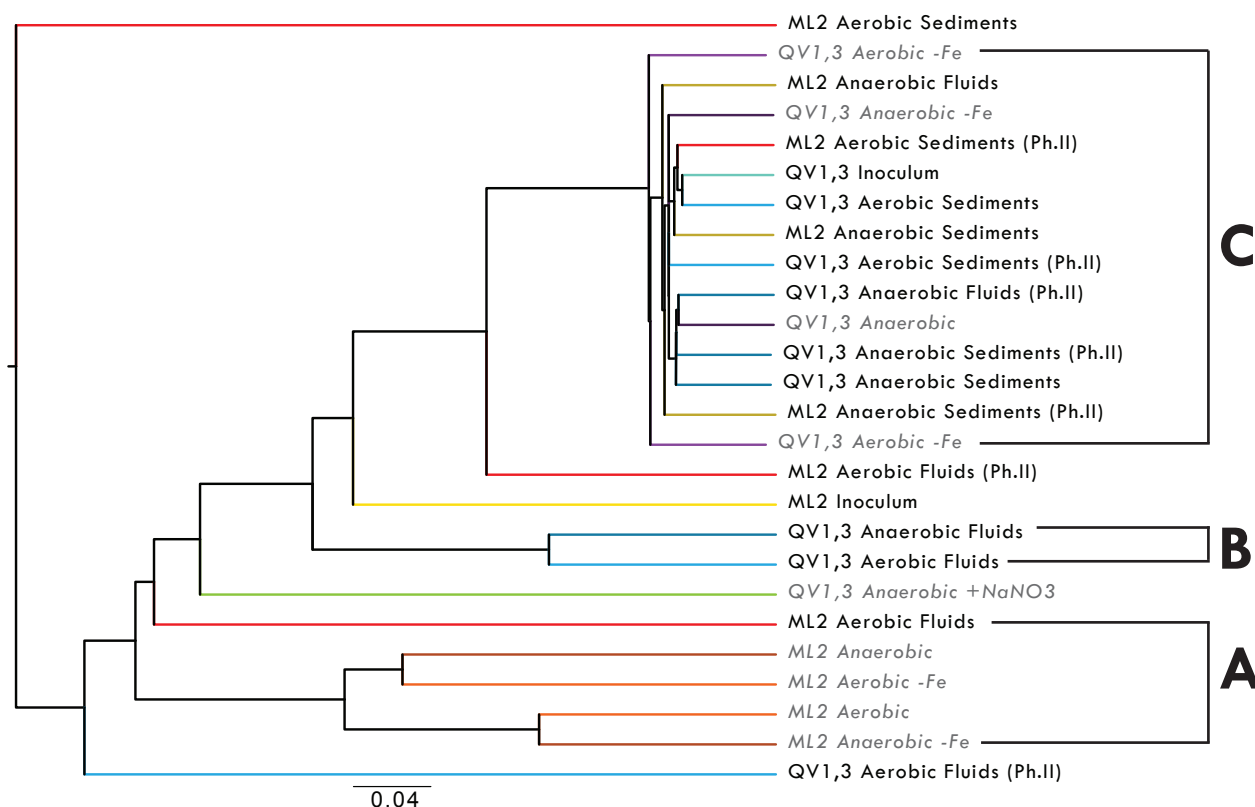


Figure 33. Beta diversity calculated with the weighted Unifrac metric showing clustering of inoculum sediment, microcosm, and culture communities (grey italic font). Cool colors (blue and purple) indicate QV1,3 communities. Warm colors (red, orange, and yellow) indicate ML2 communities. The QV1,3 NaNO₃ community is symbolized in green. Phase II microcosm experiments are denoted as “Ph. II”. Major clades are called “A, B, and C”. The scale bar indicates number of changes per site.

differences in the presence of iron. Phase I QV1,3 microcosm fluid communities formed a clade ('B' in Figure 33), indicating that QV1,3 fluids supported similar communities regardless of headspace or the presence of iron. One large clade encompasses the bulk of the communities, including all QV1,3 culture communities, the majority of Phase II QV1,3 microcosm communities, the Phase I anaerobic ML2 microcosm communities, and the QV1,3 inoculum sediments ('C' in Figure 33). This clade indicates that the compositions of those communities are very similar, suggestive of a subsurface community signature.

The unweighted beta diversity dendrogram (Figure 34), which accounts for only the presence or absence of species, shows that generally all ML2 communities cluster closely ('A' in Figure 34), with the exception of the aerobic ML2 Phase II fluid community. Again, Phase I fluid QV1,3 microcosm communities formed a clade ('B' in Figure 34), and a large clade encompasses all other QV1,3 communities ('C' in Figure 34), with the exception of the aerobic QV1,3 Phase II fluid community and the anaerobic culture with nitrate community. This large clade also includes experimental ML2 anaerobic sediment communities, indicative of a subsurface community signature.

Overall, the diversity dendrograms indicate that common communities were present among QV1,3 experiments and the QV1,3 inoculum, whereas ML2 microcosm and culture communities varied greatly, indicating that the ML2 culture experiments selected for a different set of communities. The amounts of organic carbon and iron precipitates in the culture experiments seemed to direct changes in the ML2 community structures, but not QV1,3 community structures, suggesting that these may be limiting nutrients in the ML2 microcosm experiments. The fluid chemistry at the ML2 site agrees with this idea, as the concentration of iron in ML2 spring fluids was below detection limits. The opposite may be true for QV1,3 communities, as 47 mg/L of iron was detected in QV1,3 well fluids. Iron reduction may have also been more favorable in ML2 spring fluids, with a redox potential of -424.7

Beta Diversity | Unweighted Unifrac

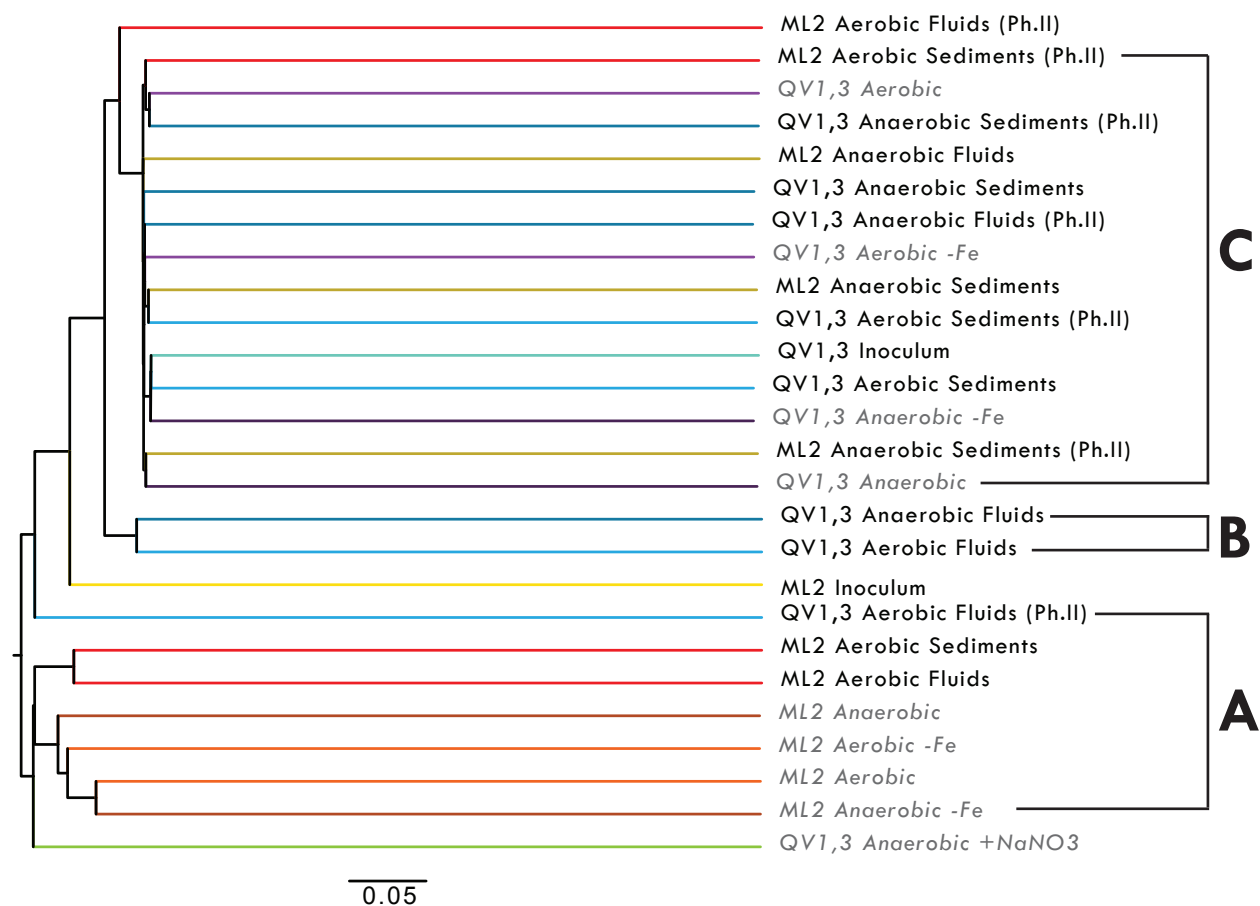


Figure 34. Beta diversity calculated with the unweighted Unifrac metric showing clustering of inoculum sediment, microcosm, and culture communities (grey italic font). Cool colors (blue and purple) indicate QV1,3 communities. Warm colors (red, orange, and yellow) indicate ML2 communities. The QV1,3 NaNO₃ community is symbolized in green. Phase II microcosm experiments are denoted as “Ph.II”. Major clades are called “A, B, and C”. The scale bar indicates number of changes per site.

in ML2 fluids compared to a redox potential of -77 in QV1,3 well fluids.

Dominant taxa in the experiments agree with metabolic interpretations that iron oxidation and reduction occurred in the culture experiments. Several taxa are known to be capable of oxidizing or reducing iron, including *Bacillus*, *Clostridium*, and *Alkaliphilus* (all dominant in ML2 cultures), as well as *Dechloromonas* (one of the dominant taxa in QV1,3 cultures) (Grossman et al. 1993; Dobbin

et al. 1999; Roh, 2007). Visual observations and the presence of biomagnetite in ML2 microcosm sediments and ML2 culture precipitates were interpreted as indications of iron reduction, which is consistent with iron-reducing taxa in communities from those experiments. The aerobic ML2 microcosm was dominated by *Pseudomonas*, known to be capable of producing siderophores (Meyer et al. 2002), as well as *Sedimentibacter* and *Sporanaerobacter*, both members of the order Clostridiales in which iron cycling organisms have been described (Whittleston et al. 2013). *Pseudomonas* and *Dechloromonas* were also dominant in experimental ML2 anaerobic microcosms and all QV1,3 microcosms and cultures, which were interpreted to host iron redox reactions.

E. Biosignature and Energy Signature Implications

Efforts have been made to quantify the amount of biomass in seafloor environments, and those estimates have been extrapolated to other subsurface environments (Kallmeyer et al. 2012), however serpentinizing subsurface environment biomass has not been directly estimated. This study supports the concept that serpentinization reactions support microbial communities in the subsurface, which may extend to depths of several kilometers, and represents a sizable fraction of potential biomass that has yet to be definitively quantified and accounted for in global carbon cycling models. Serpentinization reactions also generate gases such as hydrogen, which is interpreted in this study to play a role in microbial metabolisms in the serpentinizing subsurface and therefore may impact global gas flux models. However, gas fluxes in serpentinizing systems have yet to be well constrained. To fully address the extent of biomass and gas flux in serpentinizing systems, future drilling projects in the Zambales ophiolite serpentinizing system may require cell counts with depth and cell size and morphology characterization to calculate biomass as in Kallmeyer et al. 2012, and establishing year-round gas flux monitors. Cell counts within drilled material has been

performed at CROMO (Cardace et al. 2013), however total biomass in the Coast Range ophiolite serpentinizing subsurface system has not been estimated. CROMO wells have also been equipped with year-round data loggers, however these loggers are not monitoring gas flux.

Serpentinization could be occurring in the Martian subsurface, supported by strong evidence of the presence of liquid water on Mars (Ojha et al. 2015). If the brine comes in contact with olivine-bearing rock in the subsurface, then olivine may react with water and generate similar fluid chemistries to what is observed in terrestrial serpentinizing systems, which in turn, may also support similar microbial life. The potential for oxidized iron to be transported to the subsurface (and therefore contribute to redox gradients) by brines should also be noted, as the Martian surface has copious amounts of oxidized iron. The preservation potential of microbial life has been demonstrated in this study. Biominerals, such as nanowires, in serpentinizing systems may be a useful biosignature in Martian systems. This study contributes to the knowledge base of terrestrial serpentinizing systems that may aid in our search for extraterrestrial life in the future.

VI. CONCLUSION

The Coast Range and Zambales ophiolite serpentinizing systems were hypothesized to support subsurface microbial iron metabolisms based on fluid and gas chemistry. This study investigated iron metabolisms in these systems through microcosm and culture experiments. Microbial life has been suggested to be ubiquitous across serpentinizing systems. To address this idea, a taxonomic comparison of the communities sampled for this study were compared to serpentinizing communities described in various locations around the world.

1. Ubiquity of Microbial Communities Among Terrestrial Serpentinizing Systems

A comparison of communities from various serpentinizing systems around the world indicated that Firmicutes and Proteobacteria were dominant across all systems, suggestive of their ubiquity across global systems. Variations in global microbial communities could also be explained by analytical techniques, such as differences in primer sets used in sequencing, and local environmental variations such as climate and fluid source rock, which may affect fluid chemistries.

The communities representative of the deep subsurface in this study were those of the QV1,3 sediments drilled from the Coast Range ophiolite and the Butili rock core drilled from the Zambales ophiolite. The similarities among the QV1,3 inoculum sediment community and the communities in aerobic QV1,3 microcosm sediments and anaerobic QV1,3 and ML2 sediments, which were dominantly composed of pulverized Butili rock core, suggest a subsurface community signature. These communities also shared dominant taxa with QV1,3 microcosm fluid communities and QV1,3 culture communities, further supporting a subsurface community signature. Two dominant taxa, *Hydrogenophaga* and *Pseudomonas*, were shared with ML2 aerobic microcosm communities

and ML2 culture communities, which were inoculated with sediments sampled at the surface where serpentinizing fluids were influenced by atmospheric gases. The shared taxa among the subsurface communities (QV1,3 inoculum sediments and Butili rock core) and surface community (ML2 inoculum sediments) suggest that surface communities reflect a relict subsurface signature composed of taxa that are capable of transitioning from subsurface to surface conditions.

2. Microbial Alteration of Mineralogy

Microbe-mineral interactions were observed through microcosm experiments. SEM images of rock chips in the microcosms indicated biofilm formation on mineral surfaces, however XEDS did not establish a preference for iron-bearing minerals. Secondary mineral precipitates were observed on rock chip surfaces in both QV1,3 and ML2 microcosms, indicating a microbial influence on mineralogy. Further, a color change was observed in ML2 microcosm sediments under anaerobic conditions, which did not occur in control microcosms, indicating an influence on sediment chemistry in the presence of microbes. QV1,3 and ML2 microcosm sediment communities shared dominant taxa, indicative of a subsurface community signature reflective of QV1,3 sediment communities and the Zambales rock core communities sampled from drilling. The similarity in sediment communities across QV1,3 and ML2 microcosms is contrasted by the differences in their fluid communities, suggestive that fluids promoted microbial growth in all experiments. Dominant taxa differed between simulated surface and subsurface microcosms, which suggests that the QV1,3 and ML2 community structures were influenced by the presence of oxygen and hydrogen. The influence of oxygen was highlighted by the color change from brown to grey in ML2 sediments under anaerobic conditions, which became brown again under aerobic conditions, as well as by XPS data, which suggest that the microbes in QV1,3 and ML2 communities engaged in redox reactions.

3. Iron Redox in Terrestrial Serpentinizing Communities

Iron metabolisms were suggested to be feasible in the Coast Range and Zambales serpentinizing subsurface systems, which were investigated through culturing with iron hydroxide.

ML2 cultures enriched for microbial iron reduction, consistent with energy availability predictions for the Zambales system. Iron reduction in ML2 cultures was indicated by the precipitation of magnetite in live cultures, which did not occur in sterile controls, as well as by XPS data indicative of the iron precipitates being reduced relative to the iron in the sterile control. Fluorescence microscopy and DNA sequencing of ML2 communities indicated a difference between cultures with and without iron, which suggests that microbial community structures were influenced by the presence of iron. ML2 cultures enriched for communities composed of taxa known to be capable of iron metabolisms, such as *Pseudomonas*, *Clostridium*, *Alkaliphilus*, and *Bacillus*, and these taxa were more abundant in cultures with iron.

In contrast to ML2 culture experiments, QV1,3 cultures may have enriched for both microbial iron oxidation and reduction. These metabolisms are supported by XPS data, which show that the iron precipitates in the QV1,3 aerobic culture were oxidized relative to the control, and the precipitates in the anaerobic culture were reduced relative to the control. Fluorescence microscopy images show different cell morphologies between cultures with and without iron, indicating that the presence of iron affected QV1,3 community structures. Microbial iron oxidation and reduction in the QV1,3 cultures were further supported by DNA sequencing, which indicated communities with taxa capable of iron oxidation and reduction (*Dechloromonas* and *Pseudomonas*). Additionally, nanowire-like structures were observed in SEM images of QV1,3 culture precipitates, which were not observed in sterile control or ML2 culture precipitates, potentially indicating a mechanism of electron transport between cells and iron precipitates.

CITED LITERATURE

- Anderson, R. E., Brazelton, W. J., Baross, J. A. (2013). The deep virosphere: assessing the viral impact on microbial community dynamics in the deep subsurface. *Rev Mineral Geochem*, 75: 649-675.
- Arcilla, C. A., Pascua, C. S., Alexander, W. R. (2011). Hyperalkaline groundwaters and tectonism in the Philippines: Significance to natural carbon capture and sequestration. *Energy Procedia*, 4: 5093-5101.
- Blank, J. G., Green, S. J., Blake, D., Valley, J. W., Kita, N. T., Treiman, A. (2009). An alkaline spring system within the Del Puerto Ophiolite (California, USA): a Mars analog site. *Planetary Space Science*, 5: 533–540.
- Brazelton, W. J. (2010). Ecology of archaeal and bacterial biofilm communities at the Lost City hydrothermal field. University of Washington.
- Brazelton, W. J., Morrill, P. L., Szponar, N., Schrenk, M. O. (2013). Bacterial communities associated with subsurface geochemical processes in continental serpentinite springs. *Applied and environmental microbiology*, 79: 3906-3916.
- Cardace, D., Hoehler, T. M. (2009). Serpentinizing fluids craft microbial habitat. *Northeastern Naturalist*, 16: 272-284.
- Cardace, D., Meyer-Dombard, D., Arcilla, C., Hoehler, T., McCollom, T., Schrenk, M. (2013). Microbial metabolic landscapes derived from complementary mineralogical, aqueous geochemical, and gas data associated with high pH, actively serpentinizing springs in the Coast Range ophiolite (CA, USA) and Zambales and Palawan ophiolites (Philippines). Abstract B13C-0503 presented at 2013 Fall Meeting, AGU, San Francisco, Calif., 9-13 Dec.
- Cardace, D., Meyer-Dombard, D. R., Woycheese, K. M., Arcilla, C. (2015). Feasible metabolisms in high pH springs in the Philippines. *Frontiers in Extreme Microbiology*, 6: 1-16.
- Cardace, D., Hoehler, T., McCollom, T., Schrenk, M. O., Kubo, M. (2015). Integration of 3 Consecutive Years of Aqueous Geochemistry Monitoring in the Coast Range Ophiolite Microbial Observatory (CROMO), Northern California. Abstract #7515 presented at 2015 Meeting, AbSciCon, Chicago, Illinois, 15-19 Jun.
- Charlou, J. L., Donval, J. P., Konn, C., OndréAs, H., Fouquet, Y., Jean-Baptiste, P. and Fourré, E. (2010) High production and fluxes of H₂ and CH₄ and evidence of abiotic hydrocarbon synthesis by serpentinization in ultramafic-hosted hydrothermal systems on the Mid-Atlantic Ridge, in *Diversity of Hydrothermal Systems on Slow Spreading Ocean Ridges* (eds P. A. Rona, C. W. Devey, J. Dymont and B. J. Murton), American Geophysical Union, Washington, D. C.

- Chivian, D., Brodie, E. L., Alm, E. J., Culley, D. E., Dehal, P. S., DeSantis, T. Z., Gihring, T. M., Lapidus, A., Lin, L., Lowry, S. R., Moser, D. P., Richardson, P. M., Southam, G., Wanger, G., Pratt, L. M., Andersen, G. L., Hazen, T. C., Brockman, F. J., Arkin, A. P., Onstott, T. C. (2008). Environmental genomics reveals a single-species ecosystem deep within Earth. *Science*, 322: 275-278.
- Crespo-Medina, M., Twing, K. I., Kubo, M. D. Y., Hoehler, T. M., Cardace, D., McCollom, T., Schrenk, M. O. (2014). Insights into environmental controls on microbial communities in a continental serpentinite aquifer using a microcosm-based approach. *Frontiers in Microbiology*, 5: 604.
- Daae, F. L., Økland, I., Dahle, H., Jørgensen, S. L., Thorseth, I. H., Pedersen, R. B. (2013). Microbial life associated with low-temperature alteration of ultramafic rocks in the Leka ophiolite complex. *Geobiology*, 11: 318-339.
- Dobbin, P. S., Carter, J. P., San Juan, C. G. S., von Hobe, M., Powell, A. K., Richardson, D. J. (1999). Dissimilatory Fe (III) reduction by *Clostridium beijerinckii* isolated from freshwater sediment using Fe (III) maltol enrichment. *FEMS microbiology letters*, 176: 131-138.
- Dong, H., Fredrickson, J. K., Kennedy, D. W., Zachara, J. M., Kukkadapu, R. K., Onstott, T. C. (2000). Mineral transformations associated with the microbial reduction of magnetite. *Chemical Geology*, 169: 299-318.
- Du, M., Yvon-Lewis, S., Garcia-Tigereros, F., Valentine, D., Mendes, S., Kessler, J. (2014). High resolution measurements of methane and carbon dioxide in surface waters over a natural seep reveal dynamics of dissolved phase air-sea flux. *Environmental Science and Technology*, 48: 10165-10173.
- Ehlmann, B., Mustard, J., Murchie, S. (2010). Geologic setting of serpentine deposits on Mars. *Geophysical Research Letters*, 37: 1-5.
- Etioppe, G., Ehlmann, E., Schoell, M. (2013). Low temperature production and exhalation of methane from serpentinized rocks on Earth: A potential analog for methane production on Mars. *Icarus*, 224: 276-285.
- Fajardo-Cavazos, P., Nicholson, W. (2006). *Bacillus* endospores isolated from granite: close molecular relationships to globally distributed *Bacillus* spp. from endolithic and extreme environments. *Applied and environmental microbiology*, 72: 2856-2863.
- Greenberger, R., Mustard, F., Cloutis, E., Pratt, L., Sauer, P., Mann, P., Turner, K., Dyar, D., Bish, D. (2015). Serpentinization, iron oxidation, and aqueous conditions in an ophiolite: Implications for hydrogen production and habitability on Mars. *Earth and Planetary Science Letters*, 416: 21-34.
- van Groenigen, J. W., Huygens, D., Boeckx, P., Kuyper, T. W., Lubbers, I. M., Rütting, T., Groffman, P. M. (2015). The soil N cycle: new insights and key challenges. *Soil*, 1: 235-256.

- Grossman, T. H., Tuckman, M., Ellestad, S., Osburne, M. S. (1993). Isolation and characterization of *Bacillus subtilis* genes involved in siderophore biosynthesis: relationship between *B. subtilis* *sfpo* and *Escherichia coli* *entD* genes. *Journal of bacteriology*, 175: 6203-6211.
- Hansel, C. M., Benner, S. G., Neiss, J., Dohnalkova, A., Kukkadapu, R. K., Fendorf, S. (2003). Secondary mineralization pathways induced by dissimilatory iron reduction of ferrihydrite under advective flow. *Geochimica et Cosmochimica Acta*, 67: 2977-2992.
- Hashimoto, H., Yokoyama, S., Asaoka, H., Kusano, Y., Ikeda, Y., Seno, M., Takada, J., Fujii, T., Murakami, R. (2007). Characteristics of hollow microtubes consisting of amorphous iron oxide nanoparticles produced by iron oxidizing bacteria, *Leptothrix ochracea*. *Journal of Magnetism and Magnetic Materials*, 310: 2405-2407.
- Huang, S., Jaffé, P. R. (2015). Characterization of incubation experiments and development of an enrichment culture capable of ammonium oxidation under iron-reducing conditions. *Biogeosciences*, 12: 769-779.
- Ionescu, D., Heim, C., Polerecky, L., Thiel, V., De Beer, D. (2015). Biotic and abiotic oxidation and reduction of iron at circumneutral pH are inseparable processes under natural conditions. *Geomicrobiology Journal*, 32: 221-230.
- Kallmeyer, J., Pockalny, R., Adhikari, R., Smith, D., D'Hondt, S. (2012). Global distribution of microbial abundance and biomass in seafloor sediment. *PNAS*, 40: 16213-16216.
- Konhauser, K. (1998). Diversity of bacterial iron mineralization. *Earth-Science Reviews*, 43: 91-121.
- Kormas, K. A., Smith, D. C., Edgcomb, V., Teske, A. (2003). Molecular analysis of deep subsurface microbial communities in Nankai Trough sediments (ODP Leg 190, Site 1176). *FEMS Microbiology Ecology*, 45: 115-125.
- Kotelnikova, S. (2002). Microbial production and oxidation of methane in deep subsurface. *Earth-Science Reviews*, 58: 367-395.
- Liu, X., Millero, F. J. (1999). The solubility of iron hydroxide in sodium chloride solutions. *Geochimica et Cosmochimica Acta*, 63: 3487-3497.
- Lorenz, R., Gleeson, D., Prieto-Ballesteros, O., Gomez, F., Hand, K., Bulat, S. (2011). Analog environments for a Europa lander mission. *Advances in Space Research*, 48: 689-696.
- Lovley, D. R., Malvankar, N. S. (2015). Seeing is believing: novel imaging techniques help clarify microbial nanowire structure and function. *Environmental microbiology*, 17: 2209-2215.
- Matlakowska, R., Skłodowska, A., Nejbart, K. (2012). Bioweathering of Kupferschiefer black shale (Fore-Sudetic Monocline, SW Poland) by indigenous bacteria: implication for dissolution and precipitation of minerals in deep underground mine. *FEMS microbiology ecology*, 81: 99-

110.

- McKay, C., Porco, C., Altheide, T., Davis, W., Kral, T. (2008). The possible origin and persistence of life on Enceladus and detection of biomarkers in the plume. *Astrobiology*, 8: 909-919.
- Meyer, J. M., Geoffroy, V. A., Baida, N., Gardan, L., Izard, D., Lemanceau, P., Achouak, W., Palleroni, N. J. (2002). Siderophore typing, a powerful tool for the identification of fluorescent and nonfluorescent pseudomonads. *Applied and Environmental Microbiology*, 68: 2745-2753.
- Morrill, P. L., Brazelton, W. J., Kohl, L., Rietze, A., Miles, S. M., Kavanagh, H., Schrenk, M. O., Ziegler, S. E., Lang, S. Q. (2014). Investigations of potential microbial methanogenic and carbon monoxide utilization pathways in ultra-basic reducing springs associated with present-day continental serpentinization: the Tablelands, NL, CAN. *Frontiers in Microbiology*, 5: 1-13.
- Nation, J. L. (1983). A new method using hexamethyldisilazane for preparation of soft insect tissues for scanning electron microscopy. *Biotechnic & Histochemistry*, 58: 347-351.
- Ojha, L., Wilhelm, M. B., Murchie, S. L., McEwen, A. S., Wray, J. J., Hanley, J., Masse, M., Chojnacki, M. (2015). Spectral evidence for hydrated salts in recurring slope lineae on Mars. *Nature Geoscience*.
- Reguera, G., McCarthy, K. D., Mehta, T., Nicoll, J. S., Tuominen, M. T., Lovley, D. R. (2005). Extracellular electron transfer via microbial nanowires. *Nature*, 435: 1098-1101.
- Reguera, G., Nevin, K. P., Nicoll, J. S., Covalla, S. F., Woodard, T. L., Lovley, D. R. (2006). Biofilm and nanowire production leads to increased current in *Geobacter sulfurreducens* fuel cells. *Applied and environmental microbiology*, 72: 7345-7348.
- Roh, Y., Chon, C. M., Moon, J. W. (2007). Metal reduction and biomineralization by an alkaliphilic metal-reducing bacterium, *Alkaliphilus metalliredigens* (QYMF). *Geosciences Journal*, 11: 415-423.
- Sawicki, J., Brown, D., Beveridge, T. (1995). Microbial precipitation of siderite and protoferrihydrite in a biofilm. *The Canadian Mineralogist*, 33: 1-6.]
- Schaedler, S., Burkhardt, C., Hegler, F., Straub, K. L., Miot, J., Benzerara, K., Kappler, A. (2009). Formation of cell-iron-mineral aggregates by phototrophic and nitrate-reducing anaerobic Fe (II)-oxidizing bacteria. *Geomicrobiology Journal*, 26: 93-103.
- Schulze-Makuch, D., Haque, S., Resendes de Sousa Antonio, M., Ali, D., Hosein R., Song, Y., Yang, J., Zaikova, A., Beckles, D., Guinan, E., Lehto, H., Hallam, S. (2011). Microbial life in a liquid asphalt desert. *Astrobiology*, 11: 241-258.
- Schrenk, M. O., Kelley, D. S., Delaney, J. R., Baross, J. A. (2003). Incidence and diversity of microorganisms within the walls of an active deep-sea sulfide chimney. *Applied and*

- Environmental Microbiology, 69: 3580-3592.
- Schrenk, M., Brazelton, W., Lang S. (2013). Serpentinization, Carbon, and Deep Life. *Reviews in Mineralogy & Geochemistry*, 75: 575-606.
- Shervais, J., Choi, S. H. (2011). Subduction initiation along transform faults: The proto-Franciscan subduction zone. *Lithosphere*, 4: 484-496.
- Stevens, T. O., McKinley, J. P. (1995). Lithoautotrophic microbial ecosystems in deep basalt aquifers. *Science*, 270: 450.
- Szponar, N., Brazelton, W. J., Schrenk, M. O., Bower, D. M., Steele, A., Morrill, P. L. (2013). Geochemistry of a continental site of serpentinization, the Tablelands Ophiolite, Gros Morne National Park: a Mars analogue. *Icarus*, 224: 286-296.
- Suzuki, S., Kuenen, J. G., Schipper, K., van der Velde, S., Ishii, S. I., Wu, A., Sorokin, A. T., Meng, X., Morrill, P. L., Kamagata, Y., Muyzer, G., Nealson, K. H. (2014). Physiological and genomic features of highly alkaliphilic hydrogen-utilizing Betaproteobacteria from a continental serpentinizing site. *Nature Communications*, 5: 1-12.
- Tiago, I., Veríssimo, A. (2013). Microbial and functional diversity of a subterrestrial high pH groundwater associated to serpentinization. *Environmental Microbiology*, 15: 1687-1706.
- Wankell, S., Germanovich, L., Lilley, M., Genc, G., DiPerna, C., Bradley, A., Olson, E., Girguis, P. (2011). Influence of subsurface biosphere on geochemical fluxes from diffuse hydrothermal fluids. *Nature Geoscience*, 4: 461-468.
- Weber, K. A., Picardal, F. W., Roden, E. E. (2001). Microbially catalyzed nitrate-dependent oxidation of biogenic solid-phase Fe (II) compounds. *Environmental Science & Technology*, 35: 1644-1650.
- Weber, K. A., Achenbach, L. A., Coates, J. D. (2006). Microorganisms pumping iron: anaerobic microbial iron oxidation and reduction. *Nature Reviews Microbiology*, 4: 752-764.
- Whittleston, R. A., Stewart, D. I., Mortimer, R. J. G., Burke, I. T. (2013). Enhancing microbial iron reduction in hyperalkaline, chromium contaminated sediments by pH amendment. *Applied Geochemistry*, 28: 135-144.
- Woycheese, K. M., Meyer-Dombard, D. M., Cardace, D., Arcilla, C. (2015). Out of the dark: Transitional subsurface-to-surface microbial diversity in a terrestrial serpentinizing seep (Manleluag, Pangasinan, the Philippines). *Frontiers in Microbiology*, 6: 1-12.
- Ye, Q., Roh, Y., Carroll, S. L., Blair, B., Zhou, J., Zhang, C. L., Fields, M. W. (2004). Alkaline anaerobic respiration: isolation and characterization of a novel alkaliphilic and metal-reducing bacterium. *Applied and environmental microbiology*, 70: 5595-5602.

APPENDIX A. DOCUMENTING MICROBE-MINERAL INTERACTIONS

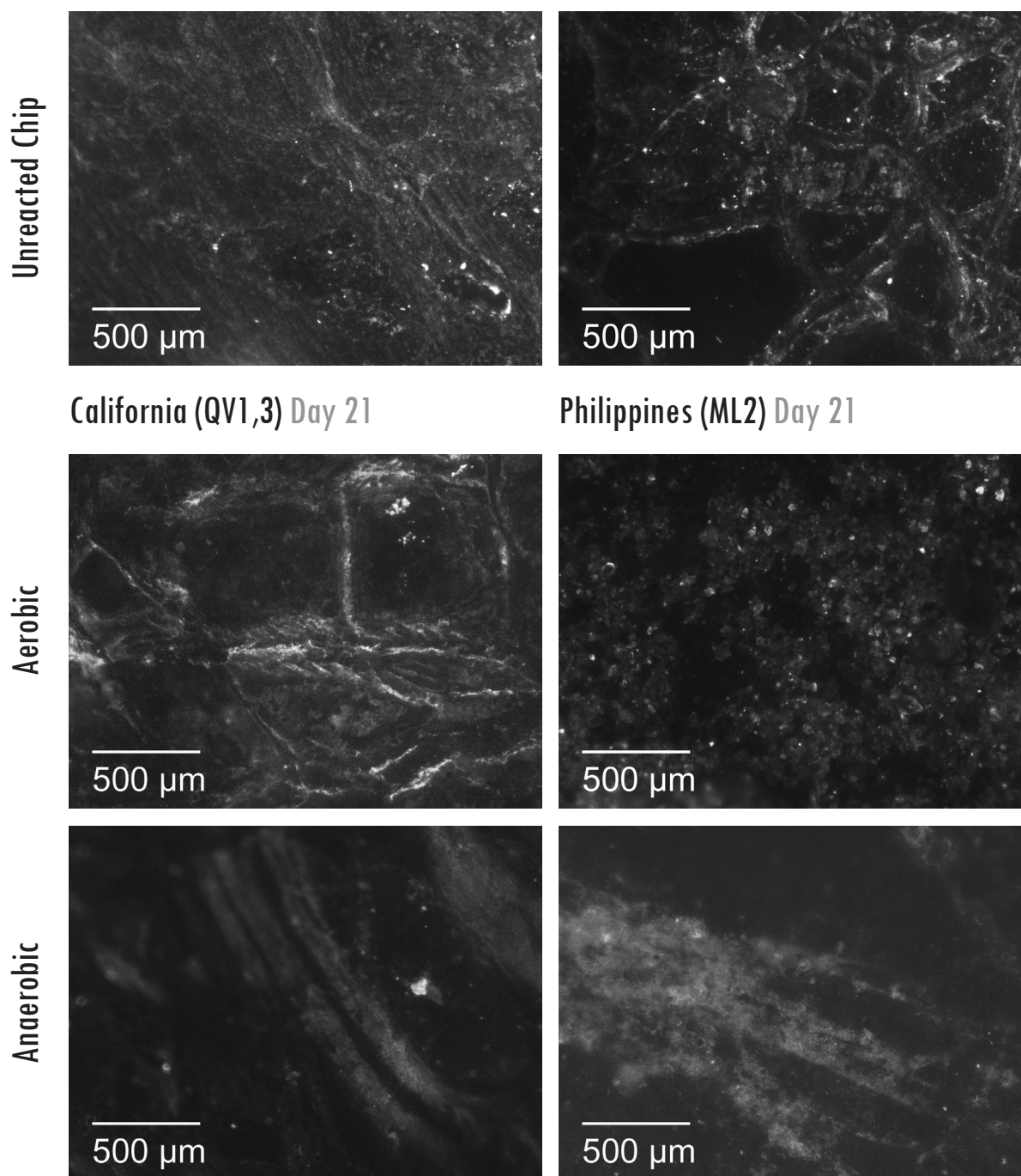


Figure 1. Fluorescence microscopy images of rock chips in microcosms showing the unreacted chip (top) and reacted chips from Phase I QV1,3 and ML2 microcosms after three weeks of growth.

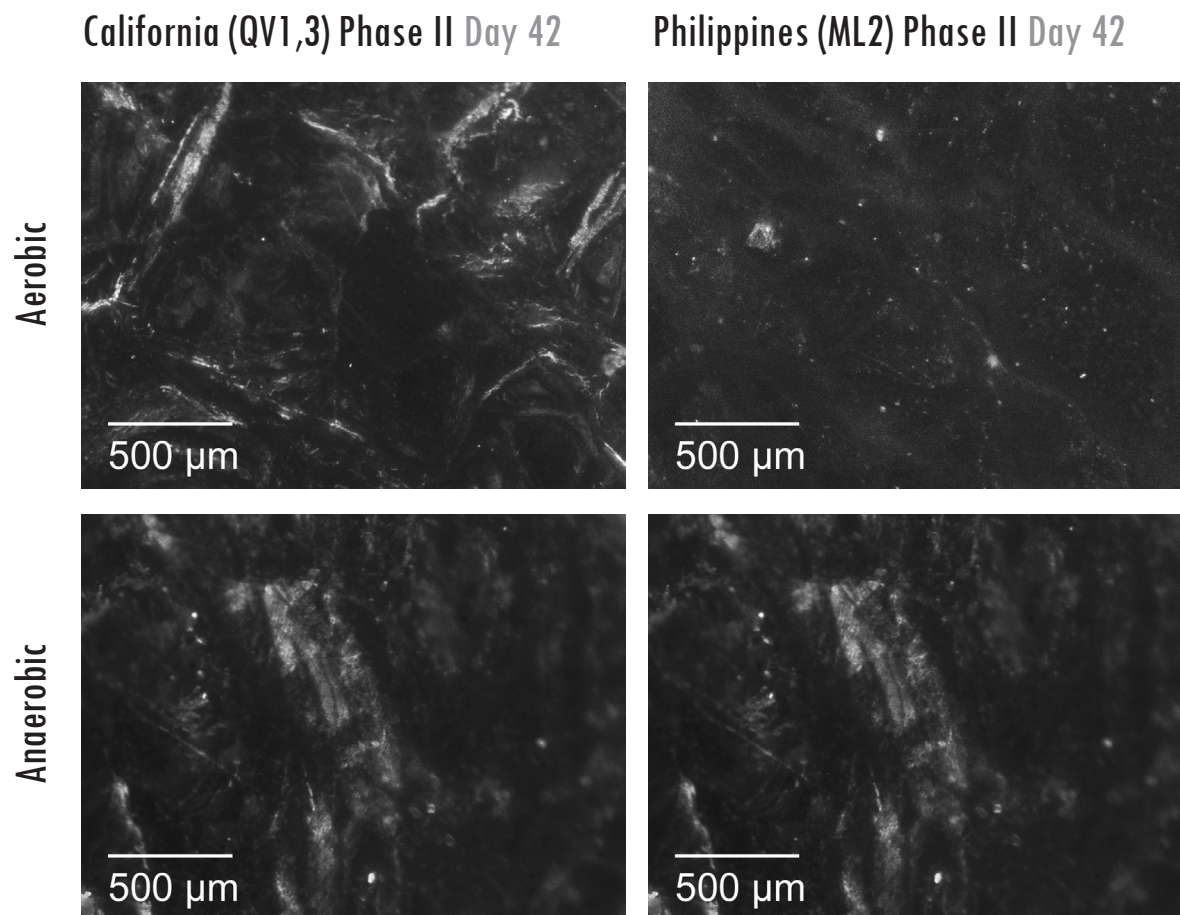


Figure 2. Fluorescence microscopy images of rock chips in microcosms showing reacted chips from Phase II (sterilized inoculum) California (QV1,3) and Philippines (ML2) microcosms after 42 days of growth.

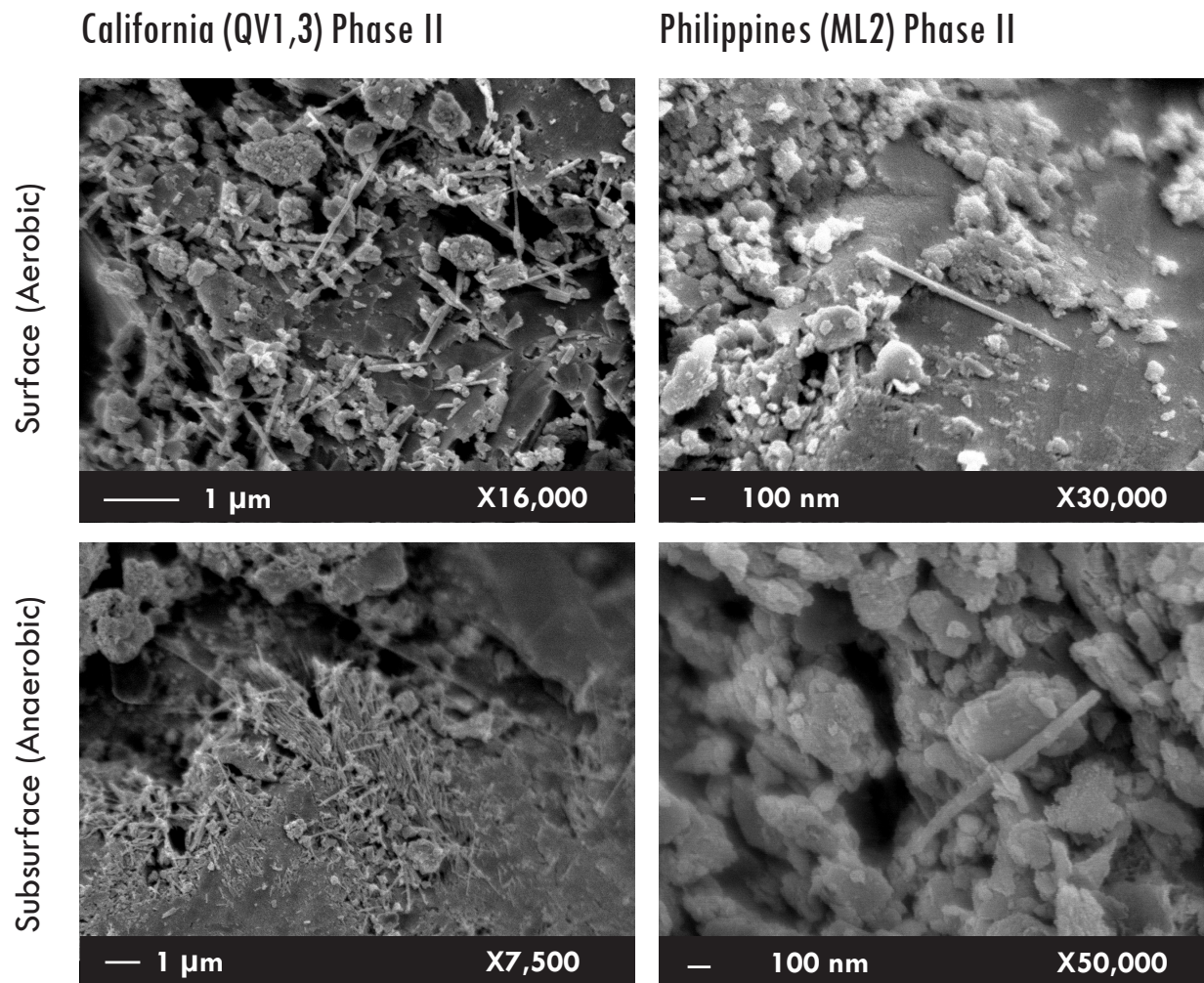


Figure 3. SEM images of rock chips in Phase II microcosms.

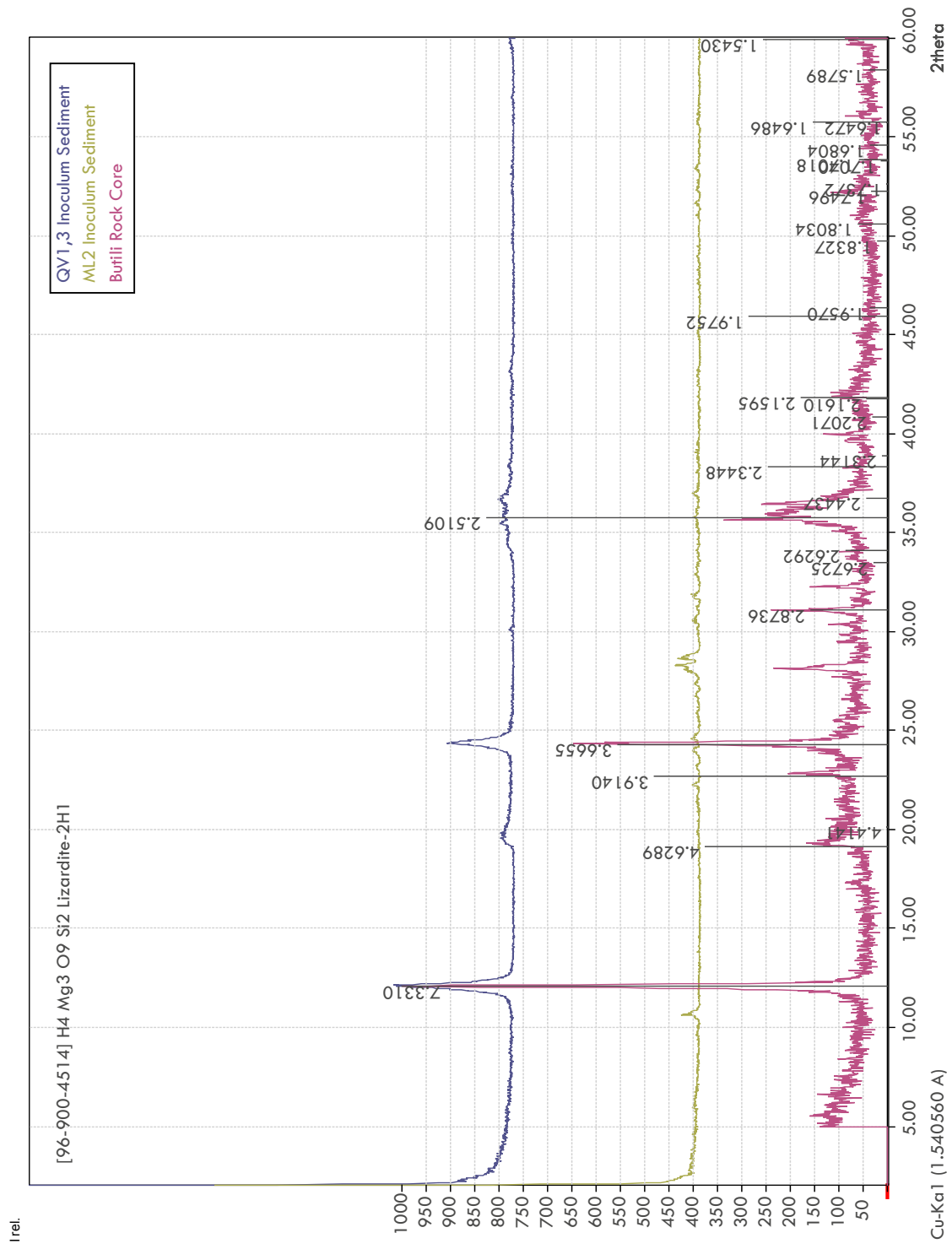


Figure 4. Inoculum sediments and rock core XRD patterns overlain with the standard pattern for lizardite (shown with d-values).

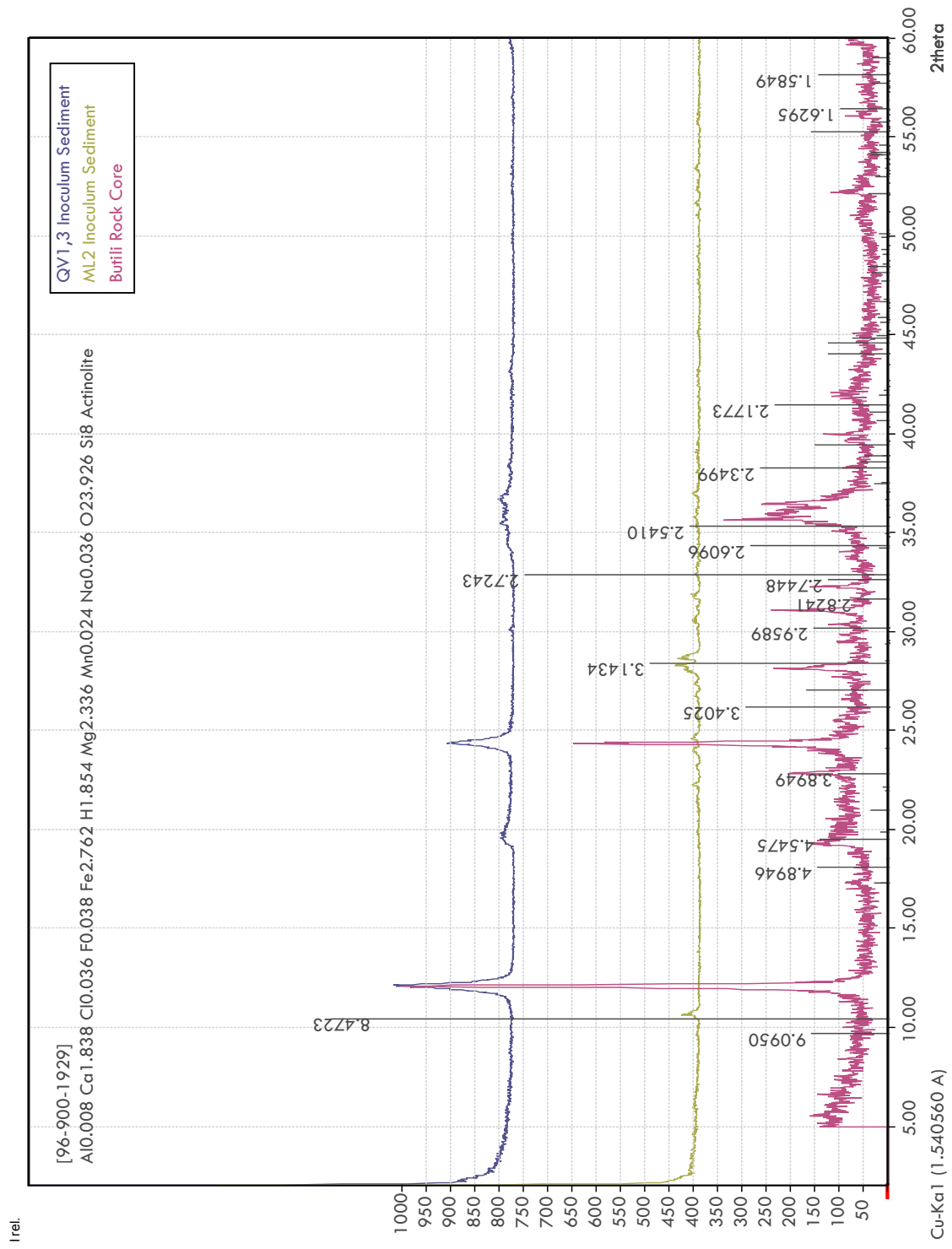


Figure 5. Inoculum sediments and rock core XRD patterns overlain with the standard pattern for actinolite (selected peaks are labeled with d-values).

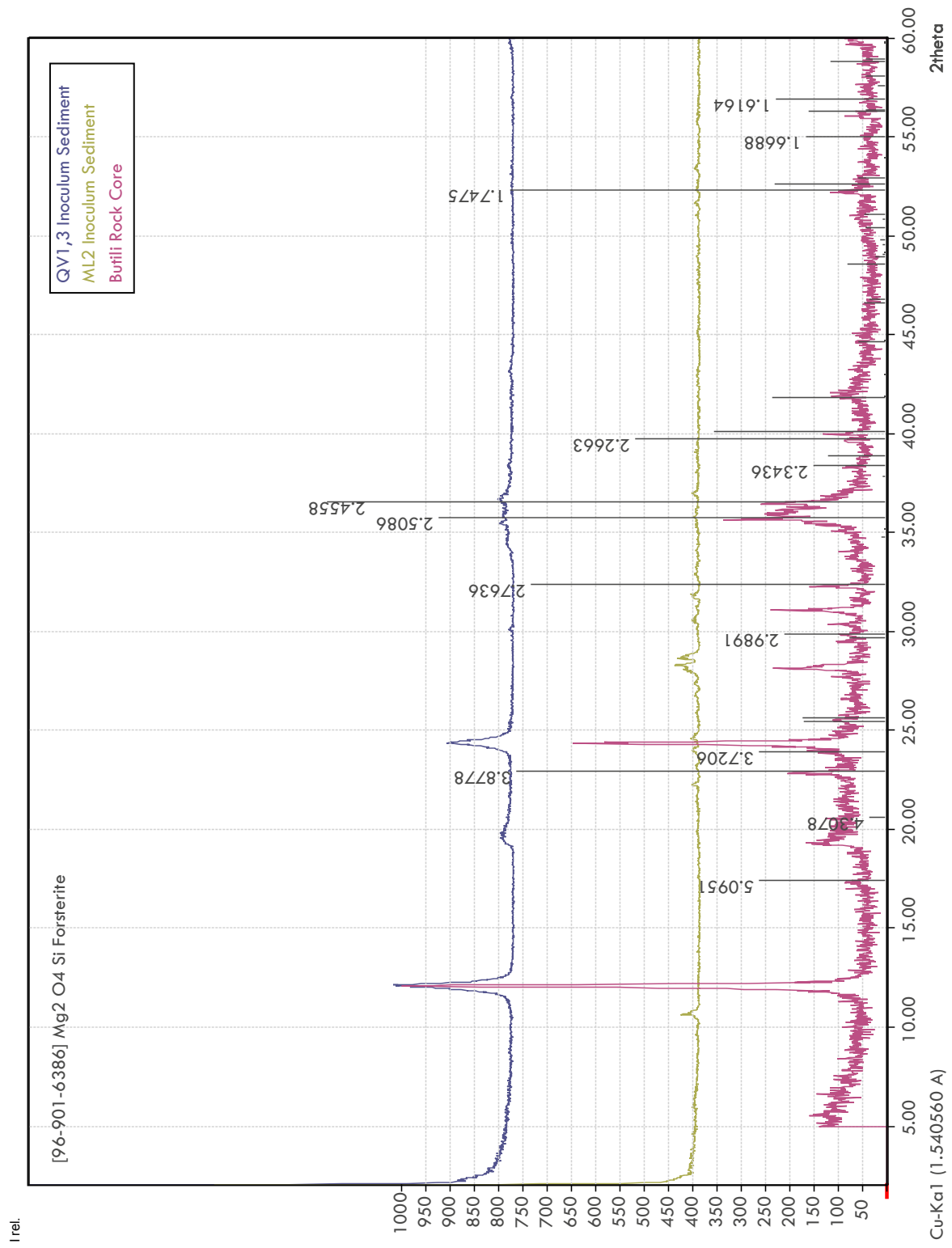


Figure 6. Inoculum sediments and rock core XRD patterns overlain with the standard pattern for forsterite (selected peaks are labeled with d-values).

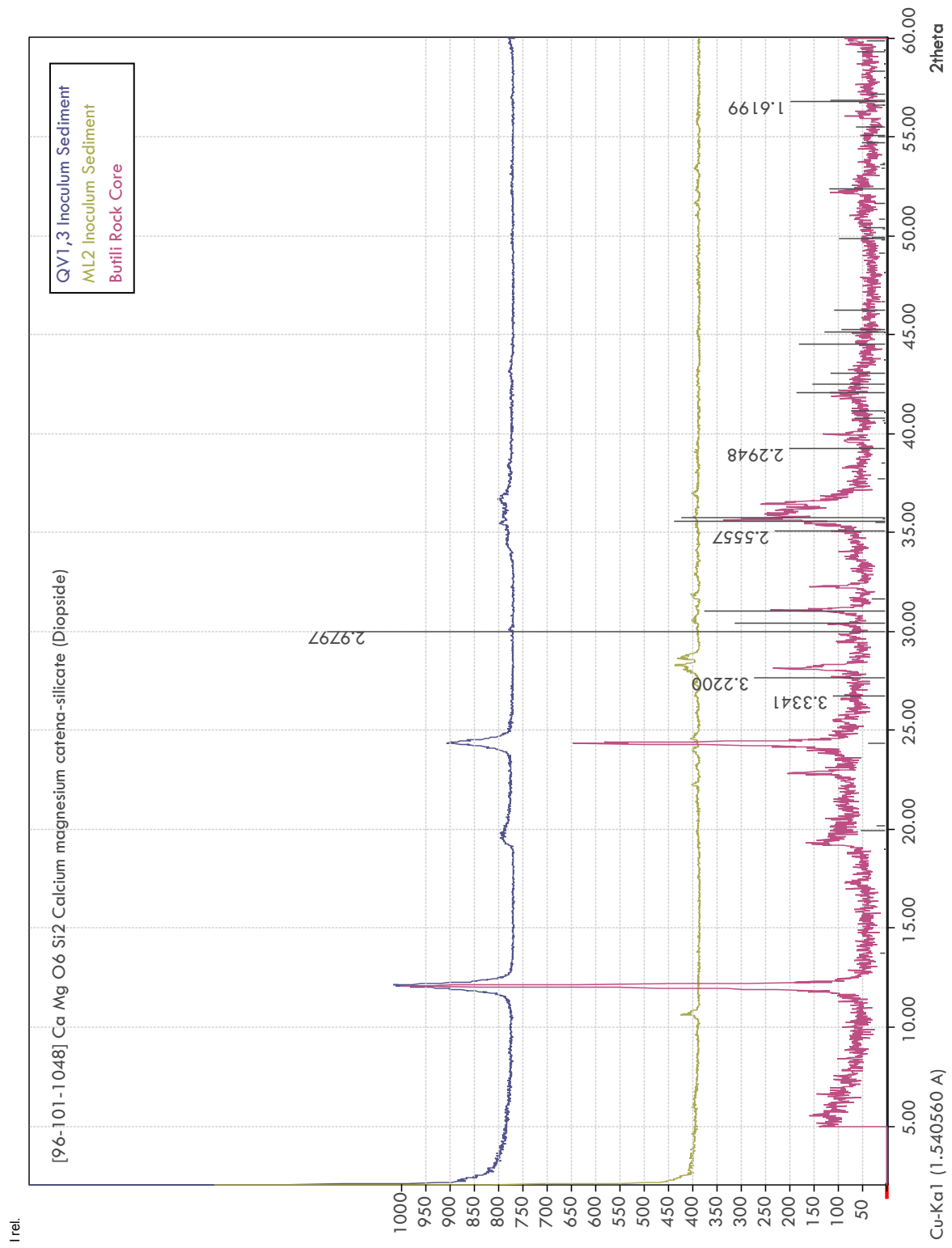


Figure 7. Inoculum sediments and rock core XRD patterns overlain with the standard pattern for diopside (selected peaks are labeled with d-values).

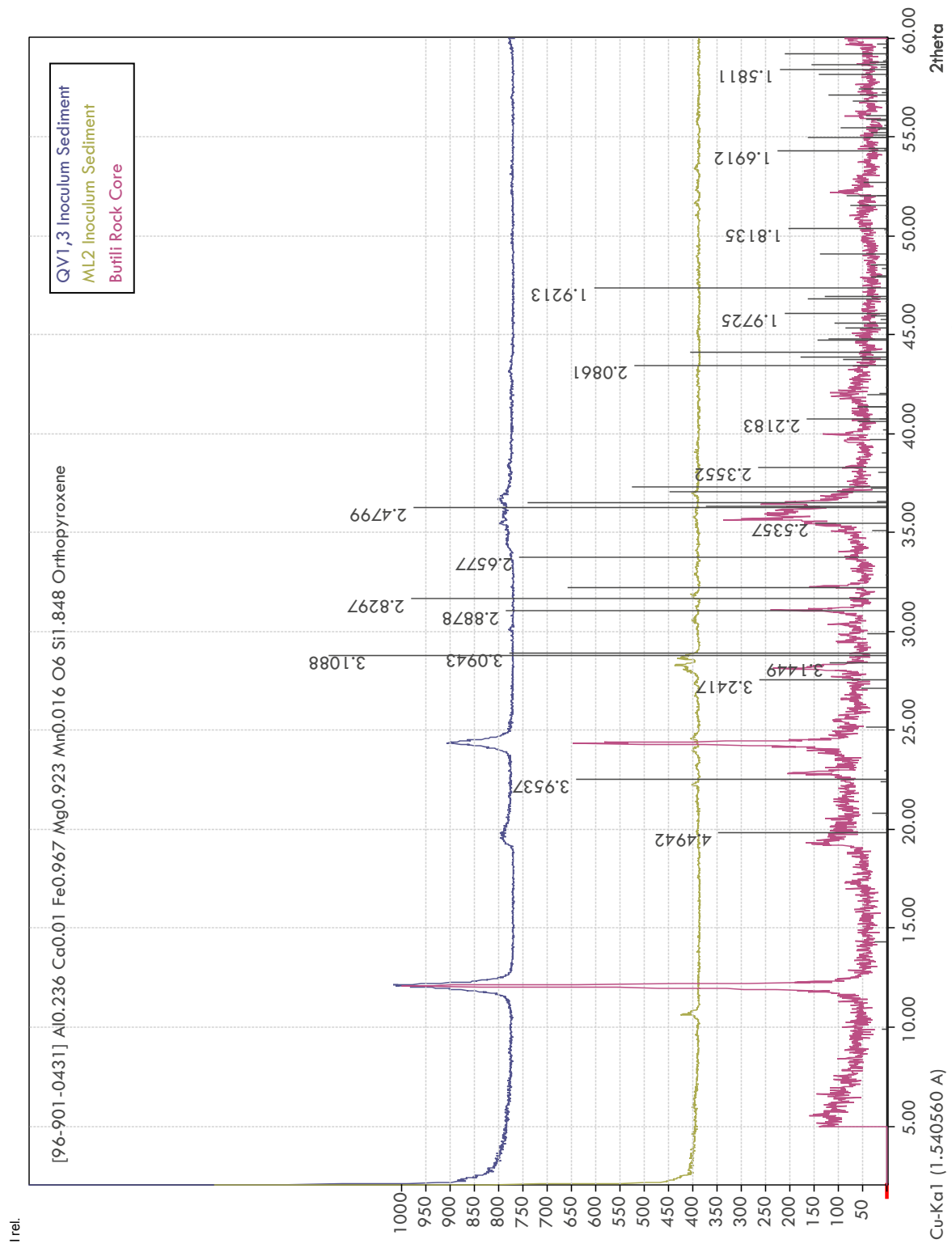


Figure 8. Inoculum sediments and rock core XRD patterns overlain with the standard pattern for orthopyroxene (selected peaks are labeled with d-values).

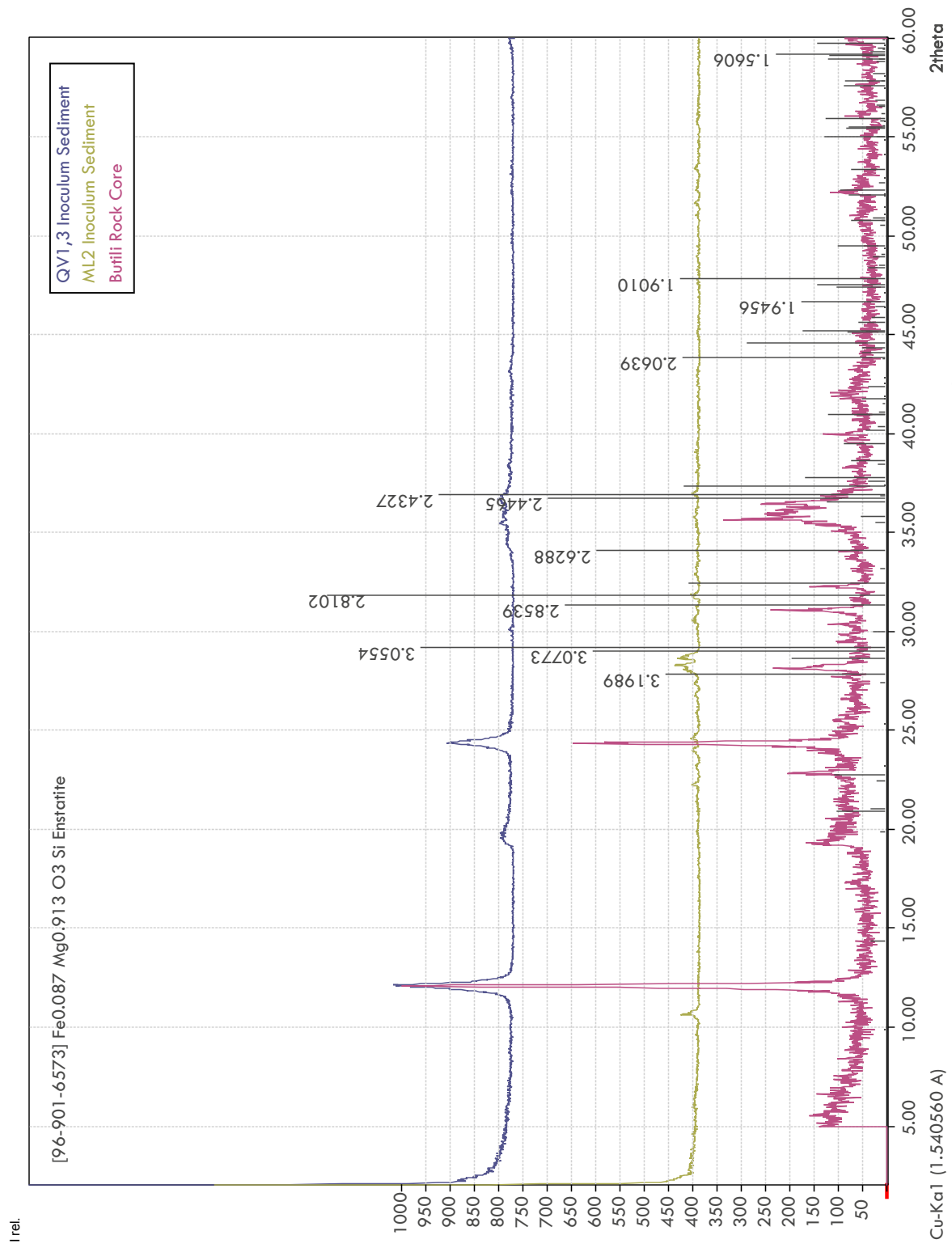


Figure 9. Inoculum sediments and rock core XRD patterns overlain with the standard pattern for enstatite (selected peaks are labeled with d-values).

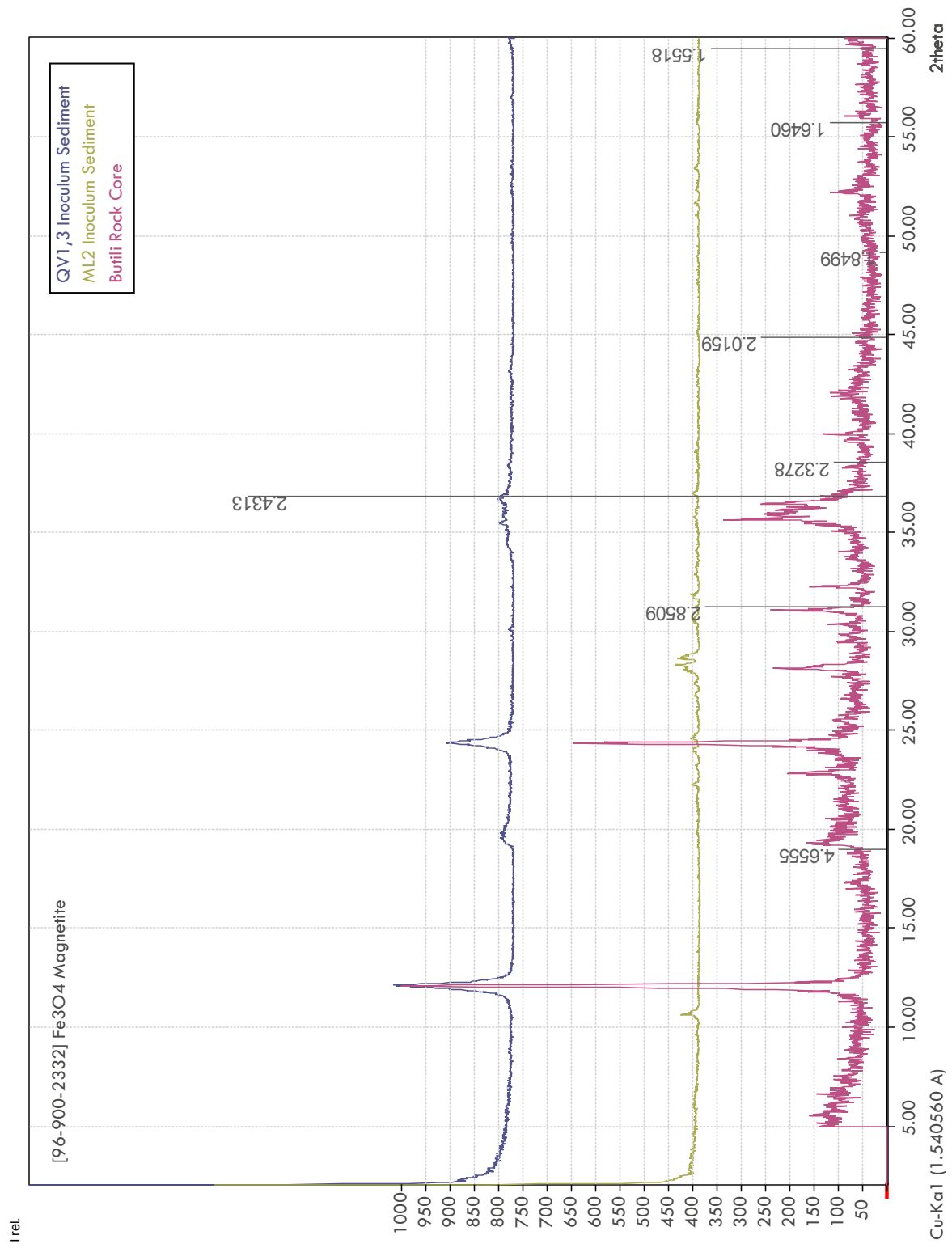


Figure 10. Inoculum sediments and rock core XRD patterns overlain with the standard pattern for magnetite(2332) (shown with d-values).

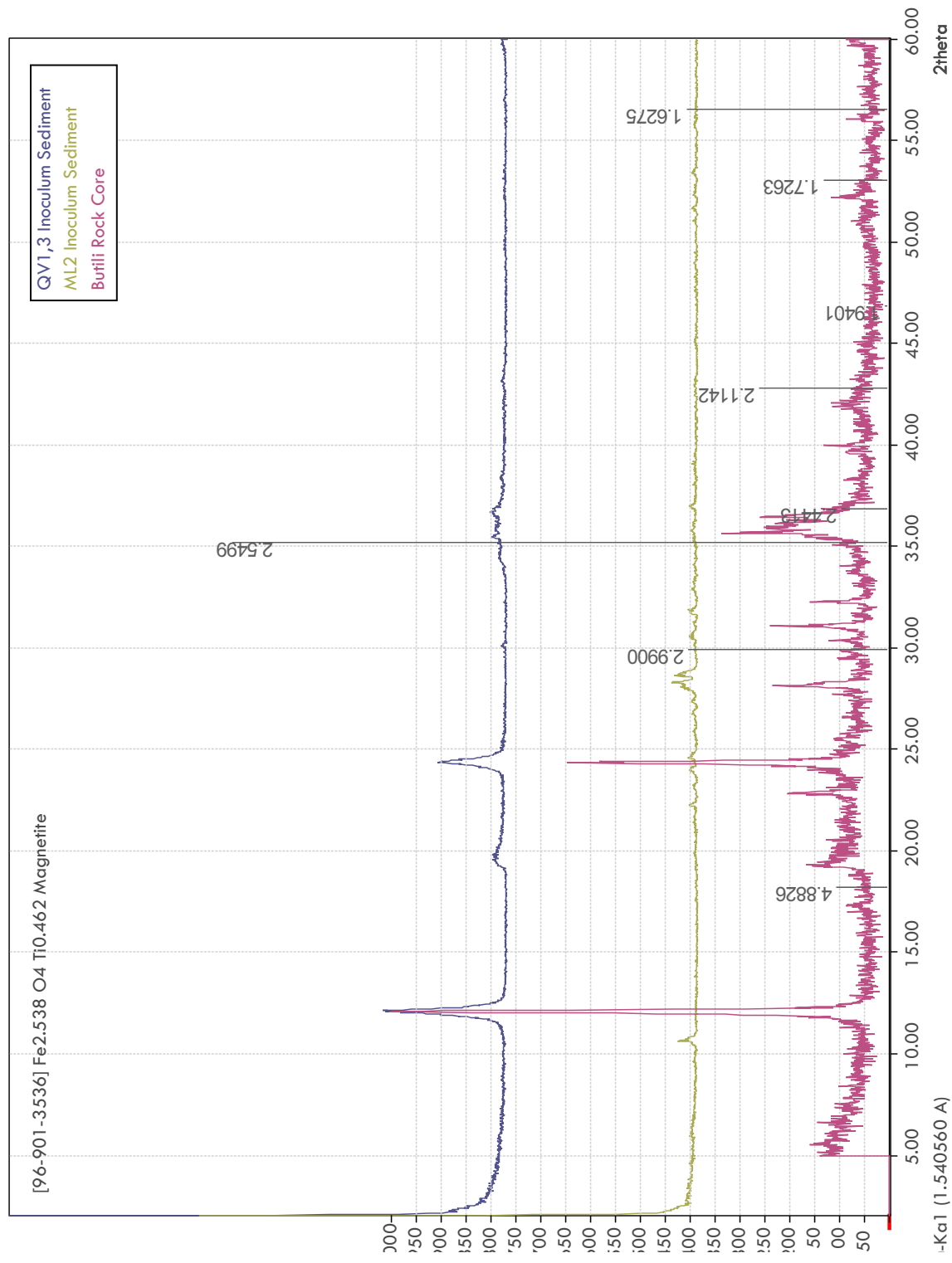


Figure 11. Inoculum sediments and rock core XRD patterns overlain with the standard pattern for magnetite(3536) (shown with d-values).

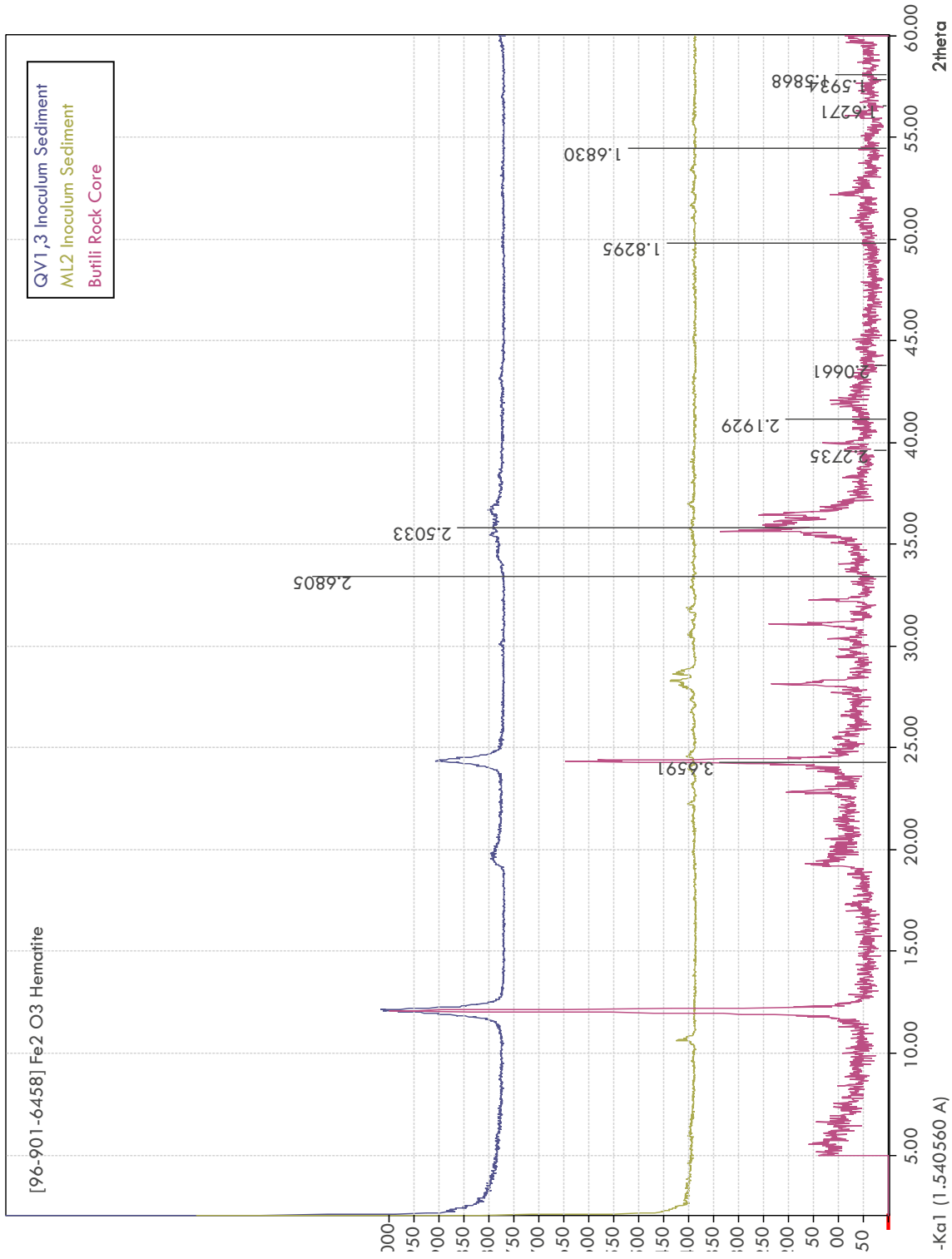


Figure 12. Inoculum sediments and rock core XRD patterns overlain with the standard pattern for hematite (shown in d-values).

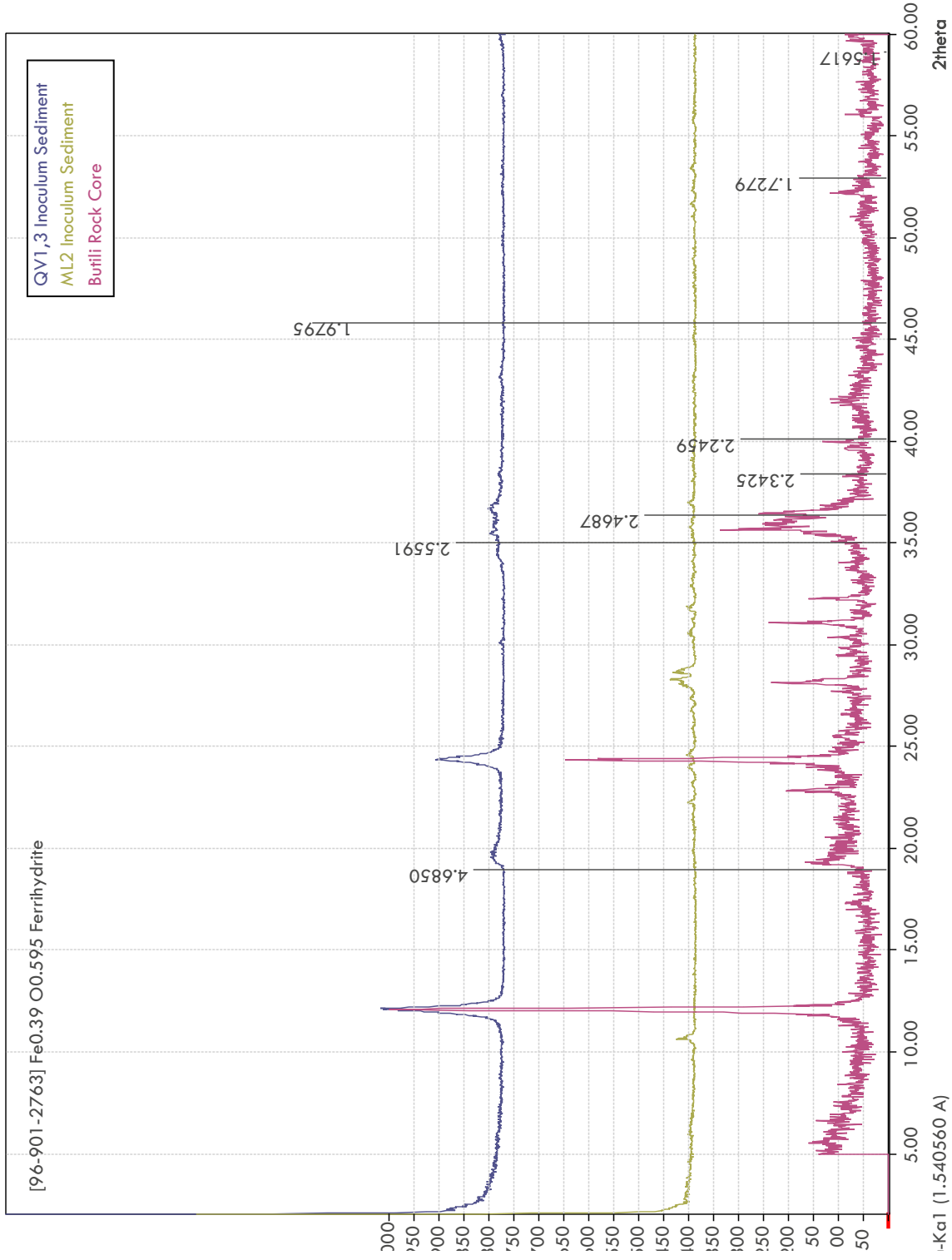


Figure 13. Inoculum sediments and rock core XRD patterns overlain with the standard pattern for ferrihydrite (shown with d-values).

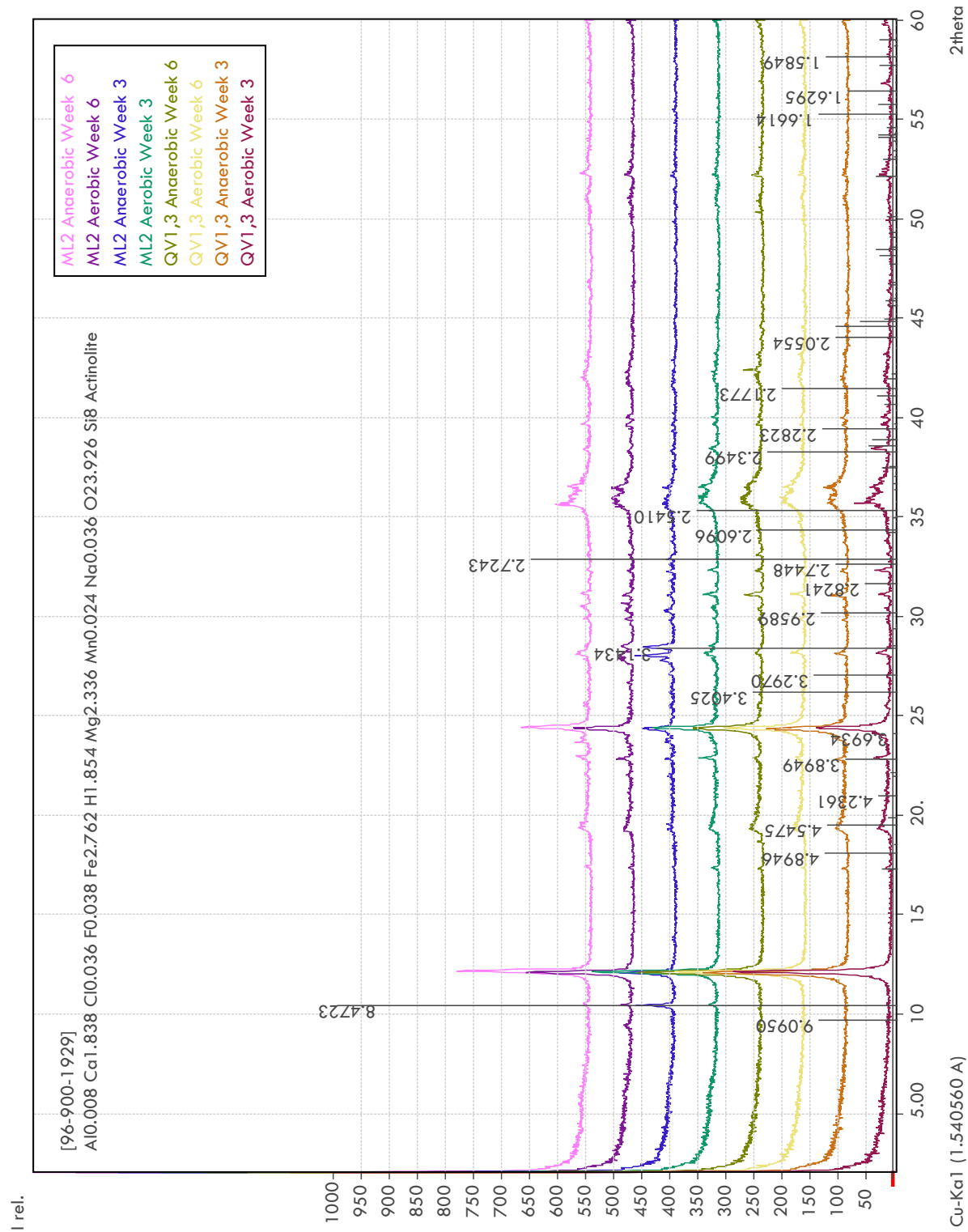


Figure 14. Phase I microcosm XRD patterns overlain with the standard pattern for actinolite (selected peaks are labeled with d-values).

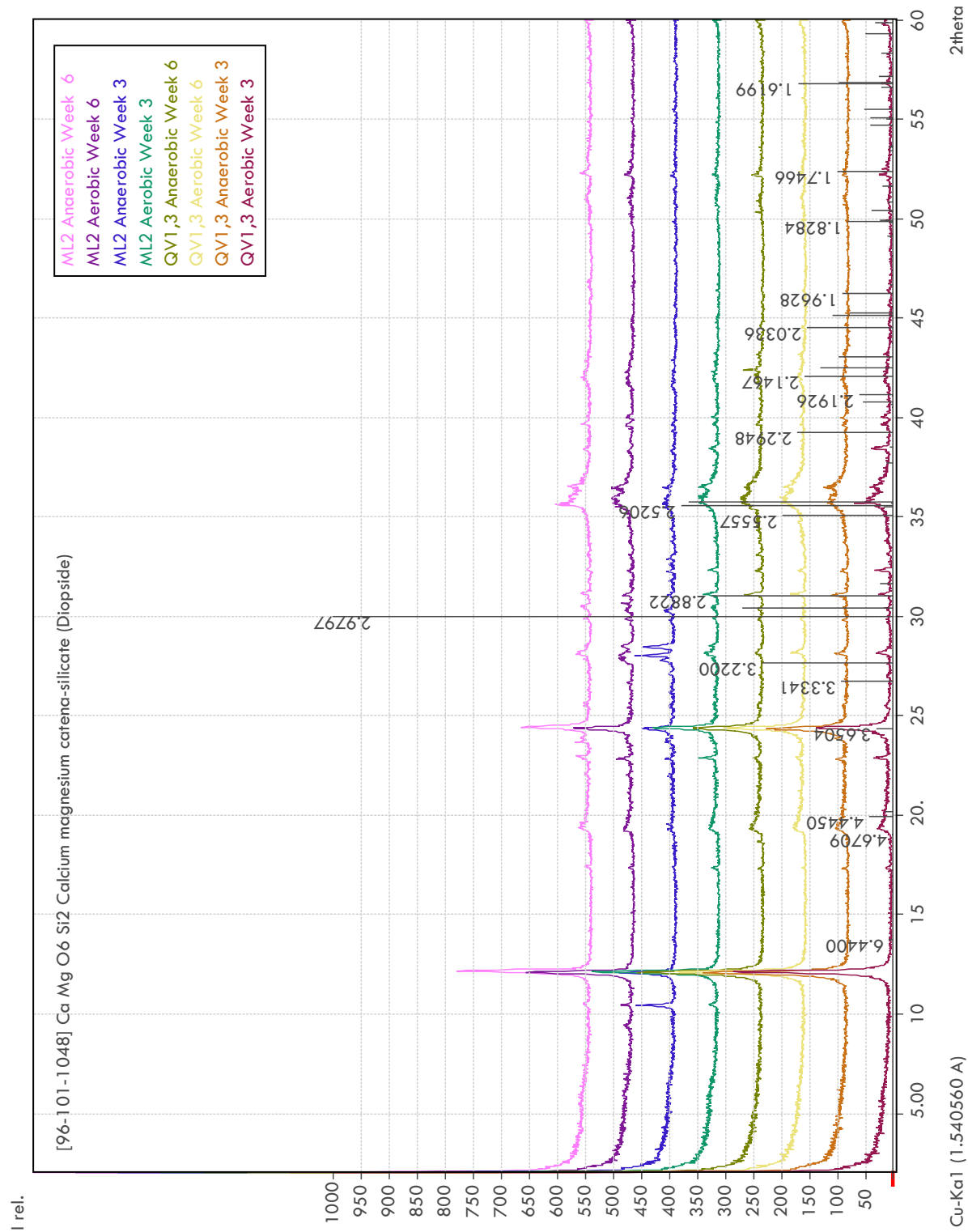


Figure 15. Phase I microcosm XRD patterns overlain with the standard pattern for diopside (selected peaks are labeled with d-values).

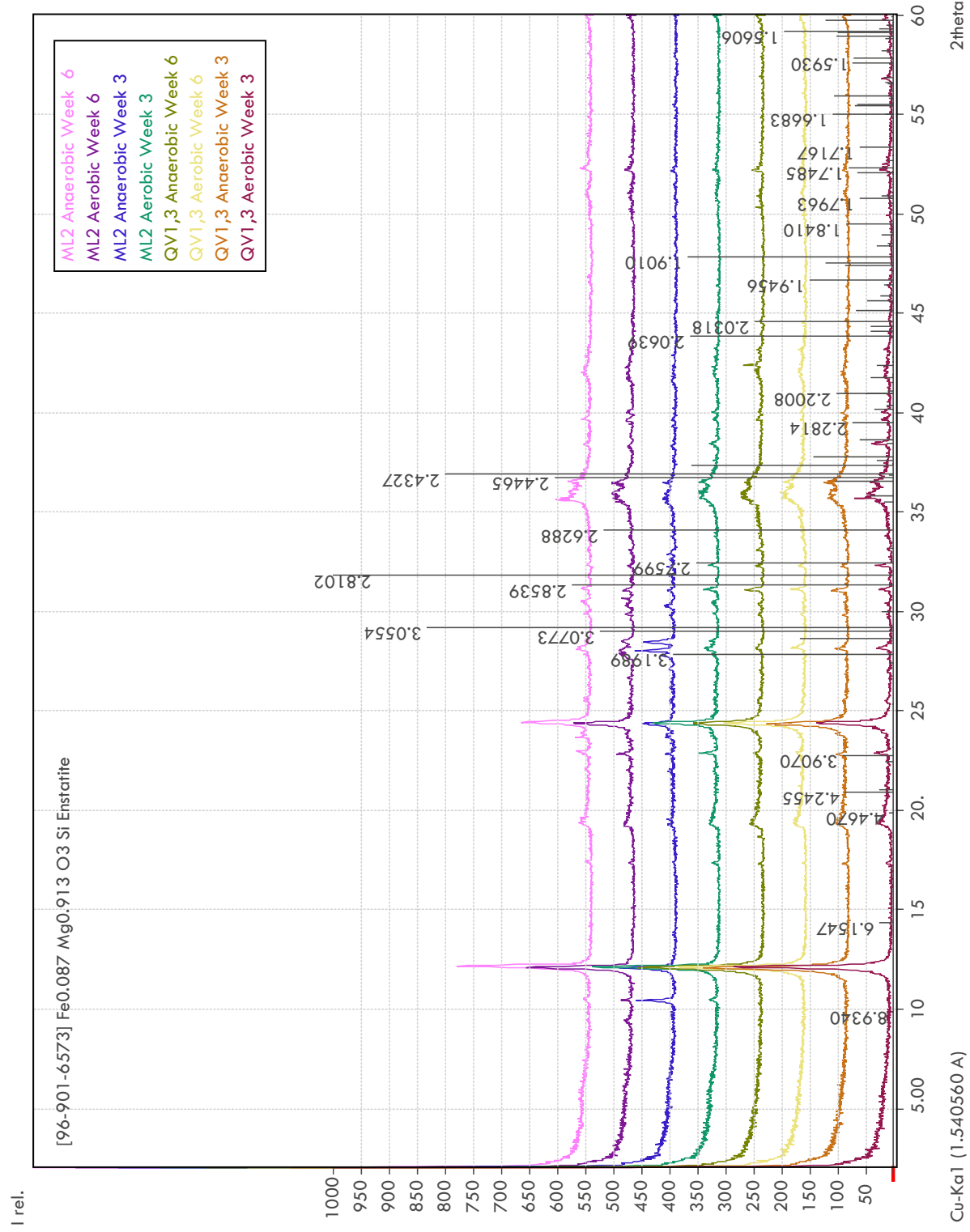


Figure 16. Phase I microcosm XRD patterns overlain with the standard pattern for enstatite (selected peaks are labeled with d-values).

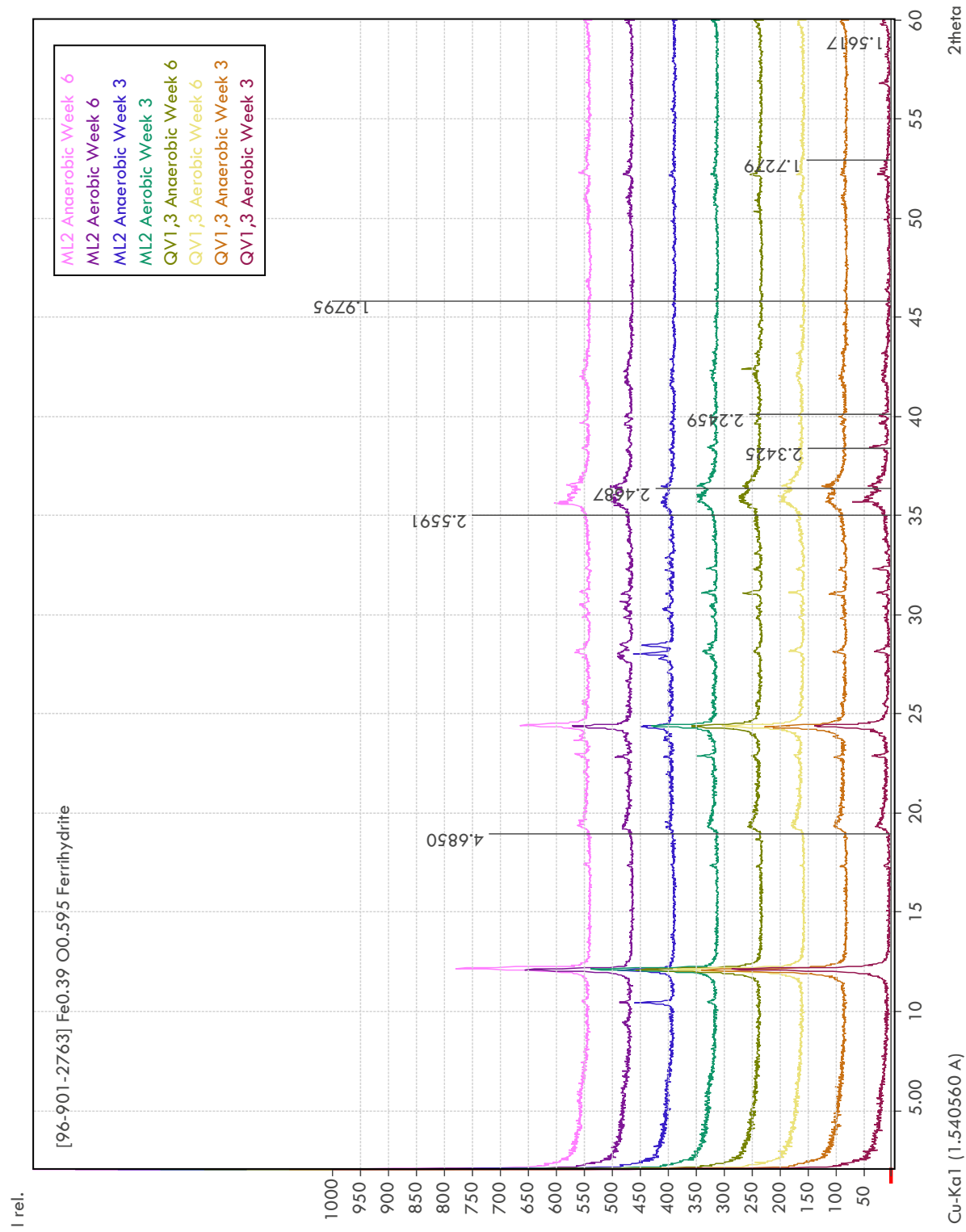


Figure 17. Phase I microcosm XRD patterns overlain with the standard pattern for ferrhydrite (shown with d-values).

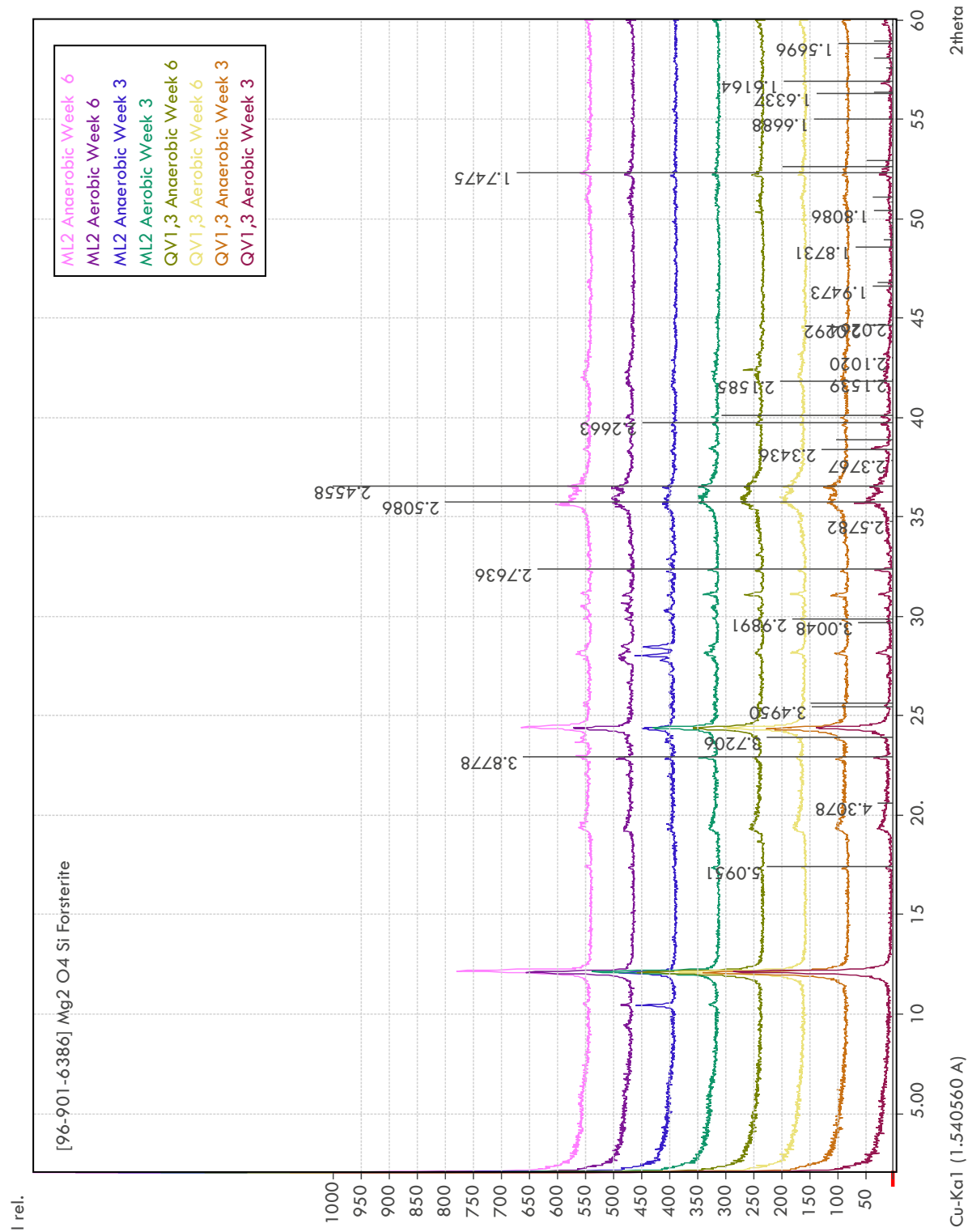


Figure 18. Phase I microcosm XRD patterns overlain with the standard pattern for forsterite (selected peaks are labeled with d-values).

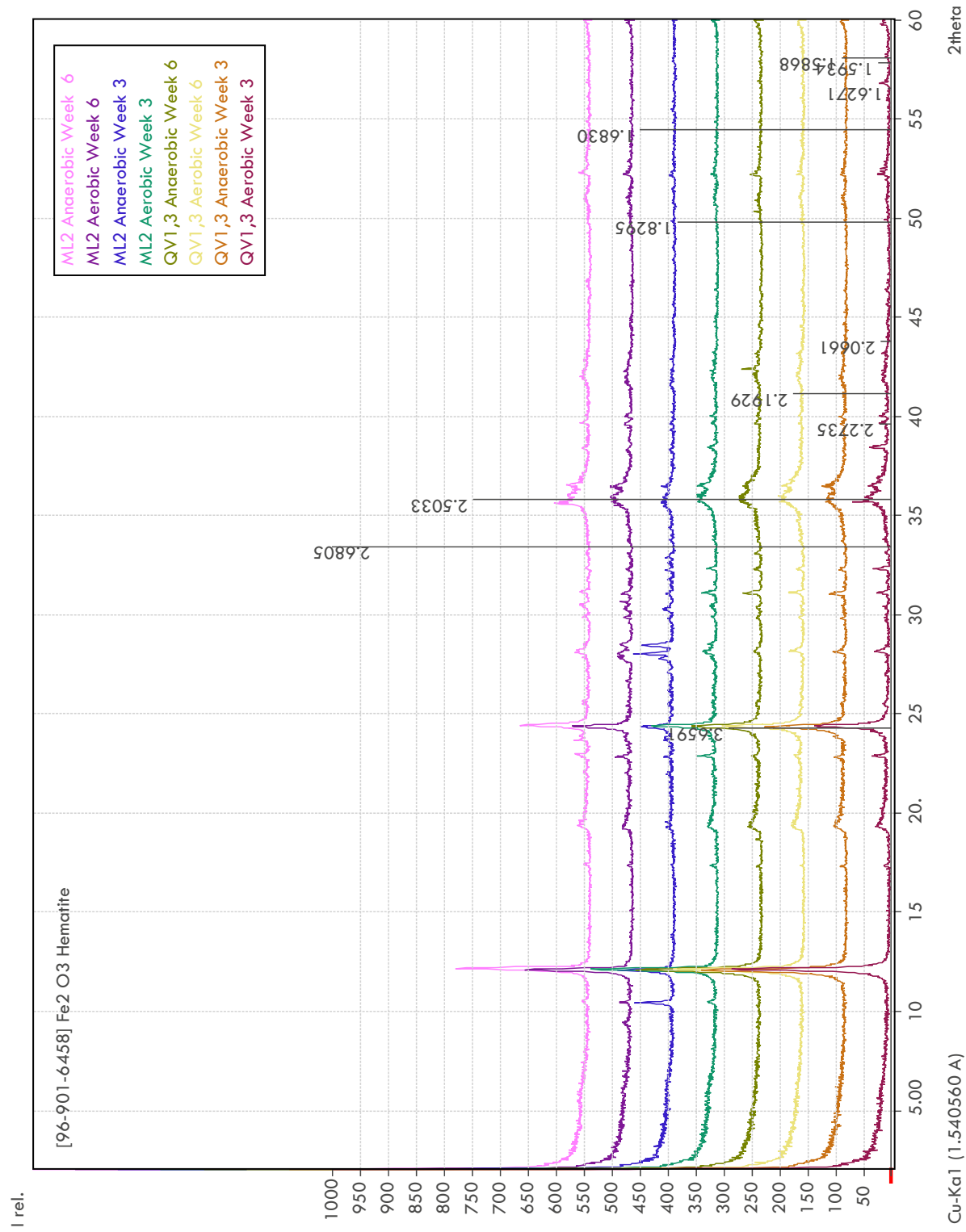


Figure 19. Phase I microcosm XRD patterns overlain with the standard pattern for hematite (shown with d-values).

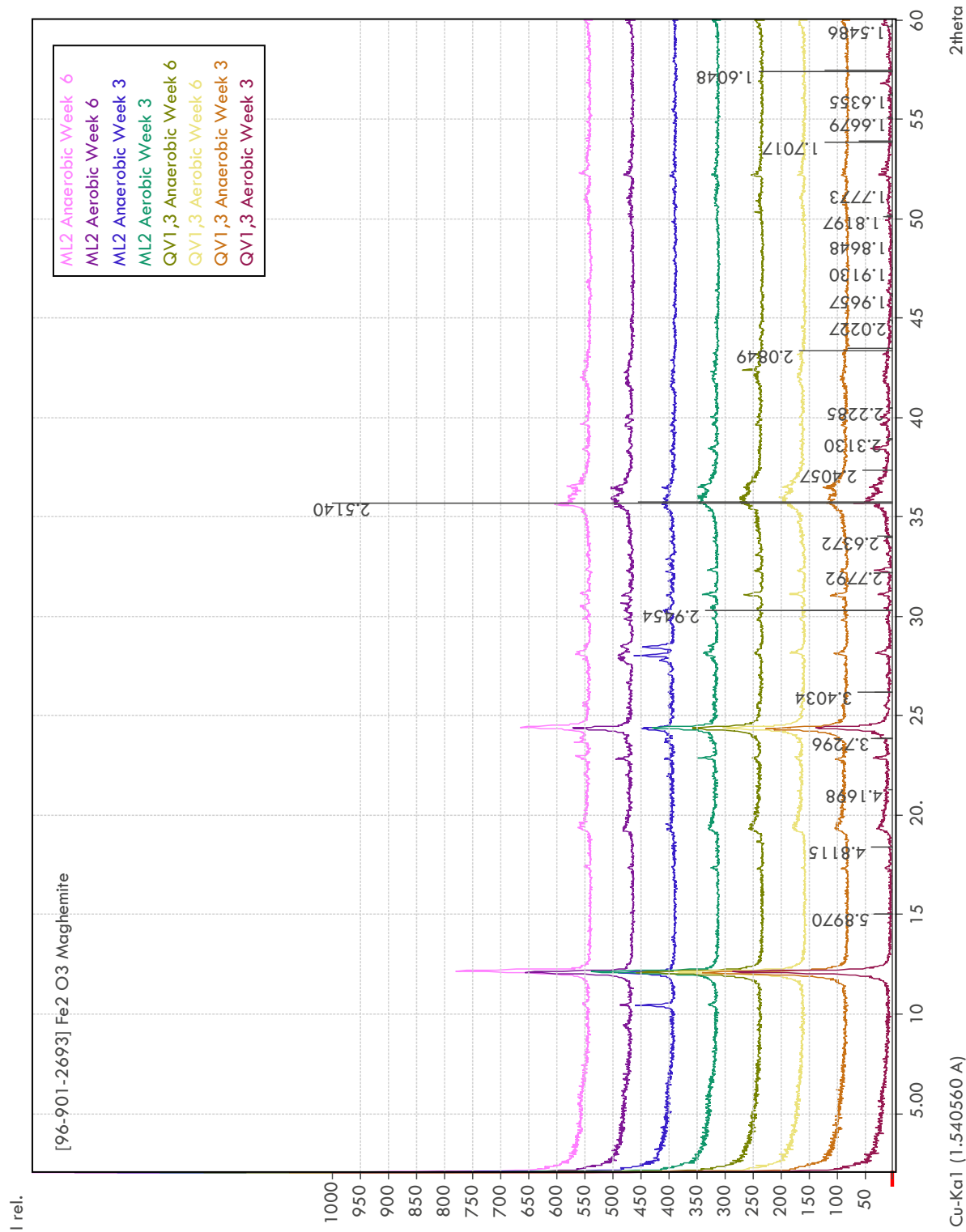


Figure 20. Phase I microcosm XRD patterns overlain with the standard pattern for maghemite (shown with d-values).

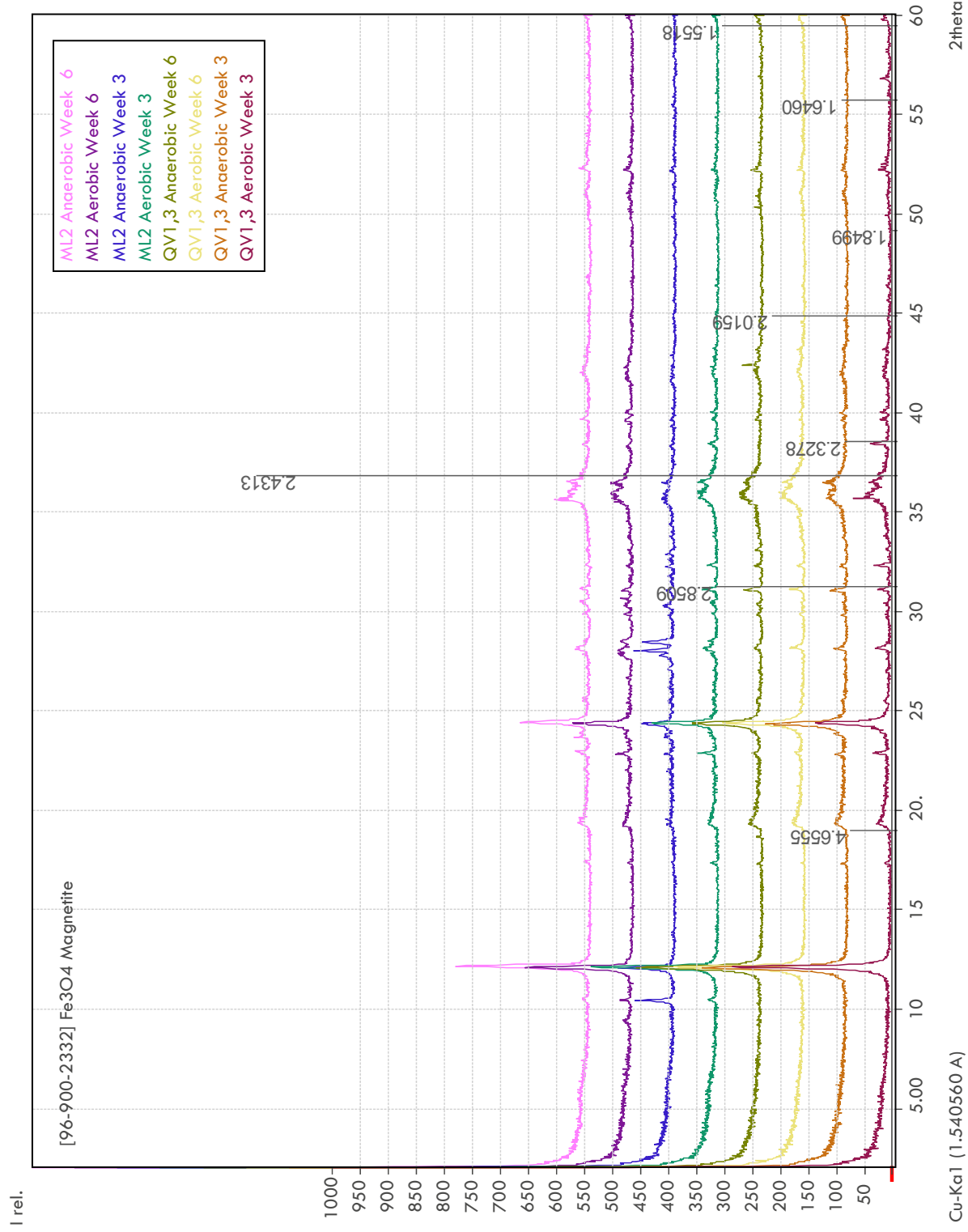


Figure 21. Phase I microcosm XRD patterns overlain with the standard pattern for magnetite(2332) (shown with d-values).

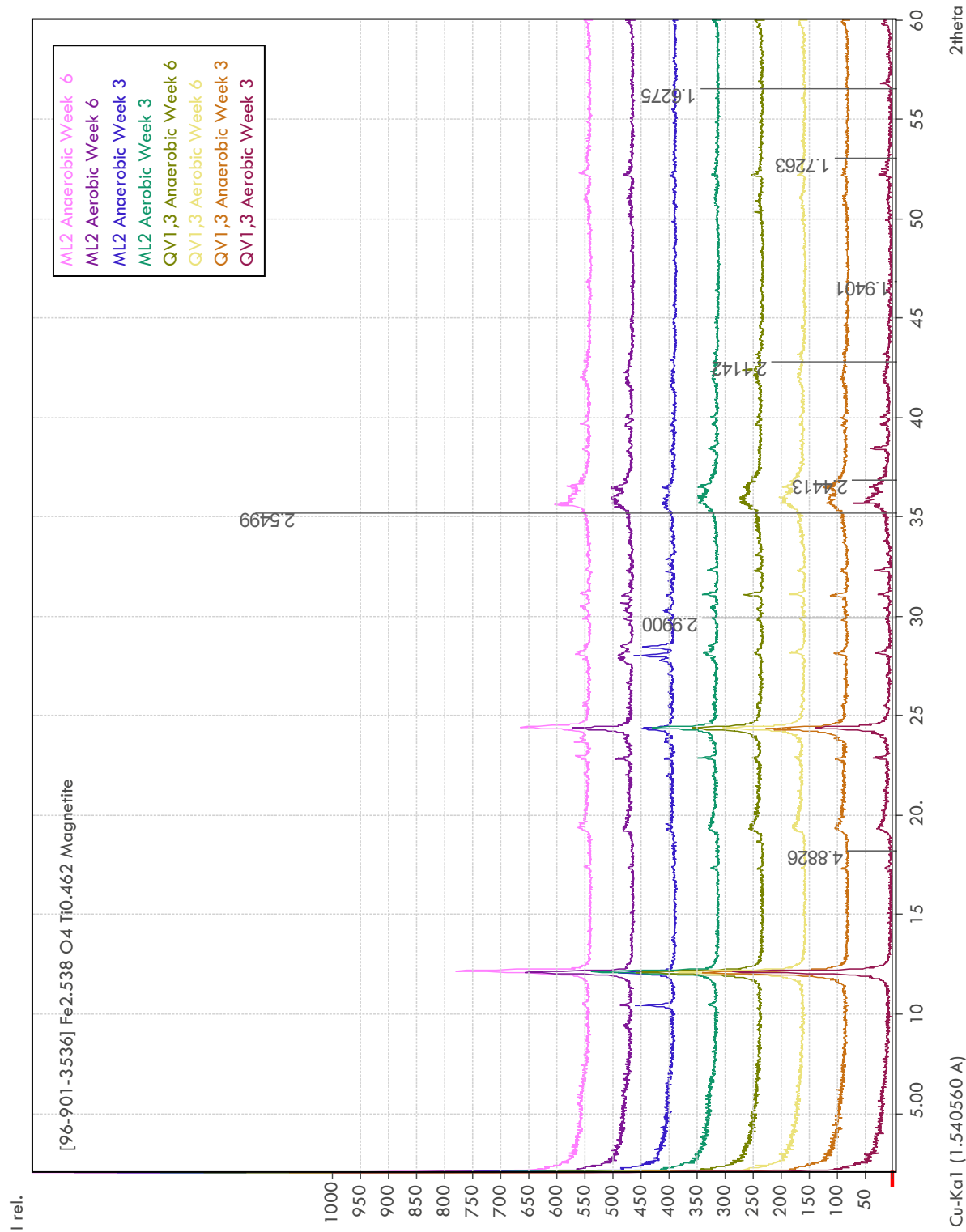


Figure 22. Phase I microcosm XRD patterns overlain with the standard pattern for magnetite(3536) (shown with d-values).

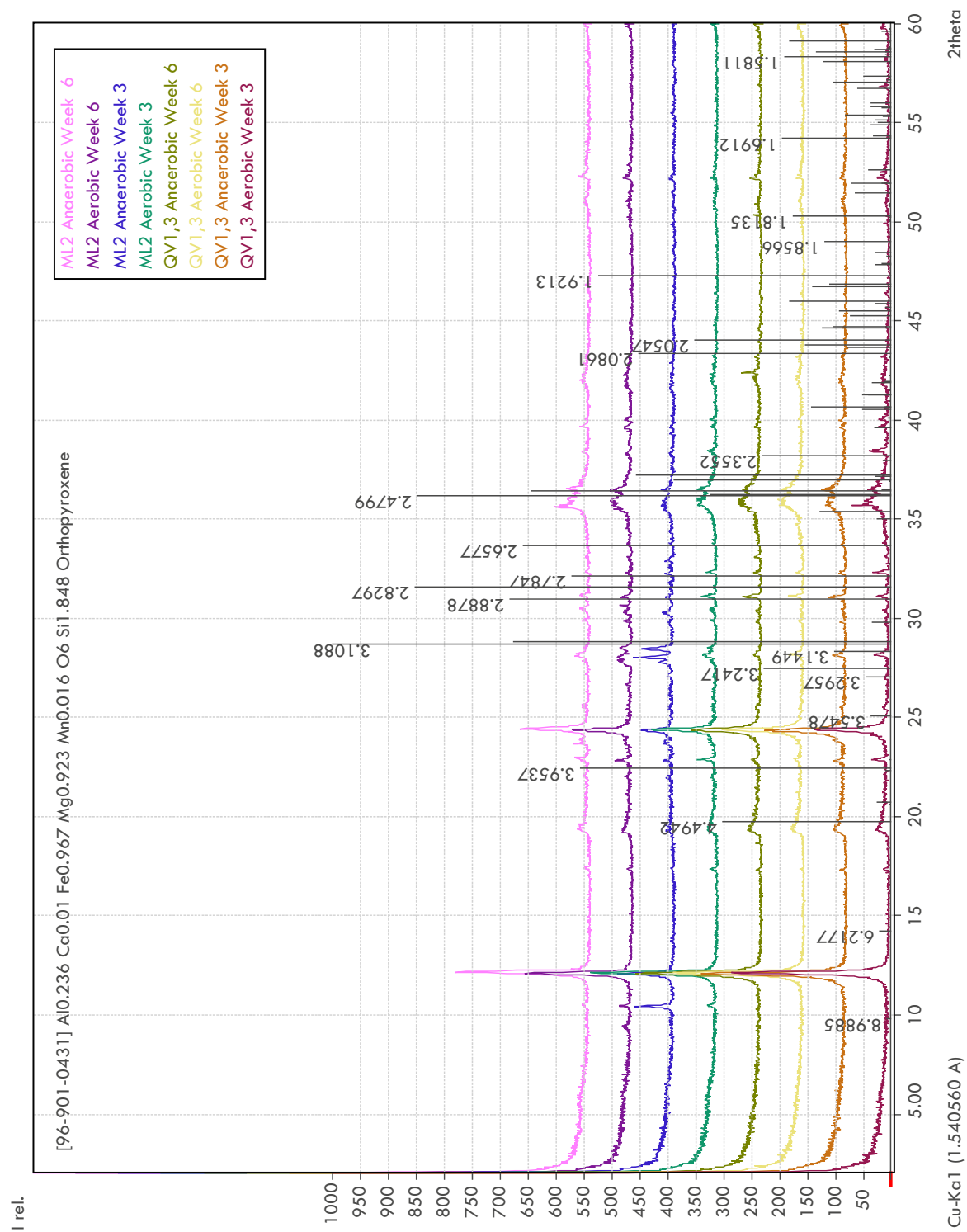


Figure 23. Phase I microcosm XRD patterns overlain with the standard pattern for orthopyroxene (selected peaks are labeled with d-values).

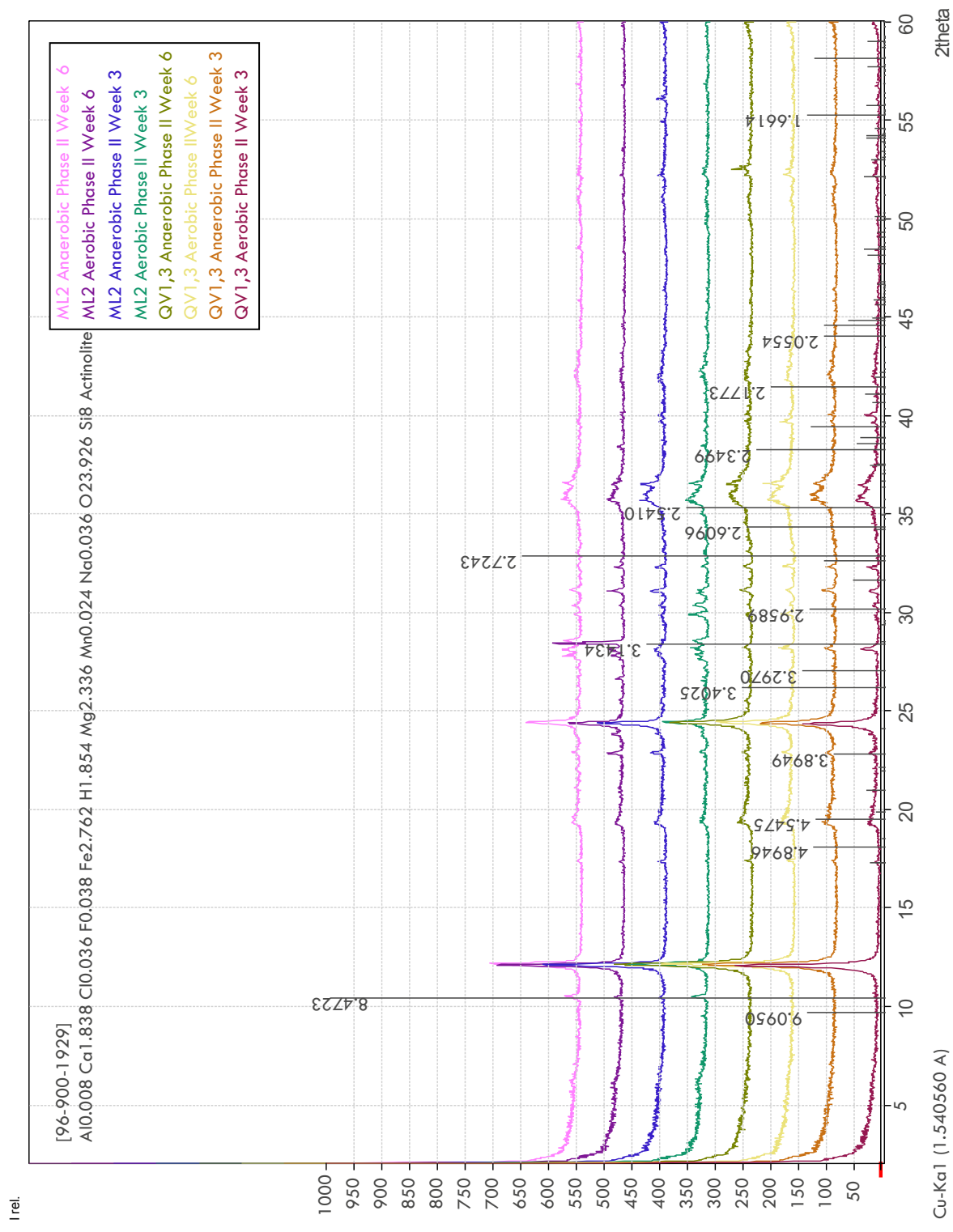


Figure 24. Phase II microcosm XRD patterns overlain with the standard pattern for actinolite (selected peaks are labeled with d-values).

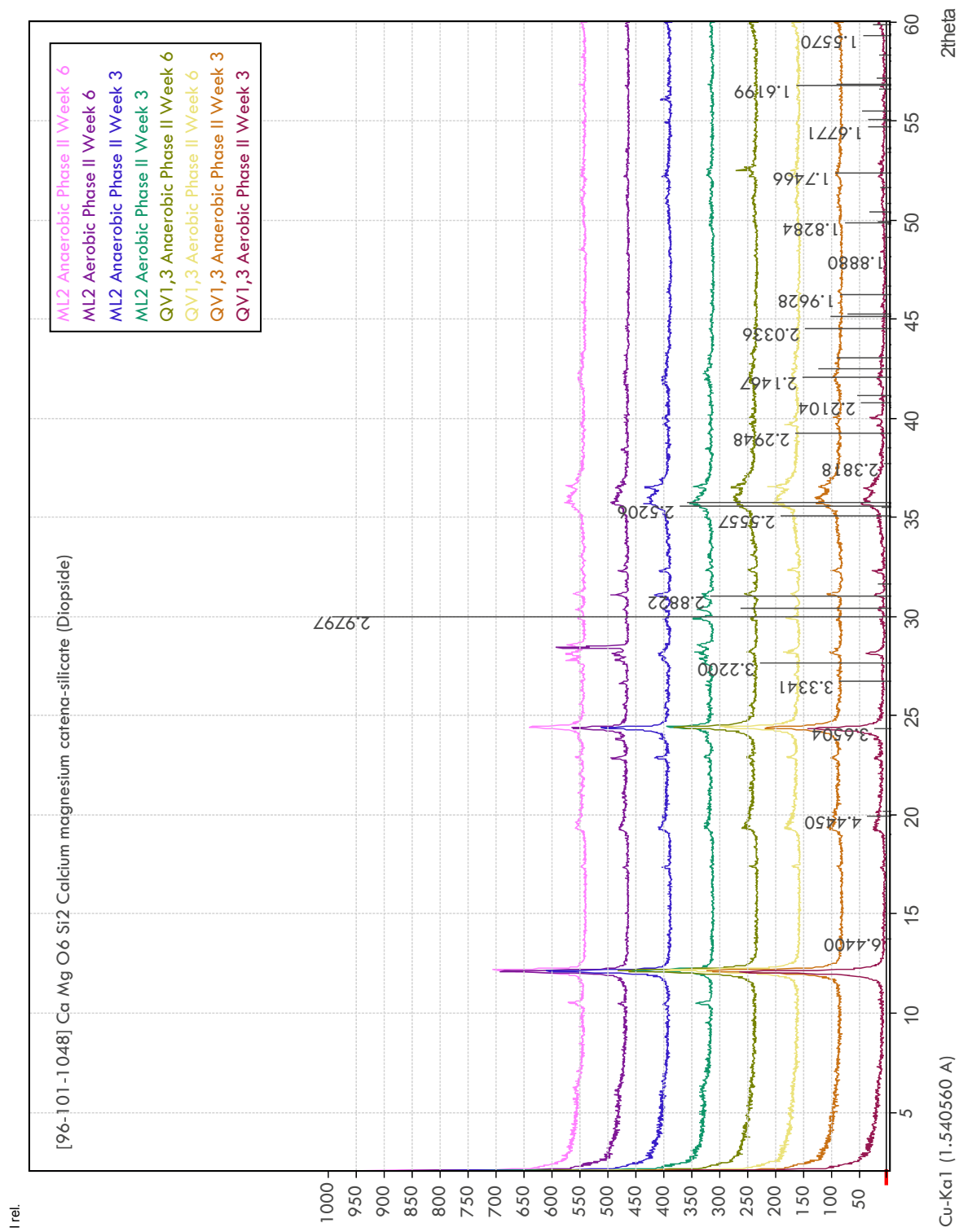


Figure 25. Phase II microcosm XRD patterns overlain with the standard pattern for diopside (selected peaks are labeled with d-values).

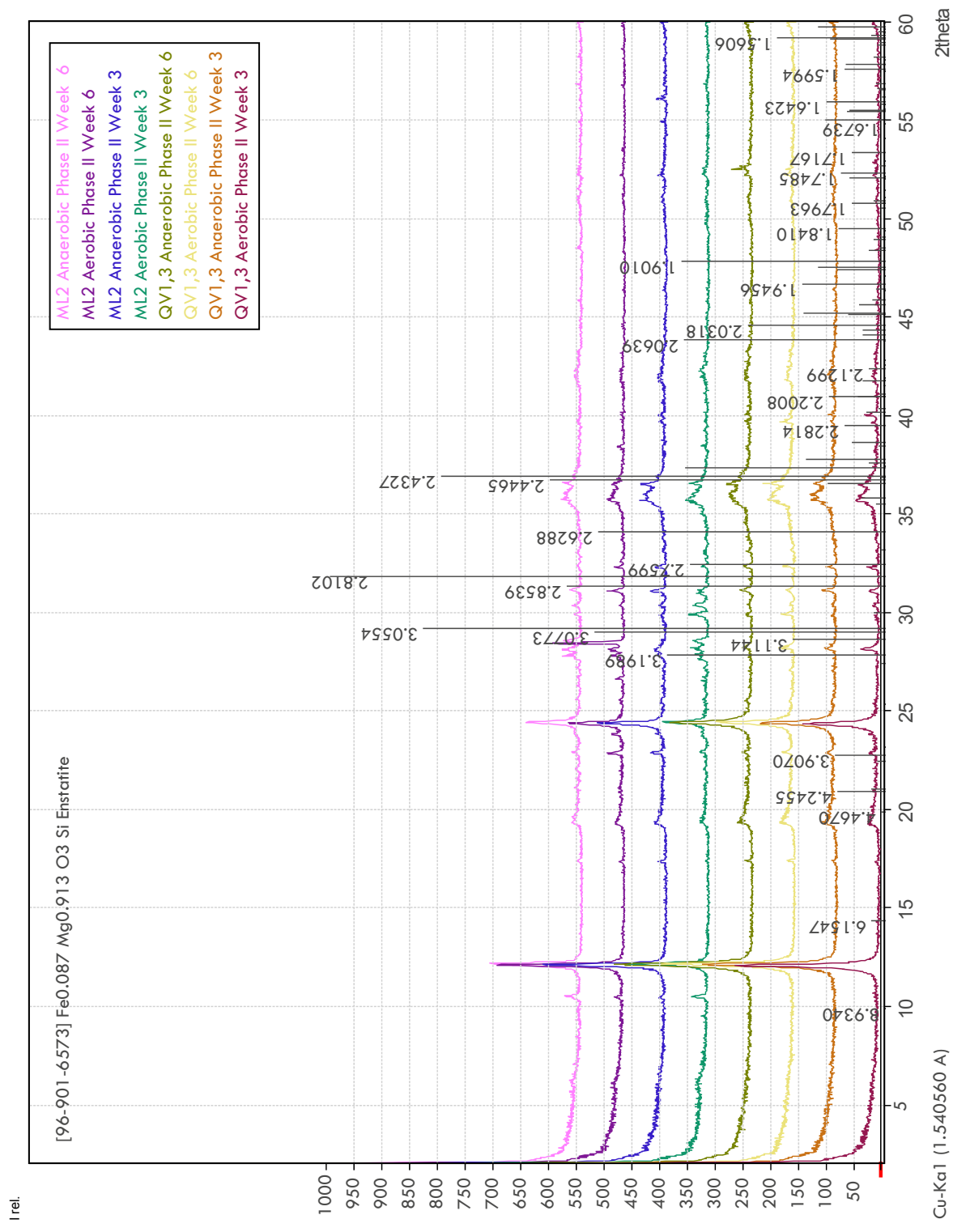


Figure 26. Phase II microcosm XRD patterns overlain with the standard pattern for enstatite (selected peaks are labeled with d-values).

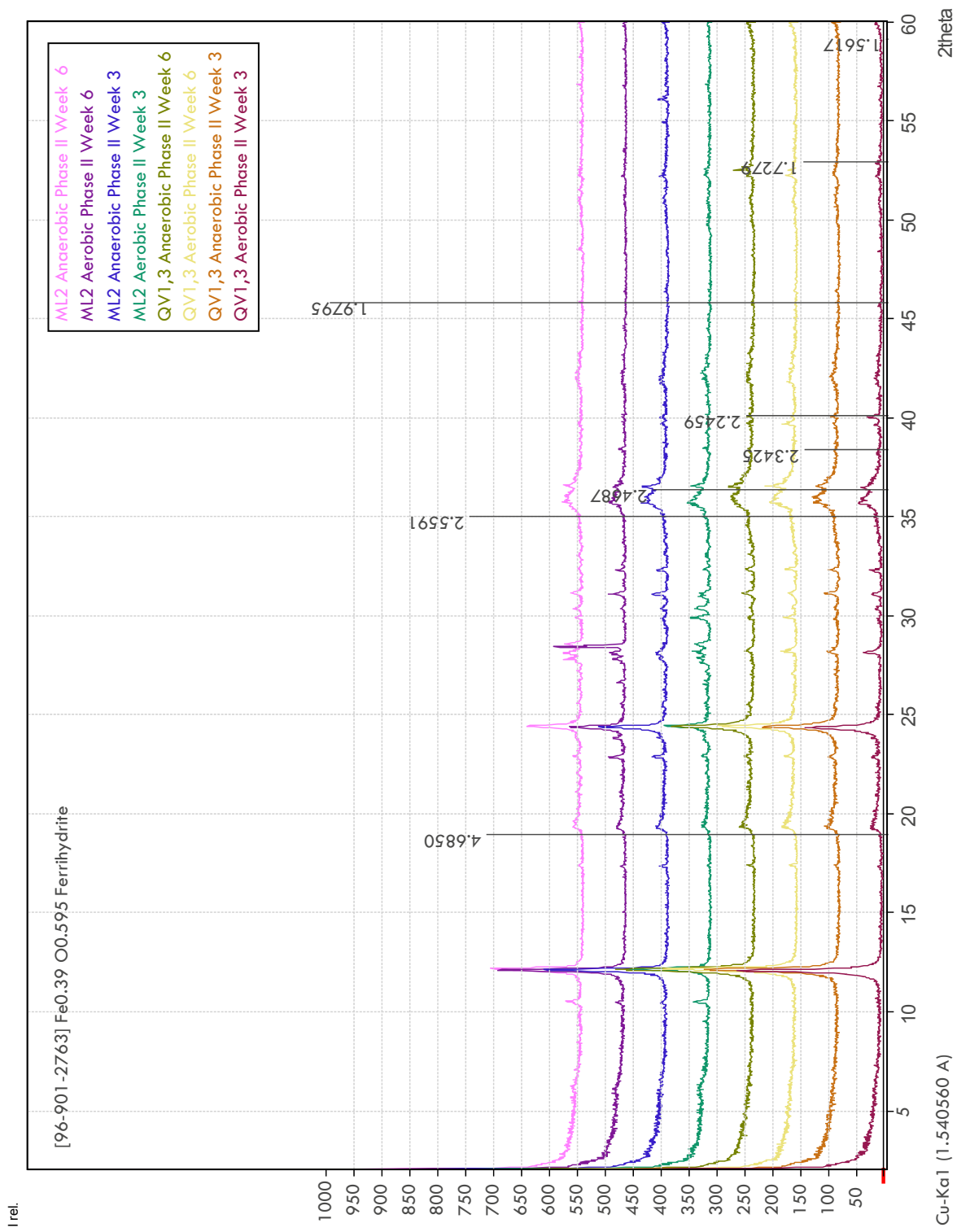


Figure 27. Phase II microcosm XRD patterns overlain with the standard pattern for ferrihydrite (shown with d-values).

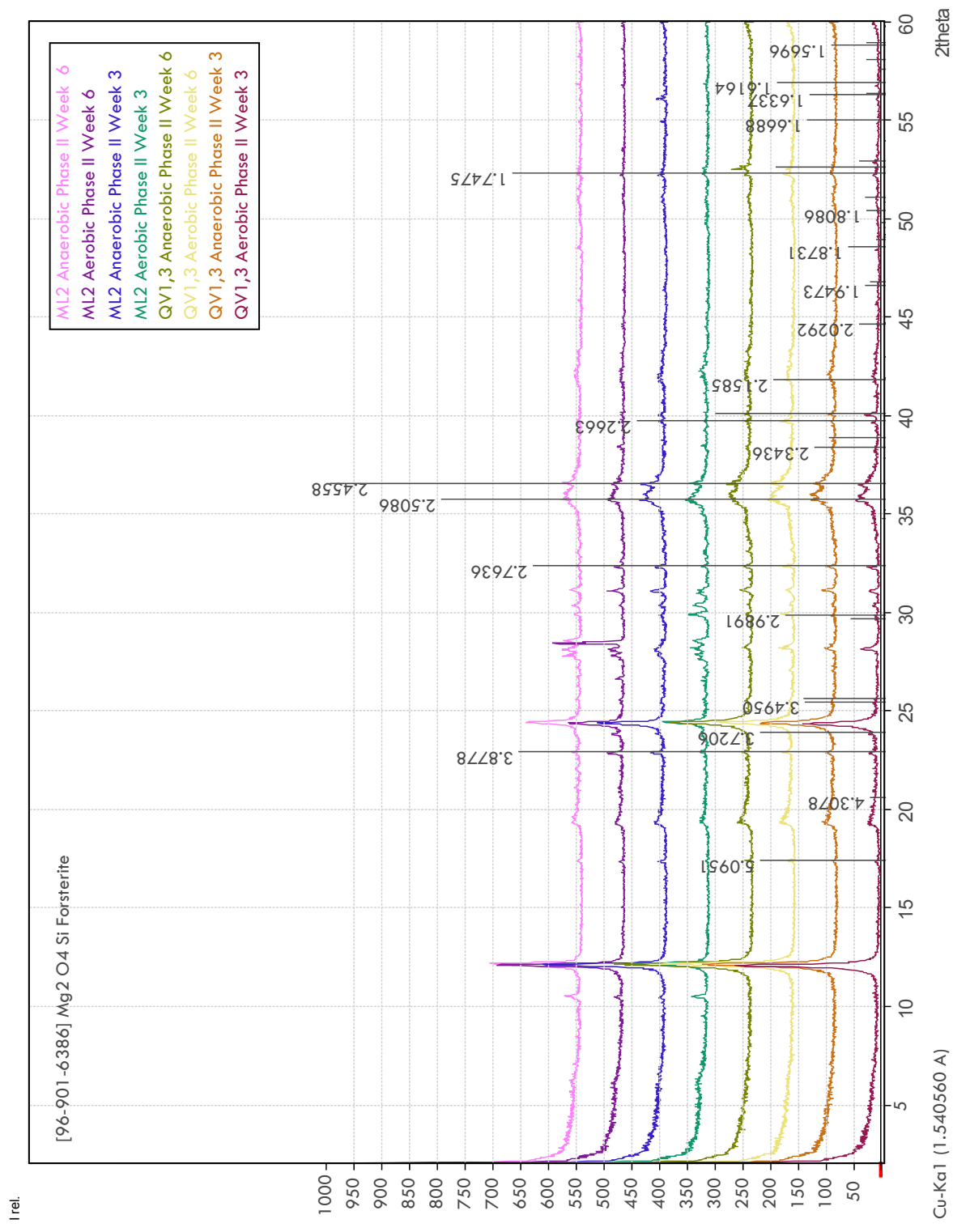


Figure 28. Phase II microcosm XRD patterns overlain with the standard pattern for forsterite (selected peaks are labeled with d-values).

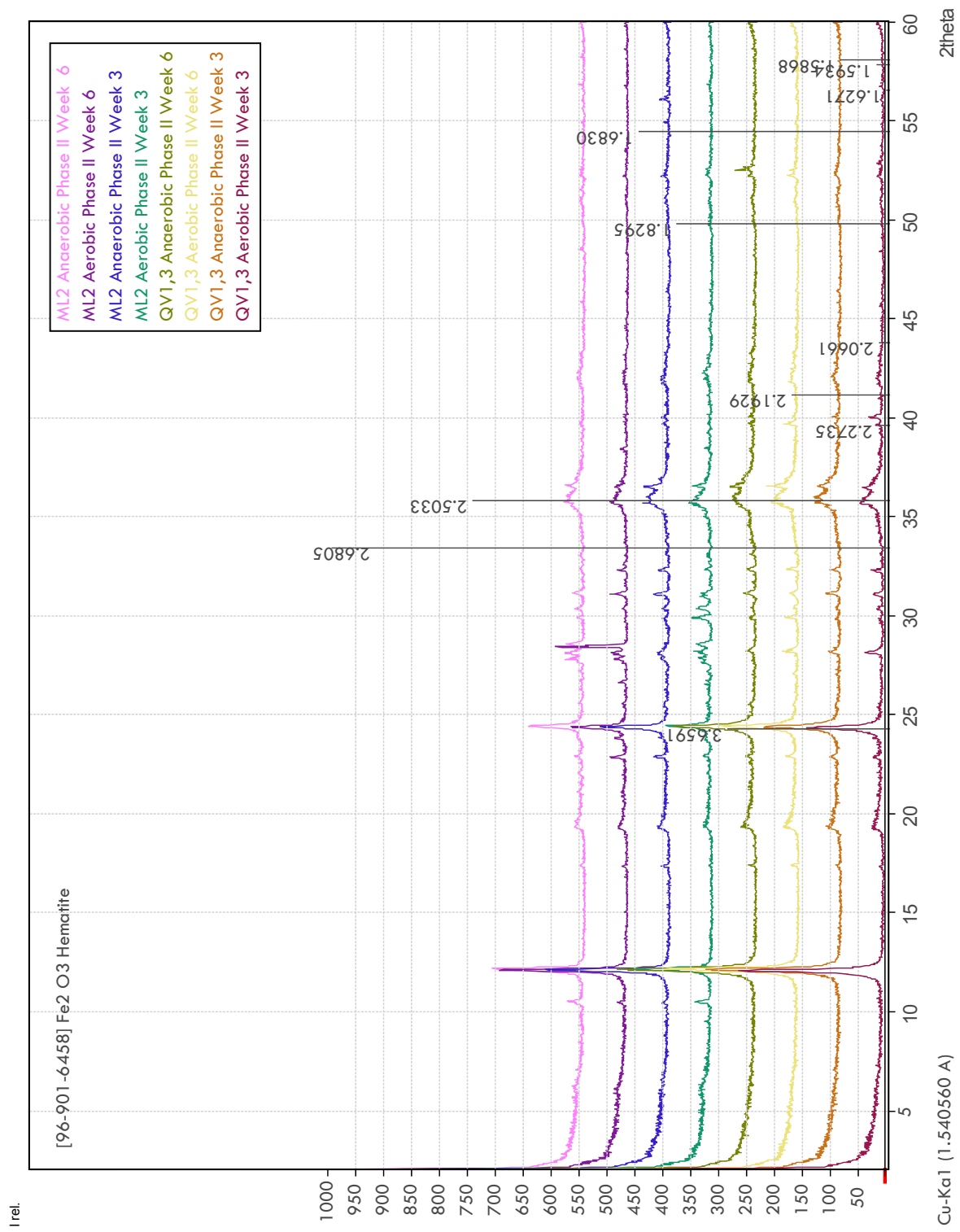


Figure 29. Phase II microcosm XRD patterns overlain with the standard pattern for hematite (shown with d-values).

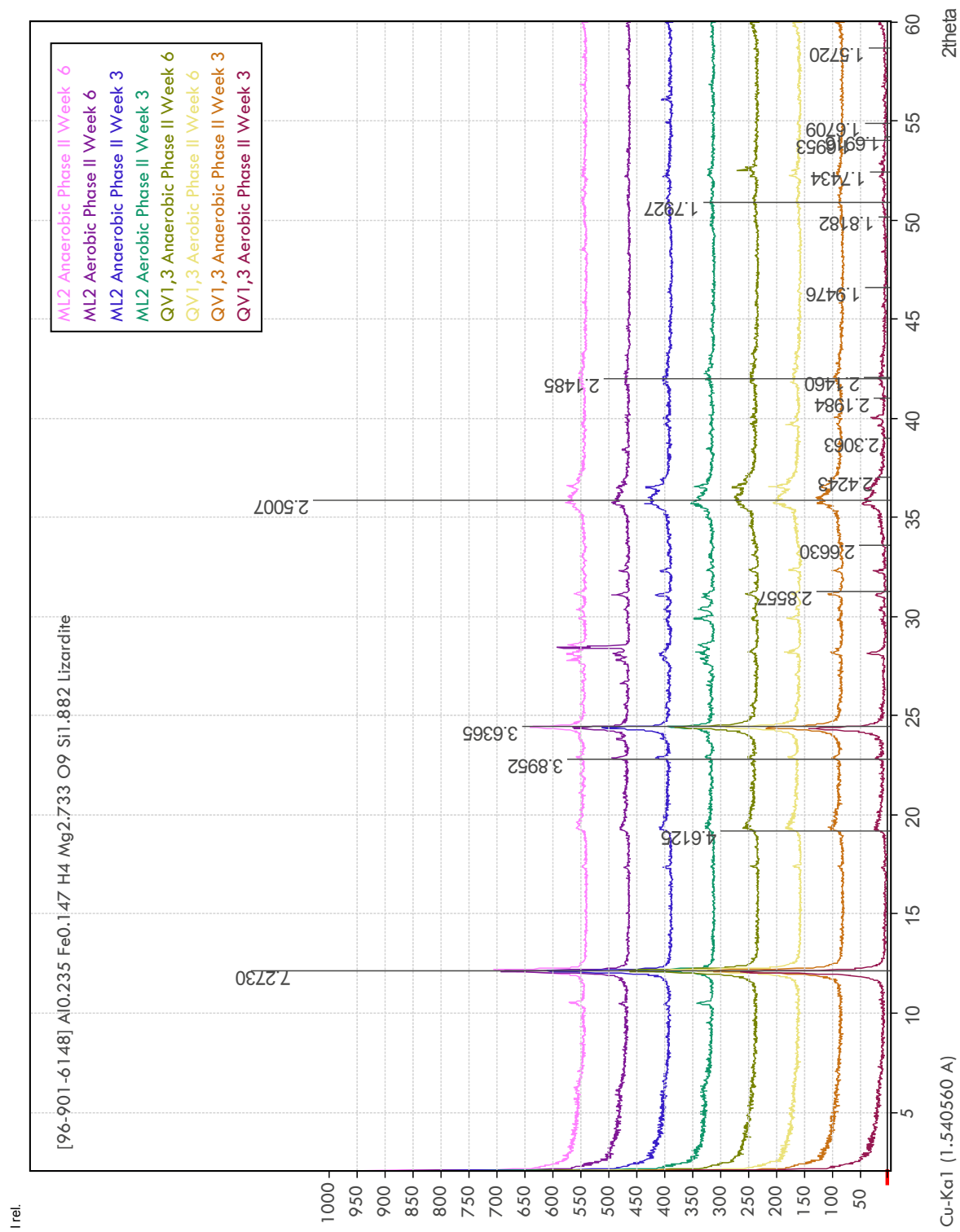


Figure 30. Phase II microcosm XRD patterns overlain with the standard pattern for lizardite (shown with d-values).

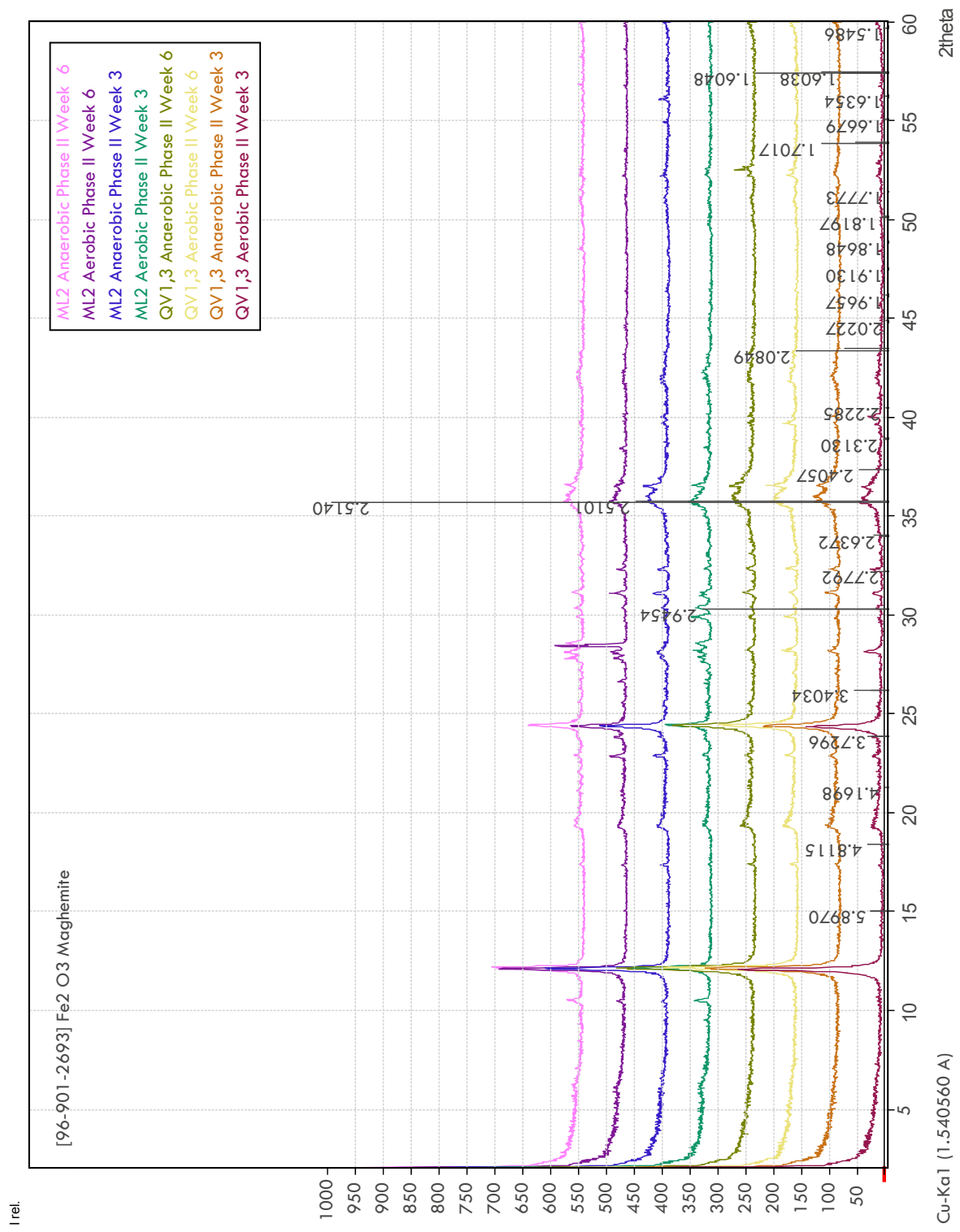


Figure 31. Phase II microcosm XRD patterns overlain with the standard pattern for maghemite (shown with d-values).

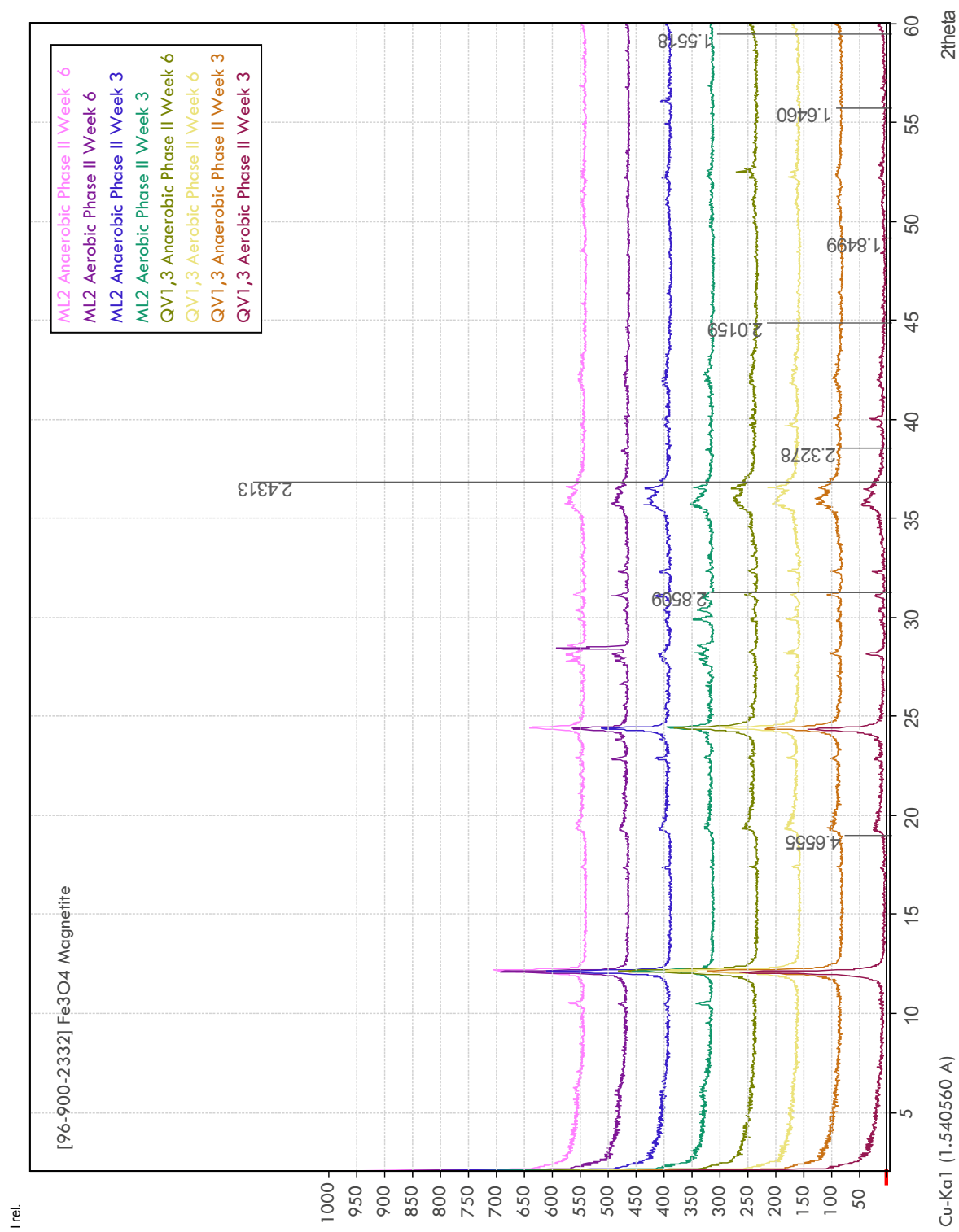


Figure 32. Phase II microcosm XRD patterns overlain with the standard pattern for magnetite(2332) (shown with d-values).

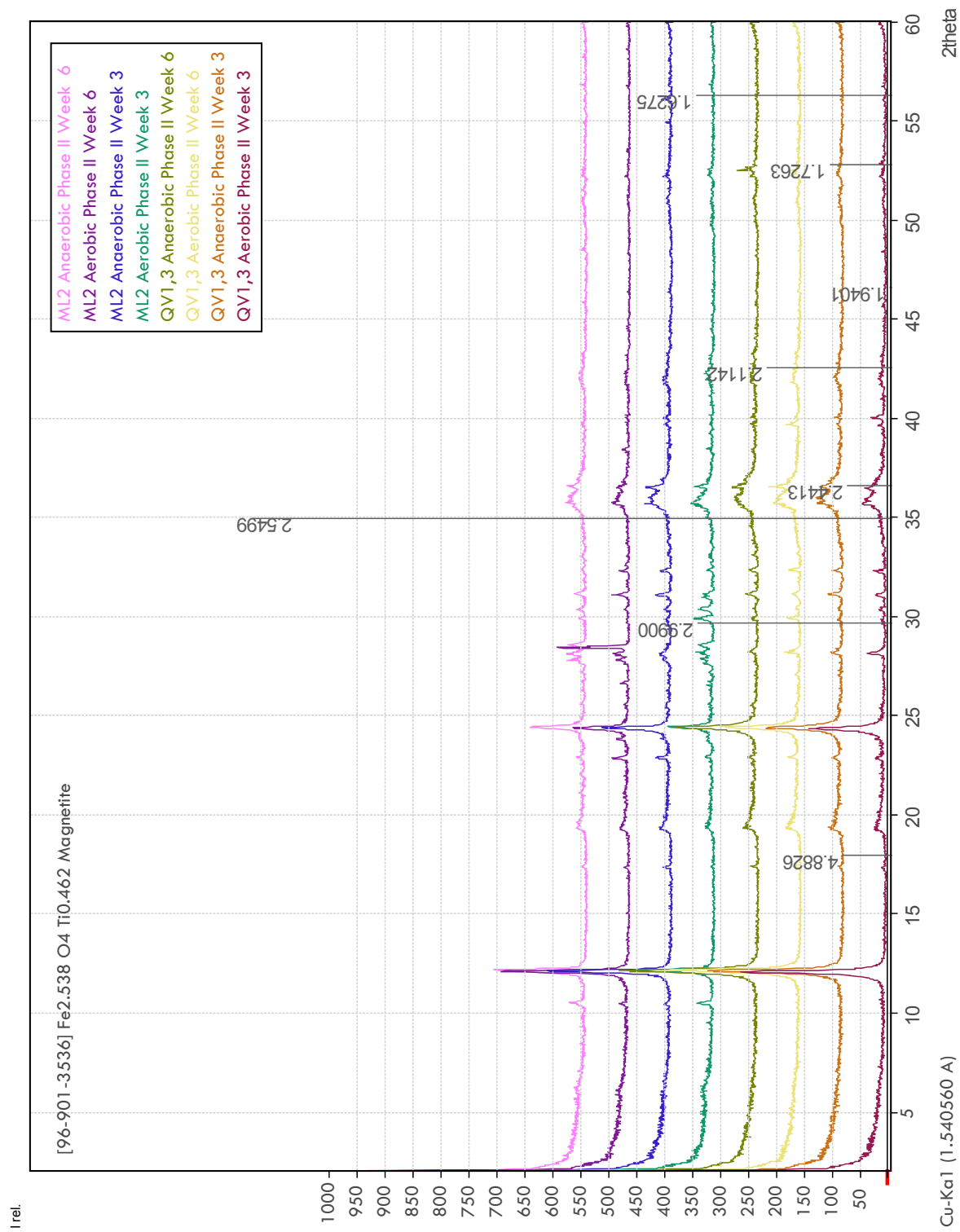


Figure 33. Phase II microcosm XRD patterns overlain with the standard pattern for magnetite(3536) (shown with d-values).

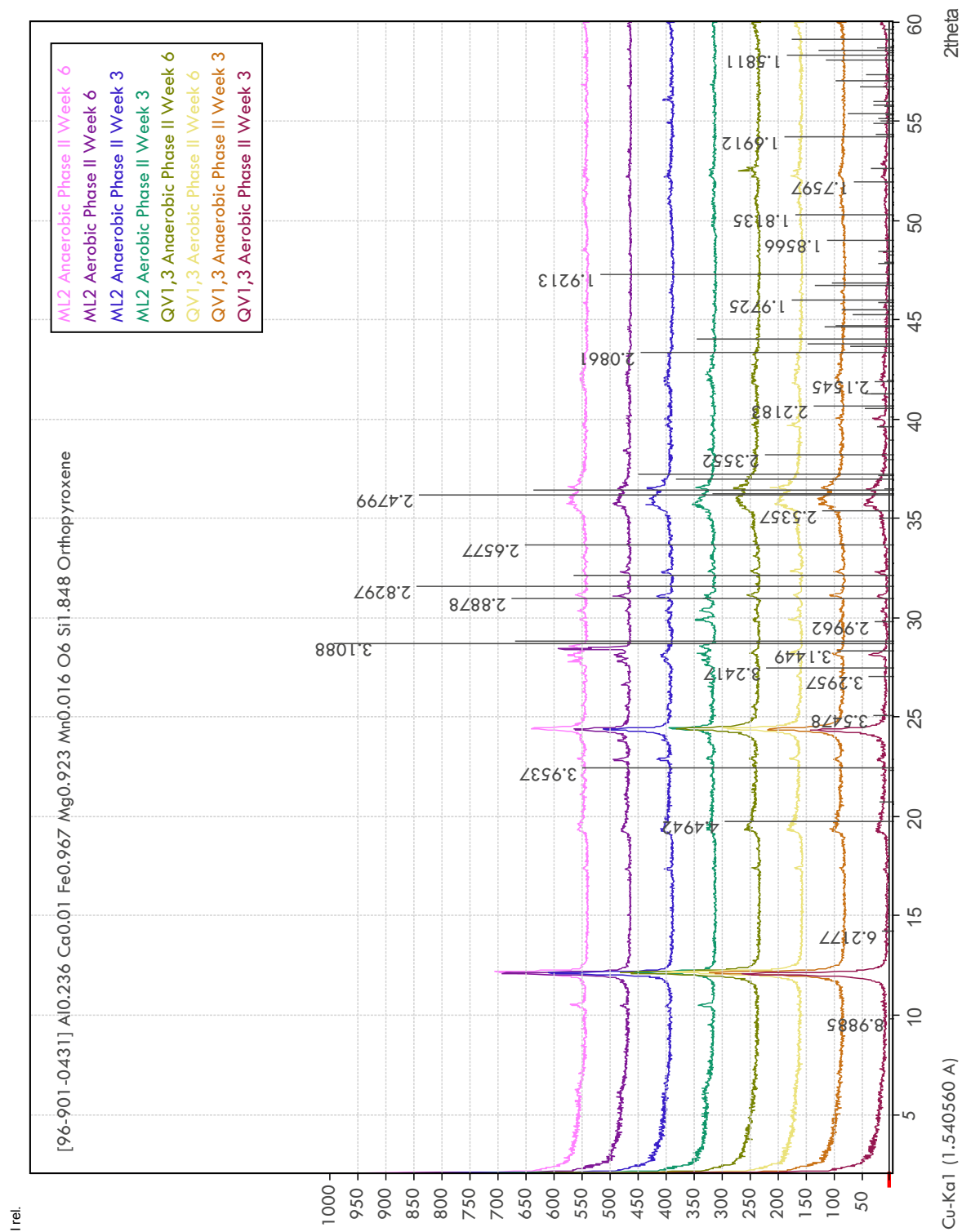


Figure 34. Phase II microcosm XRD patterns overlain with the standard pattern for orthopyroxene (selected peaks are labeled with d-values).

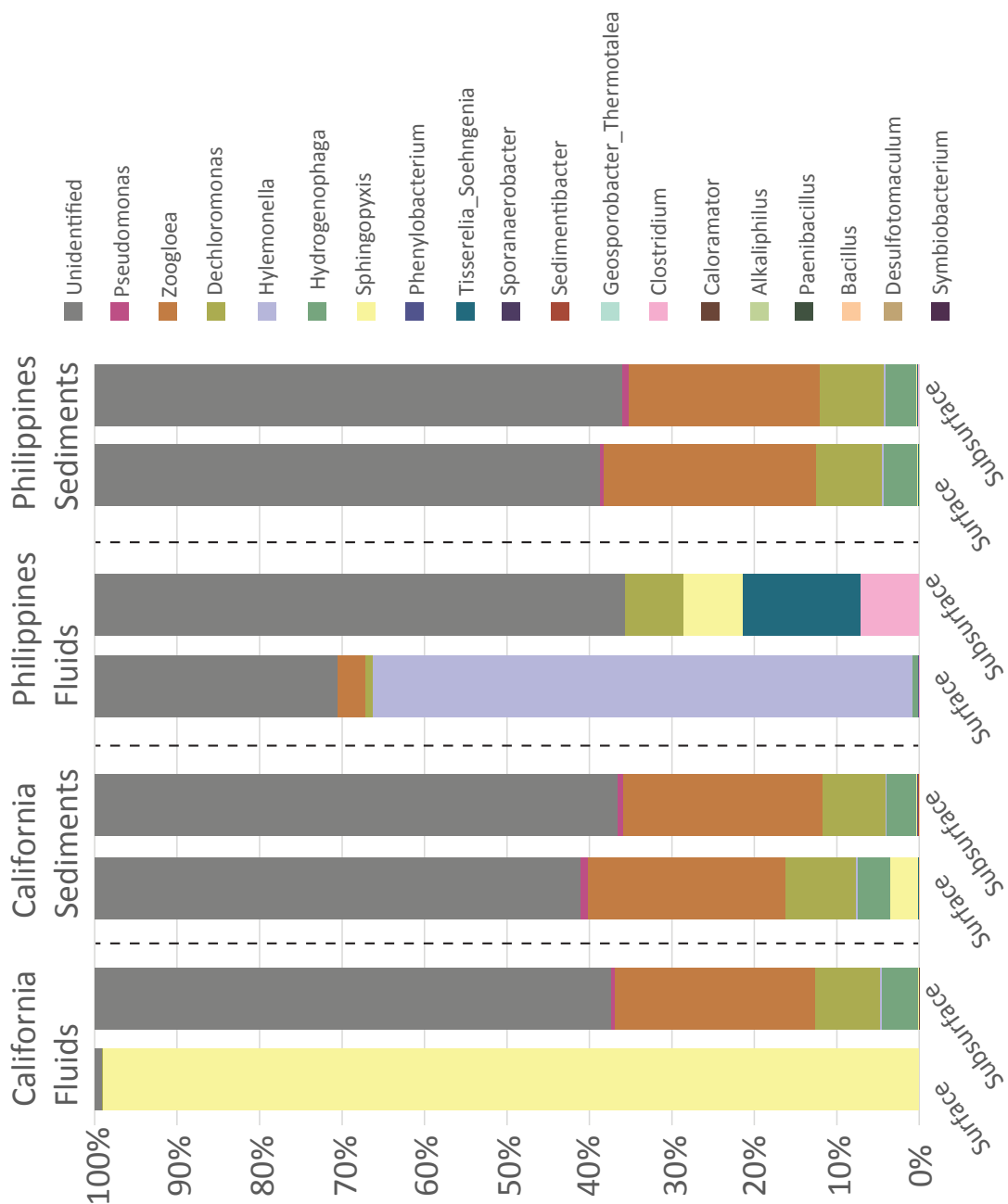


Figure 35. Relative abundances of genera in Phase II microcosm fluids and sediments after three weeks of growth. Phase II microcosms were amended with autoclave-sterilized ML2 and QV1,3 sediments, filter-sterilized QV1,3 and ML2 serpentinizing fluids, and oven-sterilized rock drilled from the Zambales ophiolite.

APPENDIX B. VERIFYING FE-METABOLISMS

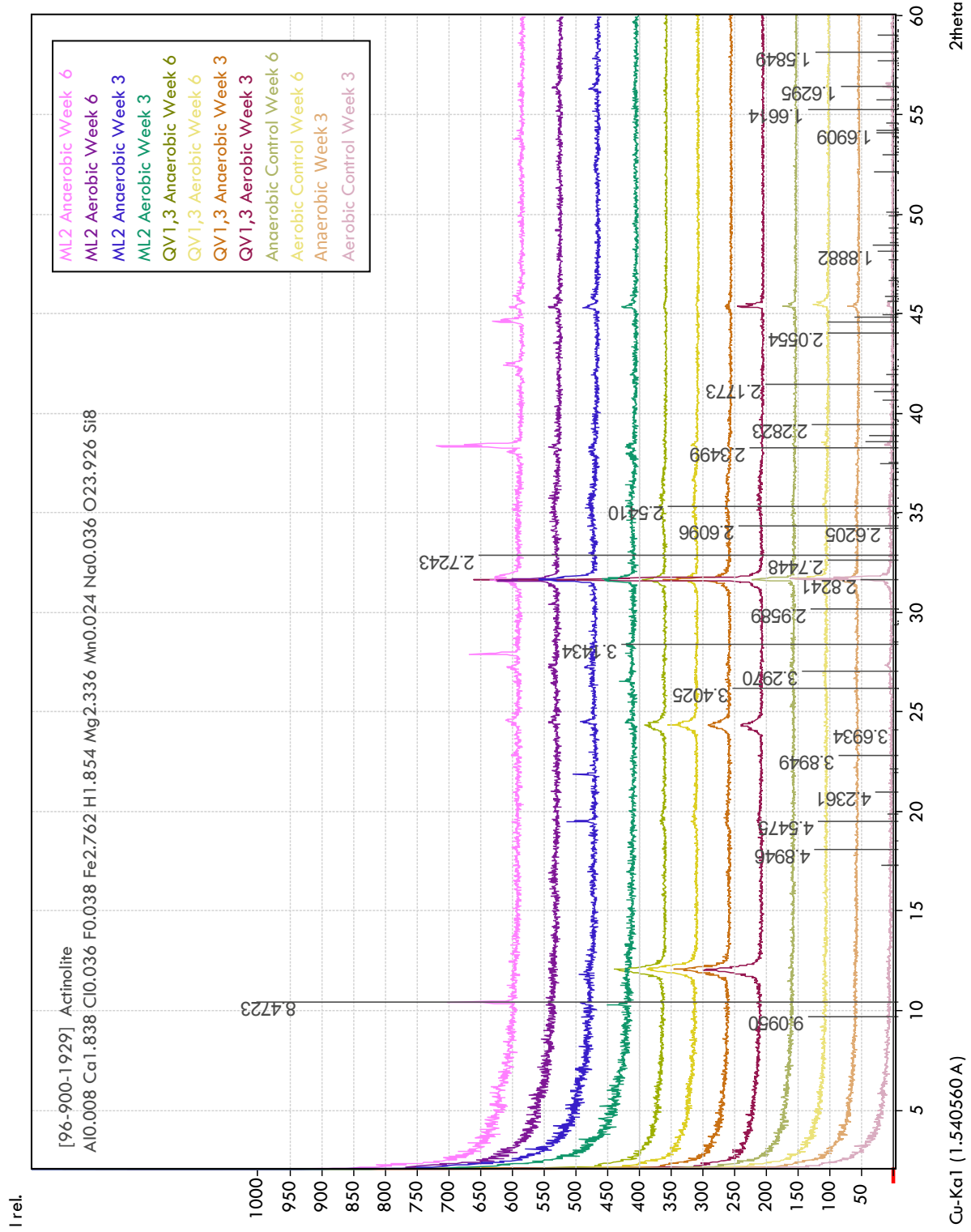


Figure 1. Culture XRD patterns overlain with the standard pattern for actinolite (selected peaks are labeled with d-values).

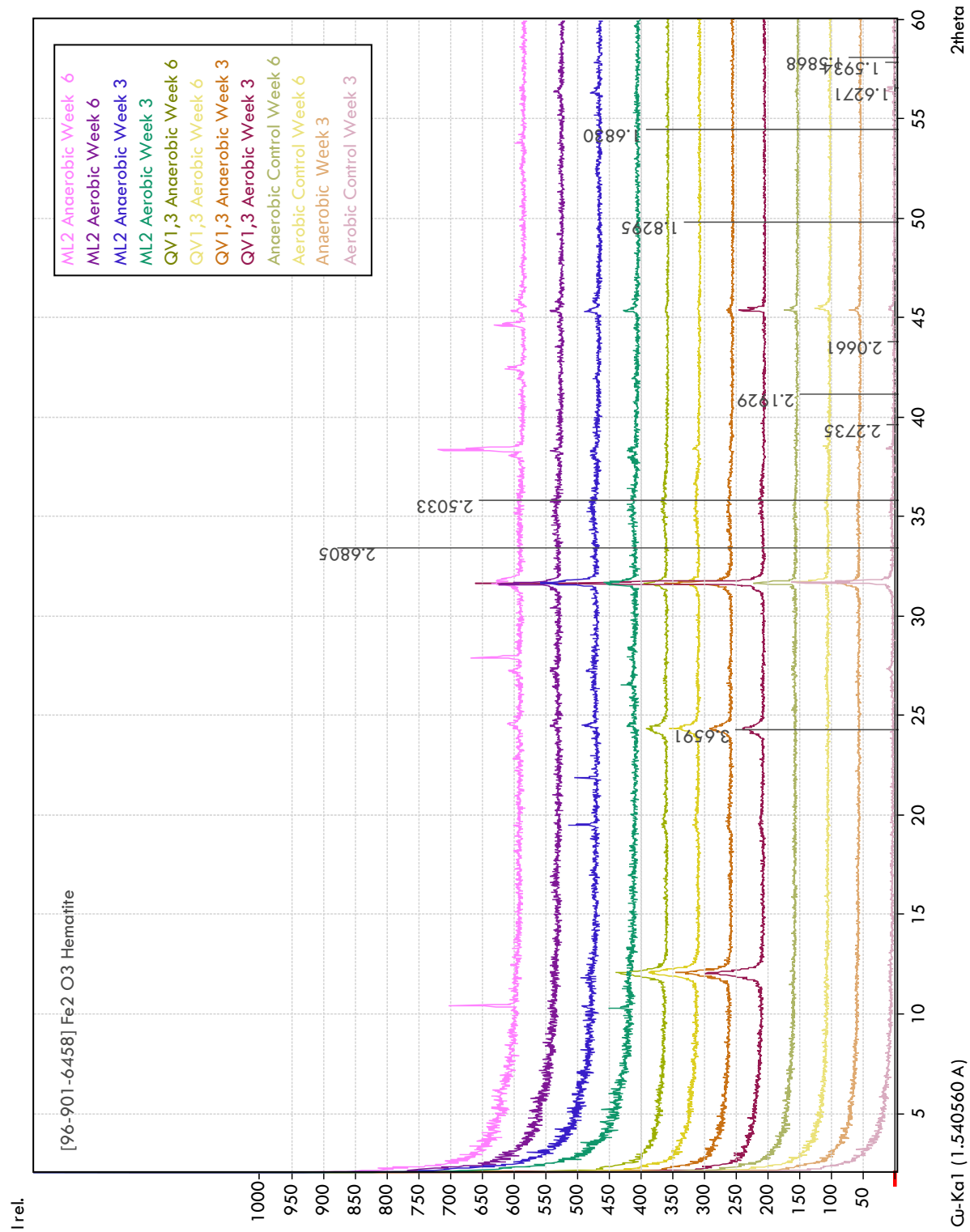


Figure 2. Culture XRD patterns overlain with the standard pattern for hematite (shown with d-values).

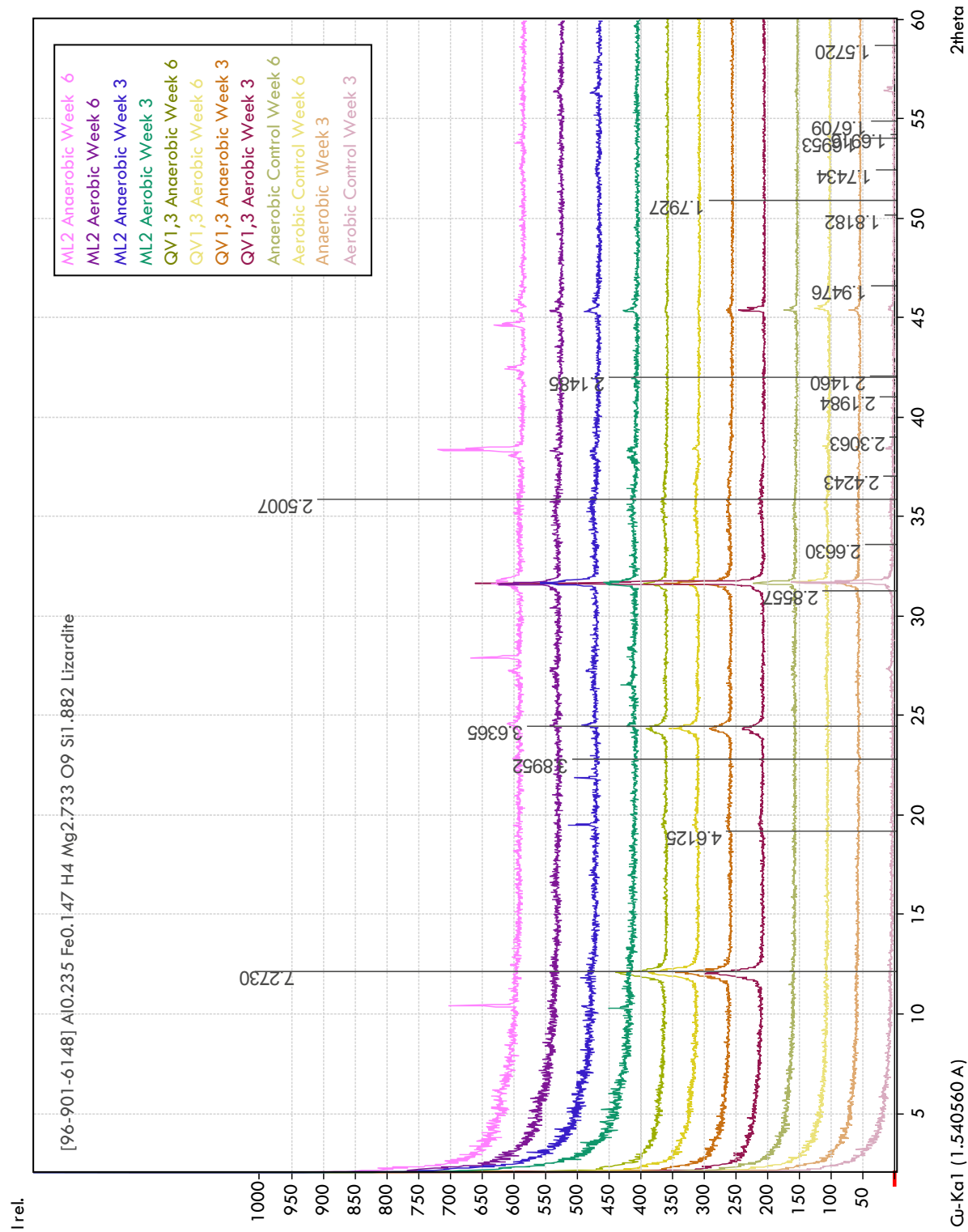


Figure 3. Culture XRD patterns overlain with the standard pattern for lizardite (shown with d-values).

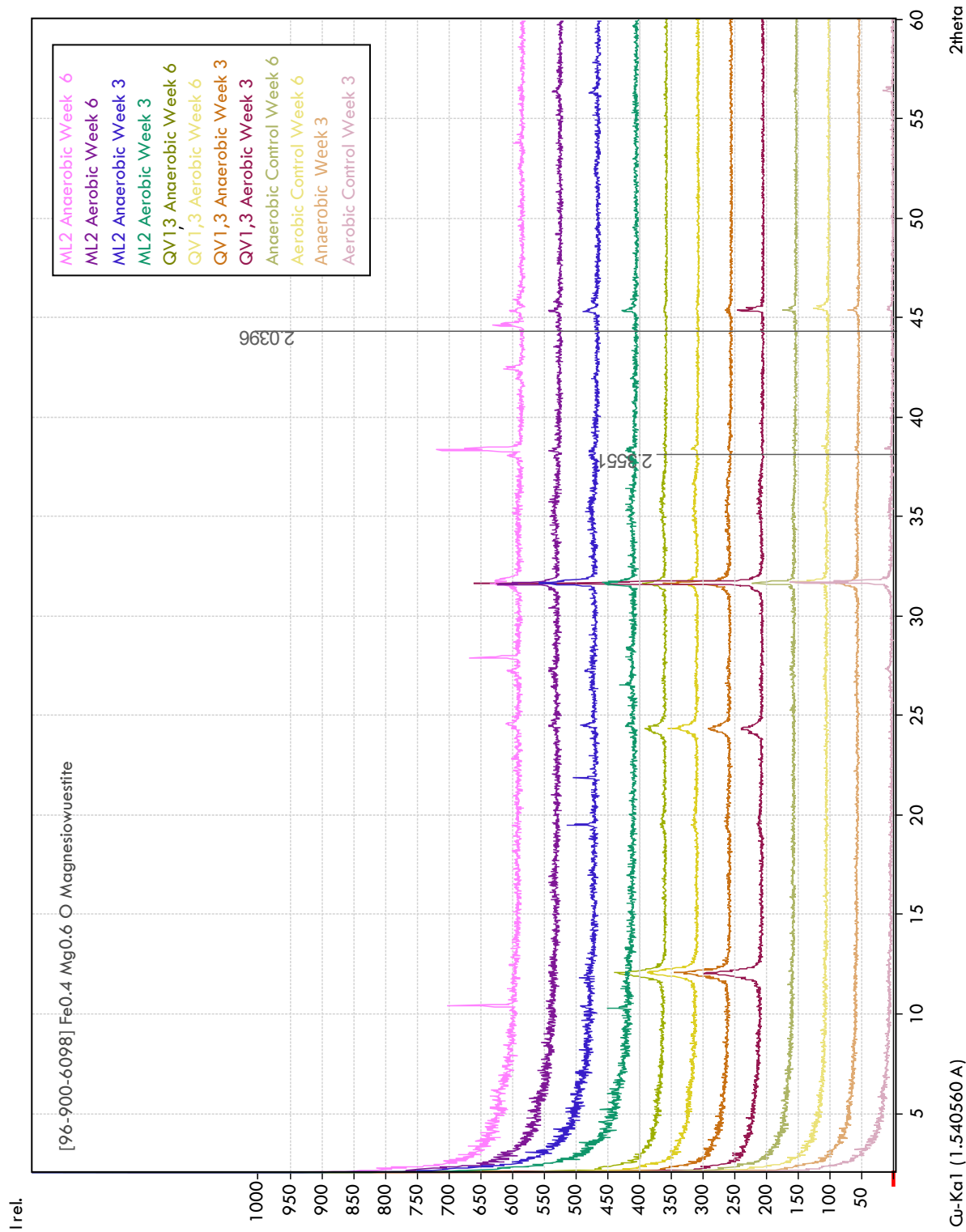


Figure 4. Culture XRD patterns overlain with the standard pattern for magnesiowuestite (shown with d-values).

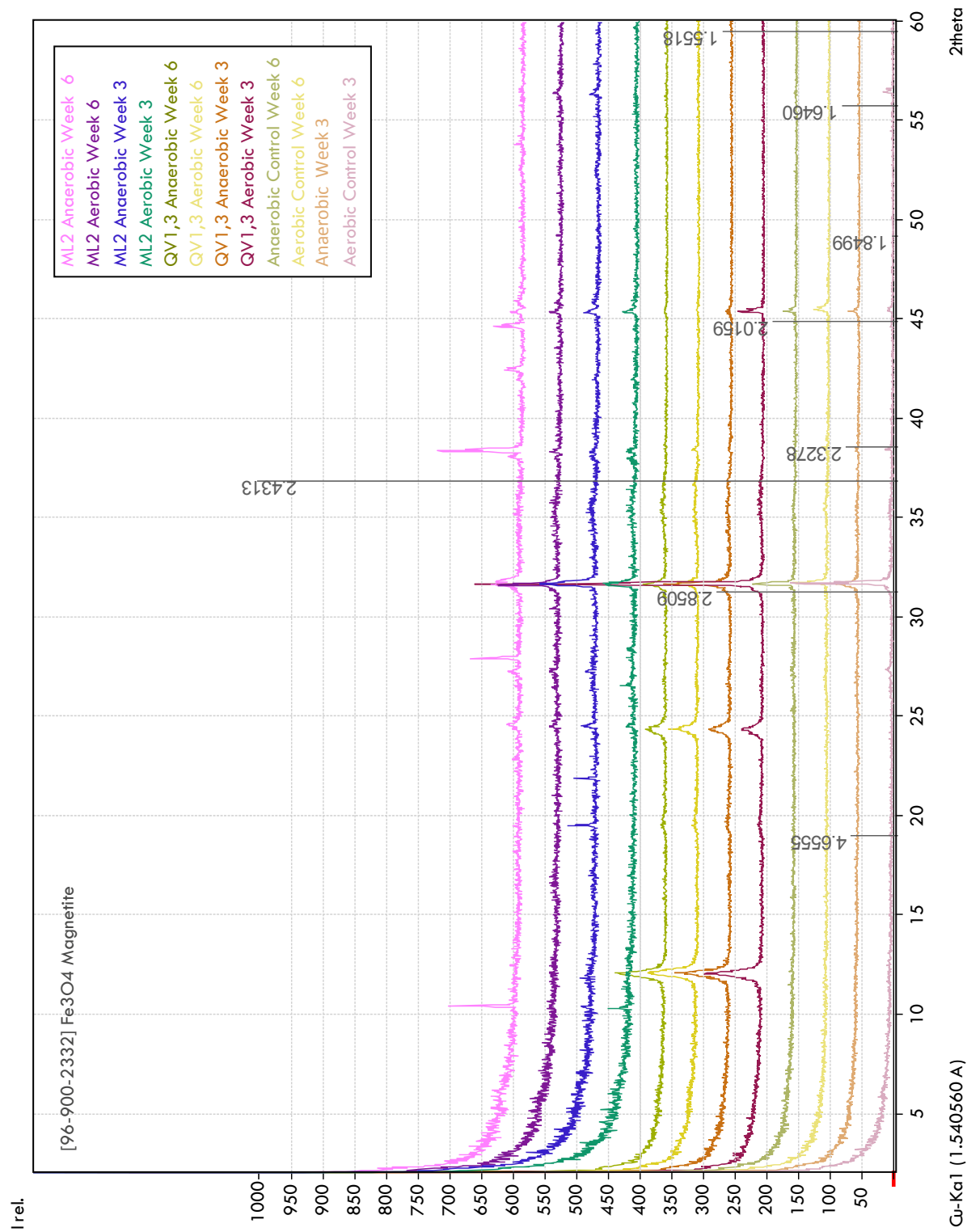


Figure 5. Culture XRD patterns overlain with the standard pattern for magnetite(2332) (shown with d-values).

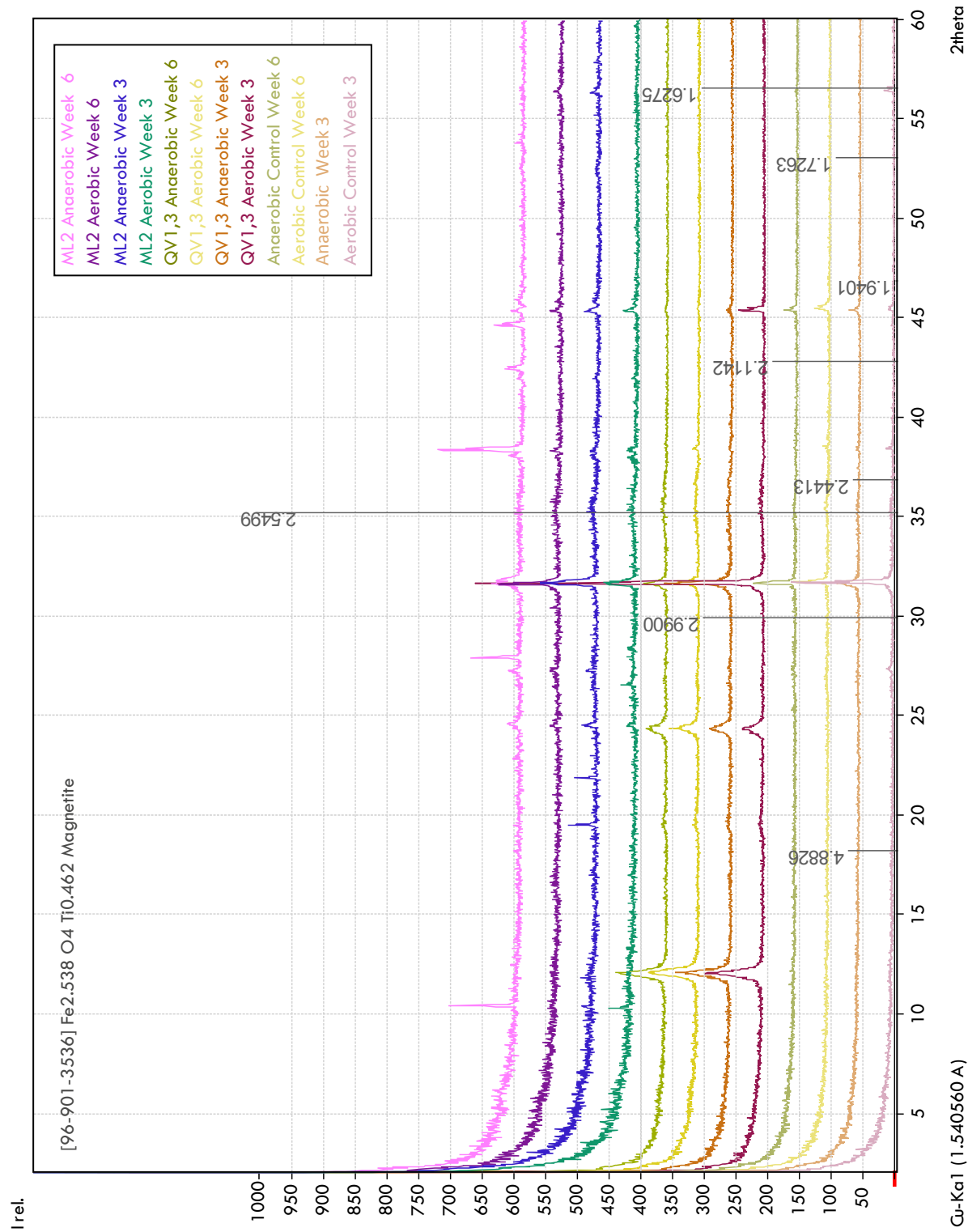
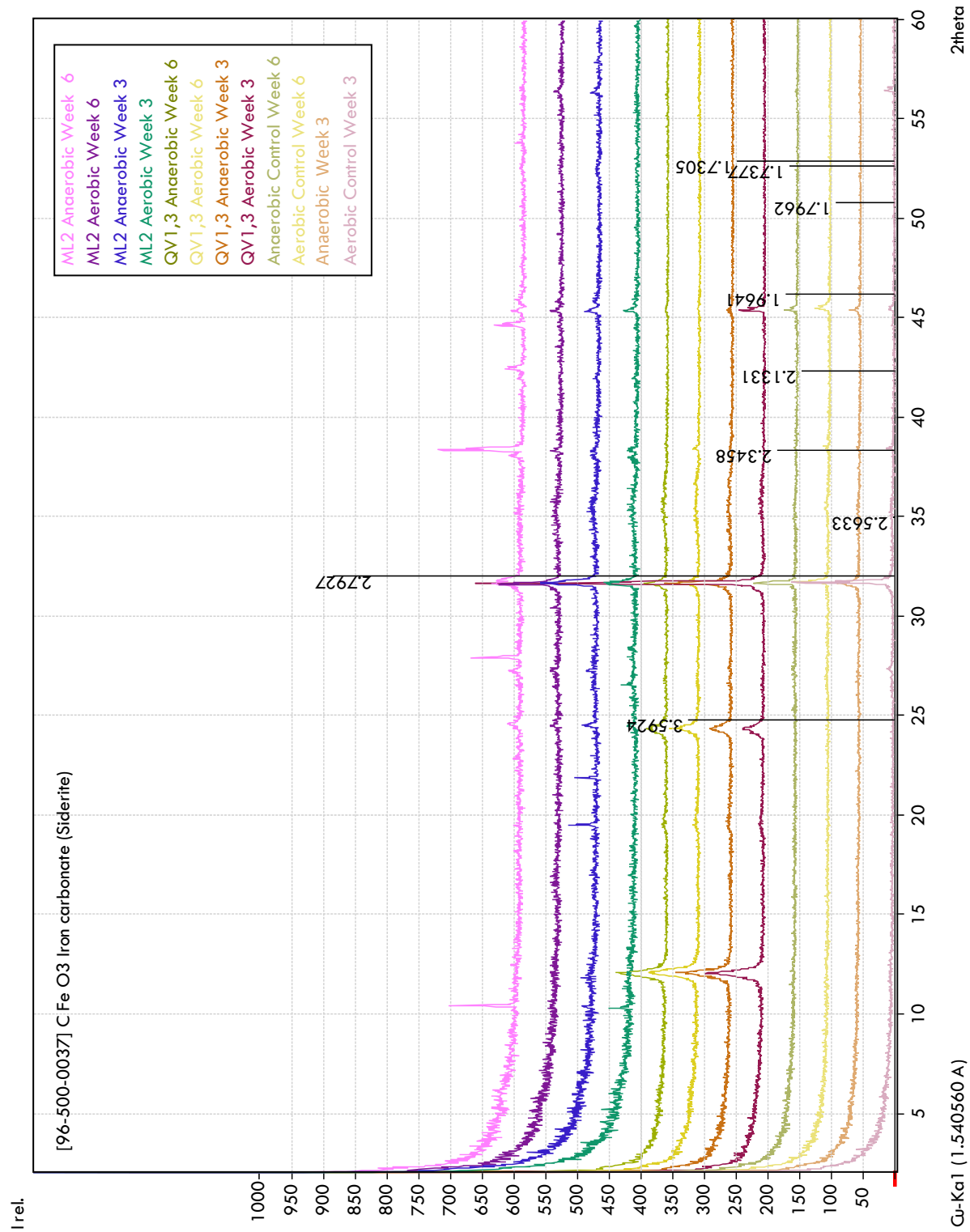


Figure 6. Culture XRD patterns overlain with the standard pattern for magnetite(3536) (shown with d-values).



2-theta

I rel.

2.7927

3.5924

2.3458

2.1331

1.9641

2.5633

1.7962

1.7377

1.7305

Figure 7. Culture XRD patterns overlain with the standard pattern for siderite (shown with d-values).

VITA

NAME: Caitlin Page Casar

EDUCATION: B.S., Geology, East Carolina University, Greenville, North Carolina, 2012

HONORS: NAGT Fellowship, 2011

ABSTRACTS: Microbially-influenced Fe-cycling within high pH serpentinizing springs of the Zambales Ophiolite, Philippines. Midwest Geobiology Symposium, Fall 2014.

Microbially-influenced Fe-cycling within high pH serpentinizing springs of the Zambales Ophiolite, Philippines. AGU, Fall 2014.

Characterizing subsurface microbial iron metabolisms in Martian analog serpentinizing systems: Zambales Ophiolite, Philippines and Coast Range Ophiolite, USA. Astrobiology Science Conference, Summer 2015.